Titre: Title:	Multi Scale Modeling of The Elastic Properties of Polymer-Clay Nanocomposites
Auteur: Author:	Maryam Pahlavan Pour
Date:	2013
Type:	Mémoire ou thèse / Dissertation or Thesis
Référence: Citation:	Pahlavan Pour, M. (2013). Multi Scale Modeling of The Elastic Properties of Polymer-Clay Nanocomposites [Thèse de doctorat, École Polytechnique de Montréal]. PolyPublie. https://publications.polymtl.ca/1163/

Document en libre accès dans PolyPublie
Open Access document in PolyPublie

URL de PolyPublie: PolyPublie URL:	https://publications.polymtl.ca/1163/
Directeurs de recherche: Advisors:	Martin Lévesque, & Pascal Hubert
Programme: Program:	Génie mécanique

UNIVERSITÉ DE MONTRÉAL

MULTI SCALE MODELING OF THE ELASTIC PROPERTIES OF POLYMER-CLAY
NANOCOMPOSITES

MARYAM PAHLAVAN POUR
DÉPARTEMENT DE GÉNIE MÉCANIQUE
ÉCOLE POLYTECHNIQUE DE MONTRÉAL

THÈSE PRÉSENTÉE EN VUE DE L'OBTENTION
DU DIPLÔME DE PHILOSOPHIÆ DOCTOR
(GÉNIE MÉCANIQUE)
JUILLET 2013

UNIVERSITÉ DE MONTRÉAL

ÉCOLE POLYTECHNIQUE DE MONTRÉAL

Cette thèse intitulée:

MULTI SCALE MODELING OF THE ELASTIC PROPERTIES OF POLYMER-CLAY NANOCOMPOSITES

présentée par: PAHLAVAN POUR Maryam
en vue de l'obtention du diplôme de: Philosophiæ Doctor
a été dûment acceptée par le jury d'examen constitué de:

M. PELLETIER Dominique, Ph.D., président
M. LÉVESQUE Martin, Ph.D., membre et directeur de recherche
M. HUBERT Pascal, Ph.D., membre et codirecteur de recherche
M. GANESAN Rajamohan, Ph.D., membre
M. PILVIN Philippe, Doctorat, membre

To my parents
Zari and Faramarz

To my loves
Farhad and Ava

ACKNOWLEDGEMENTS

I would like to thank Pr. Martin Lévesque and Pr. Pascal Hubert for their time, guidance, support and most importantly, their trust throughout this project. Your interest and insightful criticism guided me to be persistent and to gain scientific maturity. Also, I want to thank Pr. Philippe Pilvin, Pr. Rajamohan Ganesan and Pr. Ludvik Martinu for accepting to be my committee members and Pr. Dominique Pelletier as the jury president.

I owe special gratitude to the members of Laboratory for Multiscale Mechanics (LM2) research group. I would like to paricularly acknowledge the contributions of Hadi Moussaddy for numerous and fruitful discussions all along this project and his great helps and comments for improving my French. A great thank you goes to my colleagues Amine El-Mourid, Rouhollah Farahani and Elias Ghossein for their great supports and comments.

I would also like to thank the Fluids Dynamics Laboratory at École Polytechnique de Montréal for sharing computational resources that greatly facilitated the tasks.

I would like to thank the National Research Council Canada for their financial support that made this project possible.

I would like to take this opportunity to thank my parents who devoted their entire lives to my success, for providing unconditional support to me and my family. I have written my thesis in the hope of presenting something valuable to them as my heros. I would also like to thank my dear sweet daughter, Ava who made my life full of hope and energy. I impatiently look forward to seeing the day when she mentions me in her achievements. Finally, especial thanks to my dear mentor, colleague, friend, soulmate and husband, Farhad, who provides me constantly with his love and support and has been admirably encouraging along this project.

RÉSUMÉ

Les Nanocomposites Polymères-Argiles (NPA) sont reconnus pour leur capacité à améliorer les propriétés mécaniques de polymères bruts, et ce, même dans le cas de faibles fractions volumiques de nano-argiles. Cette amélioration est attribuable aux rapports de forme élevés ainsi qu'aux propriétés mécaniques des nano-argiles. En outre, la zone d'interphase résultant d'une modification des chaînes de polymère à proximité des nano-argiles joue un rôle important dans la rigidité de NPA.

Plusieurs approches analytiques existent pour la prédiction des propriétés élastiques de NPA, allant des modèles simplifiés en deux étapes aux modèles plus sophistiqués. Il n'existe toutefois aucune étude ayant déjà vérifié l'exactitude de ces modèles. Par ailleurs, les modèles numériques servant à évaluer leurs homologues analytiques sont encore loin de pouvoir modéliser la microstructure réelle de NPA. Par exemple, la majorité des modèles n'ont pas tenu compte de la microstructure tridimensionnelle de particules aléatoirement réparties, du rapport de forme élevé des nano-argiles, ou de l'intégration explicite de phases constitutives. Plus important encore, la plupart des études numériques ont été développées sans tenir compte du Volume Élémentaire Représentatif (VER) en raison du coût énorme de calculs imposé par ce dernier. Par conséquent, l'exactitude des résultats de référence ainsi obtenus est contestable.

Le but principal de cette thèse était d'évaluer l'exactitude des modèles d'homogénéisation pour la prédiction de comportement mécanique de NPA. Dans un premier temps, la validité des modèles micromécaniques analytiques couramment utilisés pour la prédiction de propriétés élastiques de NPA exfoliés a été évaluée à l'aide de simulations Éléments Finis (EF) tridimensionnelles. Une attention particulière a été accordée à l'interphase autour des nano-argiles. La stratégie de modélisation était une procédure en deux étapes se basant sur la notion de Particule Effective (PE). Dans cette approche de modélisation, les renforts multicouches ont été remplacés par des particules homogènes à effets équivalents. L'exactitude des modèles numériques dans des limites de tolérances prédéfinies était garantie grâce à la détermination rigoureuse du VER. Cette étude a révélé que la méthode de Mori-Tanaka est la plus fiable à utiliser parmi les modèles en deux étapes pour les valeurs typiques de paramètres de NPA exfoliés (contraste de module, rapport de forme et la fraction volumique). Les propriétés mécaniques de l'interphase ainsi que son épaisseur ont été estimées à partir d'une comparaison entre une étude paramétrique numérique et des résultats expérimentaux. Ceci a souligné l'importance de l'incorporation de l'interphase afin de prédire le module de Young.

Deuxièmement, les évaluations ont été étendues à une gamme plus large de modèles applicables à la fois aux morphologies intercalées et exfoliées. Des modèles analytiques ont été

adoptés afin d'explicitement modéliser l'interphase de nano-composites exfoliés ainsi que la structure stratifiée de la morphologie intercalée. Les résultats de simulations EF tridimensionnelles tenant compte de la microstructure stratifiée de PCN ont été obtenus et utilisés comme référence pour la comparaison de prédictions analytiques. Ces dernières ont été également comparées avec des données expérimentales tirées de la littérature. Il s'est avéré que les modèles basés sur l'hypothèse PE qui ne considèrent pas explicitement toutes les phases constitutives pourraient s'écarter de façon significative des résultats EF de référence. Ce résultat démontre la nécessité d'utiliser de modèles EF à microstructure stratifiée, malgré leurs coûts élevés de calculs en fonction de la microstructure et de l'exactitude recherchée.

Finalement, le modèle analytique basé sur l'hypothèse d'inclusions à revêtements multiples a été jugé plus fiable que les méthodes en deux étapes.

La principale contribution de cette thèse était d'évaluer les meilleurs modèles d'homogénéisation pour la prédiction de comportements mécaniques de NPA. En outre, des modèles analytiques ont été adoptés pour la modélisation explicite de phases constitutives dans les NPA. L'originalité de cette étude réside dans le fait que le VER a été établi et que ni les modèles analytiques ni numériques n'étaient limités par des hypothèses simplificatrices fréquemment utilisées dans plusieurs approches, dont la notion de PE.

ABSTRACT

Polymer-Clay Nanocomposites (PCN) are known to improve the mechanical properties of bulk polymers, even for modest clay loadings. This enhancement is due to the high aspect ratio and mechanical properties of the nanoclay platelets. Additionally, the interphase zone created by altered polymer chains in the vicinity of the nanoclays plays an important reinforcing role.

Several analytical approaches exist for predicting the elastic properties of PCN, ranging from simplified two-step models to more complex one-step methods. However, no thorough study has yet rigorously verified the accuracy of these models. On the other hand, the numerical models that are commonly used to evaluate the analytical models are still far from modeling the real PCN microstructure reported in the literature. For example, most of the models have failed to model the detailed 3D microstructure considering randomly positioned reinforcing particles, the large nanoclay aspect ratio and the explicit incorporation of the constituent phases. More significantly, most of numerical studies have been reported without a thorough determination of the appropriate Representative Volume Element (RVE) due its computational burden, resulting in benchmark results of questionable accuracy.

The main purpose of this thesis was to evaluate the accuracy of homogenization models for predicting the mechanical behavior of nanoclay nanocomposites.

First, the validity of commonly used analytical micromechanical models for the prediction of exfoliated PCN elastic properties was evaluated with the help of 3D Finite Element (FE) simulations. In particular, special attention was devoted to the interphase around the nanoclays. The modeling strategy was a two-step procedure relying on the Effective Particle (EP) concept, in which the multi-layer reinforcing stacks were replaced by homogenized particles. The accuracy of the numerical models was guaranteed, within a given tolerance, by rigorous determination of the RVE. It was found that the Mori-Tanaka model was the most reliable method to be used in two-step models for the possible ranges of modulus contrasts, aspect ratios and volume fractions typical of exfoliated PCN. The properties and the thickness of the interphase were estimated from comparison between a numerical parametric study and experimental results. The importance of incorporating the interphase for predicting the axial Young's modulus was highlighted.

Second, the evaluation was extended to a wider class of models applicable to both intercalated and exfoliated morphologies. Analytical models were adopted to explicitly model the interphase in exfoliated nanocomposites, as well as the layered structure of intercalated morphology. 3D FE simulations of PCN layered microstructures were performed to produce

benchmark results. The theoretical predictions were also compared to experimental data extracted from the literature. It was found that the EP-based models not explicitly considering all constituent phases may significantly diverge from the layered microstructure FE results. This observation makes use of the layered FE models inevitable, despite their high computational cost, depending on the PCN microstructure and desired accuracy. Finally, the analytical multi-coated inclusions model was found to deliver more reliable results than two-step methods.

The main contribution of this thesis was to assess the best homogenization models for predicting PCN mechanical behavior based on their evaluated accuracy. In addition, analytical models were adopted to explicitly model the constituent phases in PCN. The originality of the present work lies in the fact that the RVE was established and that neither analytical nor numerical models were limited by simplifying assumptions common in most of modeling approaches such as EP concept.

TABLE OF CONTENTS

LIST OF TABLES

LIST OF FIGURES

LIST OF APPENDICES

LIST OF SYMBOLS AND ABBREVIATIONS

a	Aspect ratio
B	A constant
l	Length of nanoclay platelet
L	Length of volume element
d	Thickness
e	Macroscopic strain component
$\mathbf{e}$	Macroscopic strain tensor
E	Young's modulus
f_{p}	Particle volume fraction
f_{m}	Matrix volume fraction
f^*	Lielens volume fraction
G	Shear modulus
Z	Desired elastic property
k	Bulk modulus
n_{VE}	Size of volume element
n_{R}	Number of realizations
N	Number of nanoclays in each stack
N_{VE}	Size of representative volume element
N_{R}	Size of ensemble of representative volume elements
s	Standard deviation
$\mathbf{u}_x$	Displacement at point $\mathbf{x}$
$\mathbf{C}$	Apparent Stiffness tensor
$\mathbf{C}^{\mathrm{eff}}$	Effective stiffness tensor
$\tilde{\mathbf{C}}$	Ensemble average of stiffness tensor
$\overline{\mathbf{C}}$	Arithmetic mean stiffness tensor
$\underline{\mathbf{C}}$	Harmonic mean stiffness tensor
$\mathbf{I}$	Identity tensor
$\mathbf{S}$	Eshelby tensor
$\mathbf{A}$	Strain localization tensor
P	Percentile
V	Volume of the volume element
V^S	Boundaries of volume element
$\mathbf{r}^k$	Position vector of disc K

$\mathbf{v^k}$	Velocity vector of disc K
R^k	Radius of disc K
a^k	Growth rate of radius of disc K
t	Time
$\mathbf{n}$	Normal vector of the surface
$\mathbf{u}$	Displacement vector
$\mathbf{x}$	Point coordinates vector

Greek symbols

ε	Strain component
$\boldsymbol{\varepsilon}$	Strain tensor
$\boldsymbol{\sigma}$	Stress tensor
σ	Stress component
$\boldsymbol{\Sigma}$	Macroscopic stress tensor
Σ	Macroscopic stress component
ν	Poisson's ratio
δ_0	Tolerance for number of realizations
δ_1	Tolerance for volume size
δ_2	Distance between the two discs in the 13-plane
δ_3	Distance between the two discs along axis 2
ϵ_{CI}	Size of the confidence interval
α	An empirical parameter

Abbreviations

VE	Volume element
RVE	Representative volume element
FE	Finite element
PCN	Polymer-clay nanocomposites
2D	Two-dimensional
3D	Three-dimensional
MT	Mori-Tanaka
SC	Self-consistent
Li	Lielens
EP	Effective Particle
Iso	Isotropic
TIso	Transversely isotropic

| RSA | Random Sequential Adsorption |
| MD | Molecular Dynamics |

INTRODUCTION

Polymer-Clay Nanocomposites (PCN) are known to improve the properties of bulk polymers. The property improvement can be achieved with modest amounts of clay (usually less than 5 wt % (Alexandre and Dubois, 2000)) for different properties: mechanical, barrier, thermal, optical, electrical and biodegradability (Chen *et al.*, 2008; Alexandre and Dubois, 2000; Ray and Okamoto, 2003). Significant increases in moduli (Kojima *et al.*, 1993; Messersmith and Giannelis, 1994; Giannelis, 1996), strength, heat resistance (Okada and Usuki, 1995), biodegradability (Schmidt *et al.*, 2002; Chen *et al.*, 2008), decrease in gas permeability (Yano *et al.*, 1997; Giannelis, 1996; Bharadwaj, 2001; Ray and Okamoto, 2003) and flammability (Giannelis, 1996; Gilman, 1999; Ray and Okamoto, 2003; Powell and Beall, 2006; Schmidt *et al.*, 2002) have triggered applications in three important industrial sectors: transportation, construction and packaging (Morgan, 2007).

Clay minerals have a layered structure constituted of silicate platelets of nanometric thickness, referred herein as nanoclays. Generally, the clay filler and the polymer matrix are not compatible with each other and the clay surface must be modified with surfactant molecules (modifiers). PCN can be classified into two morphologies, depending on the degree of separation between the silicate layers and the polymer penetration, namely, intercalated nanocomposites and exfoliated nanocomposites (Figure 0.1). Exfoliated morphology occurs when separated single nanoclays are dispersed in the polymer matrix. The intercalated morphology results from the penetration of polymer chains between parallel nanoclays lying in stacks. Interactions at the interface between the nanoclay and polymer matrix result in the formation of a modified polymer, called interphase, that has a thickness of a few nm.

Characterization and fabrication of PCN from the experimental point of view is not a straightforward task. The fabrication of PCN is still empirical and controlling their properties is complex, time consuming and costly. Therefore, computer modeling can play a helpful role in predicting and tailoring the desired properties.

There exists different analytical, as well as numerical, methods for predicting the mechanical behavior of PCN. Analytical homogenization models, generally based on ideal representations, produce quick estimations (or rigorous bounds) for the effective properties of composites. However, unless for very specific microstructures (e.g., Ghossein and Lévesque (2012)), the accuracy of their estimates has not been thoroughly evaluated. In addition, very few works have addressed to the interphase effects.

Analytical models are usually evaluated using numerical homogenization. Numerical homogenization is accomplished by simulating artificial loadings on three-dimensional (3D) or
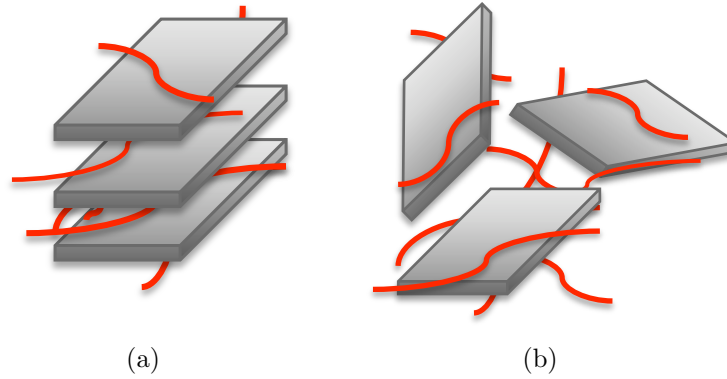
Figure 0.1 Schematic representation of two different morphologies for PCN. a) Intercalated and b) exfoliated clay stacks in PCN. The gray platelets are the nanoclays and the red lines are the polymer chains.

two-dimentional (2D) representations of the material. The behavior of the volume under the applied force is computed by numerical techniques such as the Finite Element (FE). The accuracy of numerical homogenization relies on the fundamental notion of the Representative Volume Element (RVE). The determination of the RVE is not trivial and convergence studies are required for defining a RVE that has the same effective properties as the bulk material and, concurrently, is small enough to avoid high computational costs. Most of the numerical studies did not perform a thorough determination of the appropriate RVE due its computational burden, resulting in benchmark results of questionable exactitude. In addition, numerical models are still far from modeling the real PCN microstructure reported in the literature. For example, most of the studies have failed to model the detailed 3D microstructure considering the randomly positioned reinforcing particles, the nanoclays with large aspect ratios, incorporating explicitly all the constituent phases and applying appropriate boundary conditions.

The general objective of this research was to study the homogenization models for the mechanical behavior of PCN. The study had two main themes:

– To evaluate the accuracy of different analytical homogenization models taking into account the morphology of PCN;

– To improve the numerical homogenization models, as evaluation tools, in terms of both microstucture modeling and RVE determination accuracy.

This thesis is organized as follows. Chapter 1 presents a literature review on analytical and numerical homogenization methods applicable to PCN. In Chapter 2, the research objectives are introduced along with the publication strategy of the scientific articles. The

two articles resulting from this work are presented in Chapters 3 and 4. In Chapter 3, the predictions of the effective properties using different analytical methods are compared to that of numerical modeling using well established RVEs. The evaluation is extended in Chapter 4 to a wider class of models applicable to both intercalated and exfoliated morphologies. Chapter 5 discusses the connection between the articles and the reviewed literature, as well as complementary work performed during this project. The contributions of this thesis are finally summarized and topics for future studies are recommended.

CHAPTER 1

Literature review

1.1 Analytical homogenization

The focus of this section is on the analytical homogenization models applicable to PCN. For a more thorough theoretical study on micromechanics and analytical homogenization models, one can refer to the works of (Mura, 1987; Nemat-Nasser and Hori, 1993; Suquet, 1997; Bornert *et al.*, 2001; Torquato, 2002; Milton, 2002; Böhm, 2013).

Composites are inhomogeneous materials, i.e. they consist of dissimilar phases. Micromechanics bridges the microscopic structure of the heterogeneous media, the material behavior of its constituting phases and their geometrical arrangements, to its macroscopic (*effective*) behavior. The basic idea in micromechanics, also referred to as homogenization herein, is to find the homogeneous equivalent of a micro-inhomogeneous solid sample.

1.1.1 Two-phase models studied in this work

The studied two-phase composites consisted of a matrix and embedded inhomogeneities. Homogenization computes the composite's effective stiffness tensor $\mathbf{C}^{\text{eff}}$ such that:

$$\boldsymbol{\Sigma} = \mathbf{C}^{\text{eff}} : \mathbf{e}, \tag{1.1}$$

where $\boldsymbol{\Sigma}$ and $\mathbf{e}$ are the macroscopic stress and strain responses of the composite. Bridging between the micro and macroscopic scales is performed by relating the microscopic fields to the macroscopic responses, such as:

$$<\boldsymbol{\varepsilon}(\mathbf{x})> = \mathbf{e}, \tag{1.2a}$$

$$<\boldsymbol{\sigma}(\mathbf{x})> = \boldsymbol{\Sigma}, \tag{1.2b}$$

where $\boldsymbol{\sigma}$ and $\boldsymbol{\varepsilon}$ are the local strain and stress fields, respectively, and $<.>$ denotes the volume averaging operation:

$$<\mathbf{f}(\mathbf{x})> = \frac{1}{V} \int_V \mathbf{f}(\mathbf{x}) \mathrm{d}V, \tag{1.3}$$

where V is the volume of the composite sample that is being homogenized.

The microscopic fields can be calculated by the localization relation using the mechanical

strain concentration tensor $\mathbf{A}(\mathbf{x})$ such that:

$$\boldsymbol{\varepsilon}(\mathbf{x}) = \mathbf{A}(\mathbf{x}) : <\boldsymbol{\varepsilon}>. \tag{1.4}$$

Consequently, one can obtain:

$$<\boldsymbol{\sigma}> = <\mathbf{C}(\mathbf{x}) : \mathbf{A}(\mathbf{x})> : <\boldsymbol{\varepsilon}>. \tag{1.5}$$

The knowledge of $\mathbf{A}(\mathbf{x})$ provides the solution for the homogenization problem. However, in general, the exact expressions for $\mathbf{A}(\mathbf{x})$ cannot be given analytically. Different assumptions and approximations are introduced in analytical homogenization models to obtain analytical expressions for $\mathbf{A}(\mathbf{x})$. The phase averaged strains can be related to the overall strain by the phase averaged strain localization tensors (Hill, 1965):

$$<\boldsymbol{\varepsilon}>^{\mathrm{m}} = \mathbf{A}^{\mathrm{m}} : <\boldsymbol{\varepsilon}>, \tag{1.6a}$$

$$<\boldsymbol{\varepsilon}>^{\mathrm{p}} = \mathbf{A}^{\mathrm{p}} : <\boldsymbol{\varepsilon}>, \tag{1.6b}$$

where subscripts m and p denote the matrix and the particle phases, respectively, $< \cdot >^{i}$ is the volume average in phase i and $\mathbf{A}^{i}$ is the average concentration tensor within the phase. The strain concentration tensors can be shown to fulfill the relation (Hill, 1965):

$$f_{\mathrm{m}}\mathbf{A}^{\mathrm{m}} + f_{\mathrm{p}}\mathbf{A}^{\mathrm{p}} = \mathbf{I}, \tag{1.7}$$

where f denotes the volume fraction and $\mathbf{I}$ is the fourth order identity tensor.

Under uniform displacement and traction boundary conditions on the boundaries of V, one obtains:

$$<\boldsymbol{\varepsilon}> = f_{\mathrm{m}}\langle\boldsymbol{\varepsilon}\rangle^{\mathrm{m}} + f_{\mathrm{p}}\langle\boldsymbol{\varepsilon}\rangle^{\mathrm{p}}, \tag{1.8a}$$

$$<\boldsymbol{\sigma}> = f_{\mathrm{m}}\langle\boldsymbol{\sigma}\rangle^{\mathrm{m}} + f_{\mathrm{p}}\langle\boldsymbol{\sigma}\rangle^{\mathrm{p}}. \tag{1.8b}$$

Use of Equations (1.6a) to (1.8b) leads to:

$$\mathbf{C}^{\mathrm{eff}} = \mathbf{C}^{\mathrm{m}} + f_{\mathrm{p}}(\mathbf{C}^{\mathrm{p}} - \mathbf{C}^{\mathrm{m}}) : \mathbf{A}^{\mathrm{p}}. \tag{1.9}$$

Equation (1.9) provides direct estimations for the effective stiffness tensor of two-phase composites based on the knowledge of $\mathbf{A}^{\mathrm{p}}$ (hereinafter cited as $\mathbf{A}$).

Mean field homogenization methods approximate the microfields within each phase by their phase averages so as to provide estimations for $\mathbf{A}$. Most mean field homogenization methods are based on the work of Eshelby (1957). His study dealt with the strain field of

a homogeneous ellipsoidal inclusion (i.e., inclusion with the same material as the matrix) surrounded by an infinite matrix and subjected to a uniform stress-free strain. He showed that the resulting strain field in the constrained inclusion is uniform and is given by:

$$\boldsymbol{\varepsilon}_i = \mathbf{S} : \boldsymbol{\varepsilon}_t, \tag{1.10}$$

where $\mathbf{S}$ is Eshelby's tensor, $\boldsymbol{\varepsilon}_i$ is the uniform strain in the constrained inclusion and $\boldsymbol{\varepsilon}_t$ is a uniform stress-free strain. Eshelby's tensor depends on the reinforcement shape as well as the matrix properties. Expressions for $\mathbf{S}$ can be found in (Mura, 1987) for several inclusion shapes and material symmetries. For complex shapes and material symmetries, Eshelby's tensor can be calculated numerically following the methodology of Gavazzi and Lagoudas (1990).

For dilute matrix-inhomogeneity composites, it can be assumed that the inhomogeneities do not have any interaction between each other. Such cases can be handled based on the Eshelby's theory for homogeneous inclusions, as per Equation (1.10), by replacing the heterogeneities by equivalent homogeneous inclusions subjected to a stress-free strain (Withers *et al.*, 1989). As a result, for the dilute (dil) composite, $\mathbf{A}$ can be given by:

$$\mathbf{A}^{\text{dil}} = [\mathbf{I} + \mathbf{S} : (\mathbf{C}^m)^{-1} : (\mathbf{C}^p - \mathbf{C}^m)]^{-1}. \tag{1.11}$$

The assumption of dilutely dispersed particles in the matrix ignores any interactions between neighboring particles, leading the properties predicted by Eshelby model to be accurate only at very low volume fractions (typically up to 1%) (Tucker and Liang, 1999; Böhm, 2013).

Mori-Tanaka model

In the model of Mori and Tanaka (1973) (MT), the inclusion phase average is expressed as a function of the matrix average as:

$$<\boldsymbol{\varepsilon}>^p = \mathbf{A}^{\text{dil}} : <\boldsymbol{\varepsilon}>^m. \tag{1.12}$$

An original application of MT model was performed by Benveniste (1987) for a two-phase composite material, which estimated the strain concentration tensor for MT approach as:

$$\mathbf{A}^{\text{MT}} = \mathbf{A}^{\text{dil}} : [(1 - c_p)\mathbf{I} + c_p\mathbf{A}^{\text{dil}}]^{-1}. \tag{1.13}$$

Self-consistent scheme

In the Self-Consistent (SC) scheme (Hill, 1965; Budiansky, 1965), the inclusion is assumed to be embedded in the effective material whose properties are yet unknown. The corresponding strain concentration tensor is expressed as:

$$\mathbf{A}^{\mathrm{SC}} = [\mathbf{I} + \mathbf{S}^{\mathrm{eff}} : (\mathbf{C}^{\mathrm{eff}})^{-1} : (\mathbf{C}^{\mathrm{p}} - \mathbf{C}^{\mathrm{eff}})]^{-1}, \tag{1.14}$$

and $\mathbf{S}^{\mathrm{eff}}$ is Eshelby's tensor that depends on the composite effective elastic properties ($\mathbf{C}^{\mathrm{eff}}$) as the infinite medium and the aspect ratio of the particle. The SC model is an implicit approach and must be solved iteratively. This model is mostly suitable for modeling materials whose phases are indistinguishable, e.g., polycrystals, interwoven composites, and functionally graded materials (Zaoui, 2002; Böhm, 2008).

Lielens's model

Lielens *et al.* (1997) proposed a model that interpolates between the upper and lower Hashin-Shtrikman bounds for aligned reinforcements and reads as:

$$\mathbf{A}^{\mathrm{Li}} = \hat{\mathbf{A}}^{\mathrm{Li}} : [(1 - f_{\mathrm{p}})\mathbf{I} + f_{\mathrm{p}}\hat{\mathbf{A}}^{\mathrm{Li}}]^{-1}, \tag{1.15}$$

where

$$\hat{\mathbf{A}}^{\mathrm{Li}} = \{(1 - f^*)[\hat{\mathbf{A}}^{\mathrm{lower}}]^{-1} + f^*[\hat{\mathbf{A}}^{\mathrm{upper}}]^{-1}\}^{-1}, \tag{1.16}$$

and c^* is related to the particle volume fraction as:

$$f^* = \frac{f_{\mathrm{p}} + f_{\mathrm{p}}^2}{2}. \tag{1.17}$$

$\hat{\mathbf{A}}^{\mathrm{lower}}$ and $\hat{\mathbf{A}}^{\mathrm{upper}}$ are expressed as:

$$\hat{\mathbf{A}}^{\mathrm{lower}} = [\mathbf{I} + \mathbf{S}^{\mathrm{m}} : (\mathbf{C}^{\mathrm{m}})^{-1} : (\mathbf{C}^{\mathrm{p}} - \mathbf{C}^{\mathrm{m}})]^{-1}, \tag{1.18a}$$

$$\hat{\mathbf{A}}^{\mathrm{upper}} = [\mathbf{I} + \mathbf{S}^{\mathrm{p}} : (\mathbf{C}^{\mathrm{p}})^{-1} : (\mathbf{C}^{\mathrm{m}} - \mathbf{C}^{\mathrm{p}})]^{-1}, \tag{1.18b}$$

where $\mathbf{S}^{\mathrm{p}}$ is Eshelby's tensor where the infinite medium has the properties of the particles.

Validity of two-phase models

Tucker and Liang (1999) conducted a validation study on micromechanical models applicable for short fiber composites. In their work, they assessed analytical models by comparing their estimations to 3D FE calculations of periodic arrays of fibers and also to the Ingber and Papathanasiou's boundary element predictions for randomly positioned aligned fibers (Ingber and Papathanasiou, 1997). They reported that the MT model delivers the most accurate predictions for large aspect ratio fibers (Figure 1.1(a)). The SC model was found to overestimate the axial modulus at high volume fractions (Figure 1.1(b)) but performed quite well for other elastic constants. They also pointed out that Lielens's model may improve on the MT model for higher fiber volume fractions or rigidity contrasts (Figure 1.1(b)). However, their validations were mostly performed against estimations of models with regularly arranged fibers. Furthermore, their conclusions are valid for a limited range of aspect ratios ($lenght/diameter \approx 1 - 50$). In addition, Berryman and Berge (1996); Zaoui (2002); Böhm (2008) do not recommend MT model for high volume fractions of inclusions (i.e., more than 20-30% (Berryman and Berge, 1996)).

Pierard *et al.* (2004) studied Eshelby-based homogenization techniques. They reported that for two-phase composites (when all inclusions have the same material properties, aspect ratio and orientation) the model of Lielens (Lielens, 1999) delivers perhaps the best predictions for a wide range of aspect ratios (Figure 1.2), volume fractions and stiffness contrasts. They have also mentioned that for low volume fraction of inclusions, the difference between MT and Lielens's models remains small with slightly better results obtained by the latter model.

1.1.2 Multi-phase methods

In this section, the focus is on composites made with coated or multi-coated inclusions. Various techniques have been adopted to predict the effective properties of linearly elastic composites in the presence of interphase layer, e.g., Christensen and Lo (1979); Hori and Nemat-Nasser (1993); Hervé and Zaoui (1993); Dunn and Ledbetter (1995); Sarvestani (2003); Lipinski *et al.* (2006).

Hori and Nemat-Nasser (1993) proposed a model called double-inclusion that consists of an ellipsoidal inclusion embedded in another ellipsoidal matrix, both embedded in an infinitely extended homogeneous medium. The shape and the orientation of the inclusion and the matrix, and the elastic properties of the three phases are arbitrary. By choosing the inclusion and the matrix to be aligned and identically shaped, and by taking the elastic moduli of the infinite medium to be the same as those of the matrix or the effective composite, the results
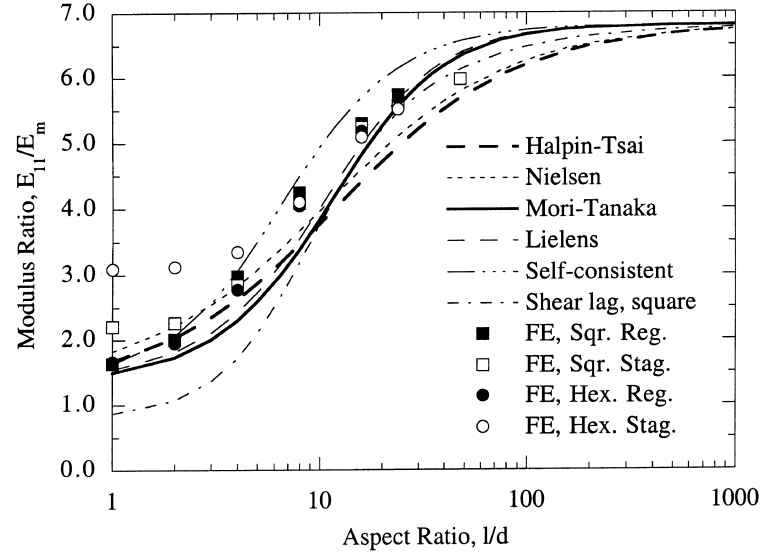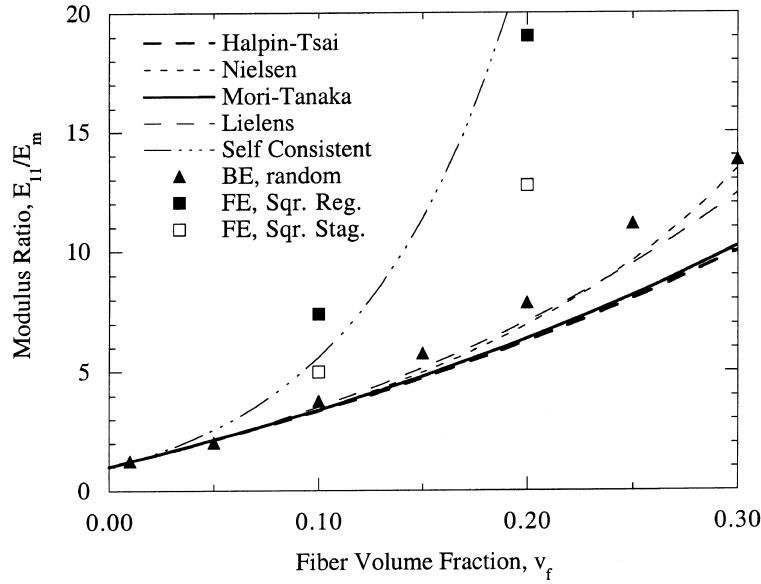
Figure 1.1 a) Analytical predictions and FE results for axial Young's modulus E_{11} for short-fiber composites with $E_{\mathrm{fiber}}/E_m = 30$ and fiber volume fraction of 20%.; b) Analytical models compared to boundary element (BE) predictions for random arrays of rigid cylinders by Ingber and Papathanasiou (1997) with $E_{\mathrm{fiber}}/E_m = 10^6$, all for aspect ratio of 10 (Tucker and Liang, 1999).

are identical to those of the MT or SC models, respectively Hu and Weng (2000). It was shown by Ju and Chen (1994) that the model of Hori and Nemat-Nasser (1993) is a *noninteracting* solution that does not take into account the interaction between particles. Ju and Chen
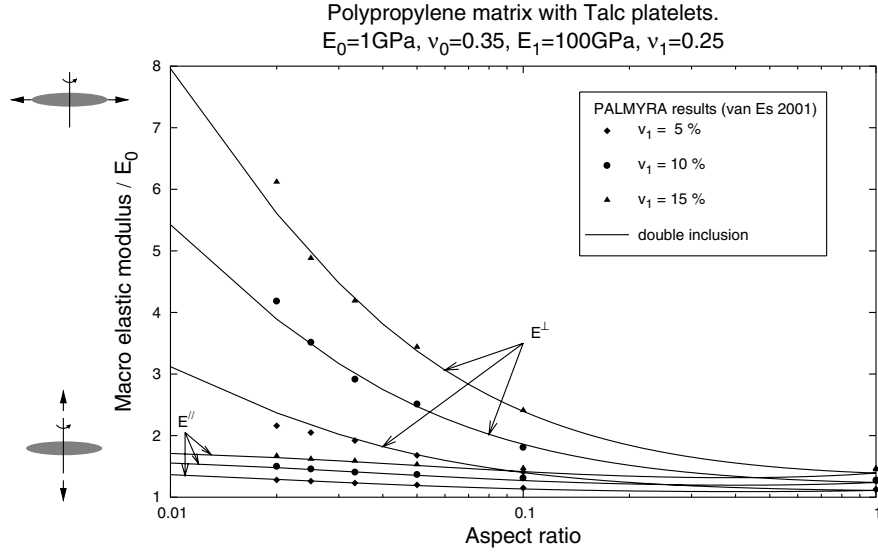
Figure 1.2 The macro elastic modulous in the direction of the revolution axis $(E^{\parallel})$ and along the radius $(E^{\perp})$ of the spheroids as a function of the talc volume fraction. Comparison between the double inclusion (Lielens's) model and FE results of VanEs (2001)(Palmyra) (Pierard *et al.*, 2004). Subscripts 1 and 0 refer to the paltelets and matrix, respectively.

(1994) derived the general governing equations for composites containing unidirectionally oriented particles by incorporating the effects of particle-particle interactions. Liu and Sun (2005) found the effective stiffness tensor for three-phase composites containing randomly distributed, yet aligned, spheroidal particles with interlayers (cited hereinafter as *Interacting Double-Inclusion (IDI) model*).

Christensen and Lo (1979) solved the elementary problem of a coated spherical inclusion in a three-phase model where the coating represents the real matrix with the thickness adjusted in consideration of the inclusion volume fraction. The coated inclusion is then embedded in the composite with yet unknown effective properties. This model is known as the generalized self-consistent scheme. Hervé and Zaoui (1993) extended the three-phase model to an n-layered spherical inclusion. Their method of resolution is based on the energy condition of Christensen and Lo (1979) for the three-phase model. More recently, Lipinski *et al.* (2006) provided a general framework to deal with a heterogeneous problem, where the inhomogeneity consists of a n-layered inclusion composed of n concentric ellipsoids (Figure 1.3) made of anisotropic elastic materials. The methodology is based on a combination of interface operators with Green's function techniques, capturing the stress and strain jumps at the interfaces between two adjacent coatings, which are considered perfectly bonded. The model of (Lipinski *et al.*, 2006) can be applied, through a generalized self-consistent scheme, to

describe the overall behavior of real composite materials with complex microstructures that are significantly influenced by the presence of the interphase, in particular the composite made with multi-coated ellipsoidal inclusions. This model is cited hereinafter as *multi-coated* model. All the equations related to the IDI and the multi-coated models are reported at Section 4.

Kernel c^1 Coating c^2 Coating c^i Coating c^n

Matrix c^0
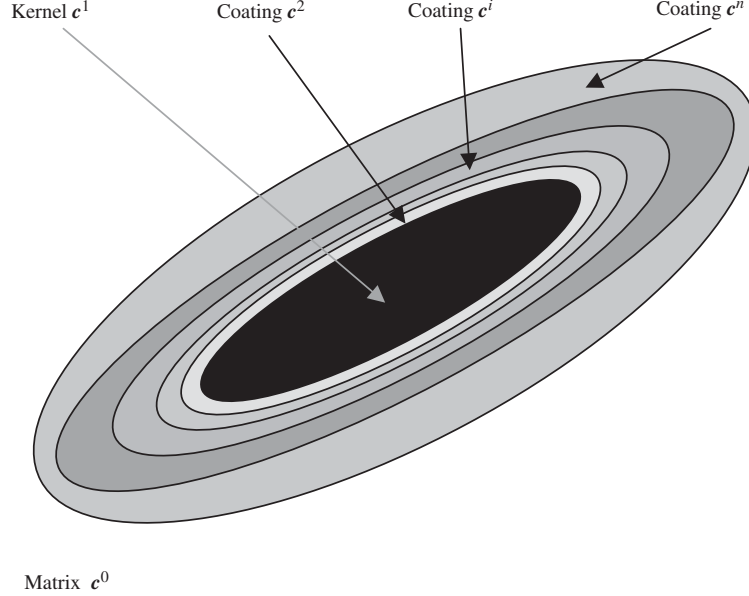
Figure 1.3 The n-layered ellipsoidal inclusion composed of n concentric ellipsoids (Lipinski *et al.*, 2006).

1.2   Numerical homogenization

In contrast to analytical models, numerical methods compute accurate local stress and strain fields for geometries where the matrix and heterogeneities are explicitly represented. The effective properties are subsequently computed from the volume average of these fields. Therefore, numerical homogenization is considered as an accurate homogenization method, provided that the simulated volume is a RVE. However, due to computational constraints in the numerical modeling, one is often limited to analyze volumes smaller than the RVE. Following the terminology of Huet (1990), the properties of such volumes are referred to as *apparent properties*, whereas that of the RVE are referred to as *effective properties*. When the volume under study is large enough (mathematically infinite), the apparent properties of random materials become equivalent to the effective properties under any set of boundary conditions, as proved by Sab (1992).

The simulation process of a single given volume is described in Section 1.2.1. The RVE concept and determination methods are then reviewed in Section 1.2.2.

1.2.1 Numerical homogenization of an arbitrary material volume

Random microstructure generation methods

A 3D microstructure can be either generated by imagery of a real microstructure sample or by a computer using random generation algorithms. Experimental image reconstruction techniques (Huang and Li, 2013) require expensive specialized equipments and involves destructive imaging of experimental samples. The focus of this work is on computer random generation methods.

The Random Sequential Adsorption (RSA) algorithm (Feder, 1980; Talbot *et al.*, 1991) has been the most commonly used method for random generation of microstructures, due to its simplicity. In this algorithm, the position of the first particle is randomly generated. The positions of the subsequent particles are also randomly generated with the condition that they must not interfere with the existing particles. If a newly added particle interferes with other particles, it is removed and then repositioned randomly. This operation is repeated until the particle location is accepted. Non-overlapping particles are sequentially added until the target volume fraction is reached. Achievable microstructures using RSA algorithm are limited to low volume fractions, also known as jamming limit (Feder, 1980).

Lubachevsky and Stillinger (1990) proposed an algorithm based on Molecular Dynamics (MD) and applied it for discs and spheres (Lubachevsky *et al.*, 1991). In their algorithm, all particles are all created at once in the volume, but with a null volume. They are then put in motion and the volume of each particle progressively increases. The particles can collide with each other or with the faces of the cell and the computations end when the target volume fraction is reached. This method is able to generate very high volume fractions (74%) of spherical particles in a volume (Ghossein and Lévesque, 2012).

There are also another method for generating random microstructure such as Monte-Carlo simulations and the recent random-walk methods proposed by Altendorf and Jeulin (2011a). Monte-Carlo methods have shown relatively low jamming limits (Lusti and Gusev, 2004). The random-walk process has been developed for fiber composites and was able to achieve high volume fractions (i.e., up to 65% for randomly oriented bent fibers having an aspect ratio of 10 (Altendorf and Jeulin, 2011a). However, such high volume fractions is limited to cases where fiber bending is permitted (Altendorf and Jeulin, 2011b).

Numerical resolution methods

FE and Fast Fourier Transforms (Moulinec and Suquet, 1994, 1998; Ghossein and Lévesque, 2012) have been extensively used to compute the local stress and strain fields of a given 3D microstructure. A list of some other numerical methods can be found in Böhm (2013) and Pierard (2006). Most numerical methods require the discretization of the microstructure geometry into smaller elements. The accuracy of the solution depends on the fineness degree of the discretization and the discretized elements must be smaller than the intrinsic microstructure length scales. Therefore, very fine discretization is required in the presence of large length scale contrasts within the microstructure, as is the case for microstructures with very thin discs. The solution of such microstructures necessitates long processing times and large computational memory to perform and store all the computations over the numerical system. The FFT solution scheme requires uniform discretization of a 3D microstructure image into cubic volume elements of equal size called *voxels*. The number of voxels required to adequately represent the geometry of high aspect ratio particles is generally high, leading to prohibitively large computational costs. In contrast, the FE method permits for a non-uniform discretization of microstructure allowing different levels of mesh refinements in different parts of the microstructure. Moreover, different shapes of elements (e.g., tetrahedrons) can be used, enabling the FE to discretize thin disc-shaped microstructures with fewer elements, when compared to the FFT method. However, in opposition to the FFT based methods, the FE method requires user interventions, which makes its automation challenging (Ghossein and Lévesque, 2012).

Boundary conditions

Homogenization can be performed under any set of boundary conditions (BC). Enforcing different BC on the same volume element smaller than the RVE yields different apparent properties. Applying appropriate BC is one of the key issues in obtaining accurate estimations.

Uniform traction boundary conditions underestimate the effective properties and more precisely leads to a lower bound (Huet, 1990). These BC are given by:

$$\boldsymbol{\sigma}(\mathbf{x}) \cdot \mathbf{n} = \boldsymbol{\Sigma} \cdot \mathbf{n} \quad \forall\, \mathbf{x} \in V^S, \tag{1.19}$$

where V^S is the surface of the volume element and $\mathbf{n}$ is the normal vector at position $\mathbf{x}$ on V^S.

Uniform displacement boundary conditions overestimate the effective properties, delivers an upper bound and are expressed as:

$$\mathbf{u}(\mathbf{x}) = \mathbf{e} \cdot \mathbf{x} \quad \forall\, \mathbf{x} \in V^S, \tag{1.20}$$

where $\mathbf{u}$ is the displacement vector. For high contrasts of phases properties, the properties computed using above BCs are very far apart and do not deliver accurate estimations of the effective properties.

On the other hand, Periodic Boundary Conditions (PBC) were shown by (Gusev, 1997; Kanit *et al.*, 2003) to yield more accurate effective properties with a minimum computational effort. PBC can be enforced on the volume element with the help of the following relation:

$$\mathbf{u}(\mathbf{x} = \mathbf{x}_0) - \mathbf{u}(\mathbf{x} = \mathbf{x}_0^*) = \mathbf{e} : (\mathbf{x}_0 - \mathbf{x}_0^*), \tag{1.21}$$

where $\mathbf{x}_0$ and $\mathbf{x}_0^*$ represent each two homologous points on opposite faces of the material volume, and $\mathbf{e}$ is the applied infinitesimal macroscopic strain tensor that can be chosen arbitrarily and is discussed in the following.
In contrast to the FFT formulation that is based on periodic fields, the implementation of PBCs in the FE model requires L-periodic (L is the edge length of volume element V) nodal positions. It means exactly homologous nodes should be located at each two opposite faces. This requirement makes the FE meshing procedure difficult and requires the volume element to be also periodic. A periodic microstructure is such that a particle that intersects a surface of volume continues from the opposite surface (see Figure 1.4).

Microstructure periodicity and matching nodes requirements for enforcing PBC were stated in several works as complex processes, (Böhm, 2013; Hbaieb *et al.*, 2007; Mortazavi *et al.*, 2013). To overcome the difficulties in applying PBC, Hbaieb *et al.* (2007) used symmetrical boundary conditions in their 3D FE modeling. Recently, Nguyen *et al.* (2012) suggested adapting the PBC to non-matching meshes. They presented a new FE formulation to impose PBC on arbitrary meshes using polynomial interpolation. However, finding the appropriate polynomial parameters (e.g., order of Lagrange interpolation, number of segments in the spline interpolation) to reach a given accuracy is not trivial.
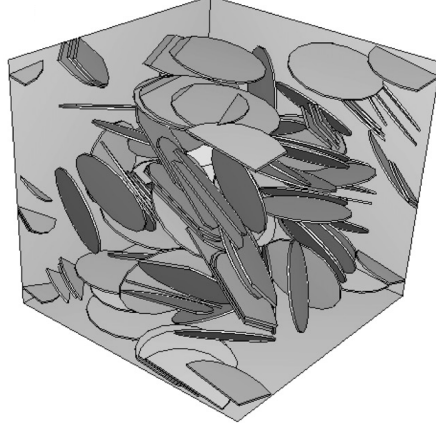
Figure 1.4 A 3D periodic volume element including randomly oriented and distributed nanoclay discs. The volume fraction of particles is 5%. Particles that cut one or two boundary faces are split into two or four parts with those remaining (that would otherwise be outside of the volume) relocated to opposite faces (Hbaieb *et al.*, 2007).

Computing apparent properties

Using the major and minor symmetries of the stiffness tensor, the macroscopic constitutive behavior for a finite volume can be written in a matrix notation (modified Voigt notation) as:

$$
\begin{bmatrix} \Sigma_{11} \\ \Sigma_{22} \\ \Sigma_{33} \\ \Sigma_{23} \\ \Sigma_{13} \\ \Sigma_{12} \end{bmatrix} = \begin{bmatrix} C_{1111} & C_{1122} & C_{1133} & \sqrt{2}C_{1123} & \sqrt{2}C_{1131} & \sqrt{2}C_{1112} \\ C_{2211} & C_{2222} & C_{2233} & \sqrt{2}C_{2223} & \sqrt{2}C_{2231} & \sqrt{2}C_{2212} \\ C_{3311} & C_{3322} & C_{3333} & \sqrt{2}C_{3323} & \sqrt{2}C_{3331} & \sqrt{2}C_{3312} \\ \sqrt{2}C_{2311} & \sqrt{2}C_{2322} & \sqrt{2}C_{2333} & 2C_{2323} & 2C_{2331} & 2C_{2312} \\ \sqrt{2}C_{3111} & \sqrt{2}C_{3122} & \sqrt{2}C_{3133} & 2C_{3123} & 2C_{3131} & 2C_{3112} \\ \sqrt{2}C_{1211} & \sqrt{2}C_{1222} & \sqrt{2}C_{1233} & 2C_{1223} & 2C_{1231} & 2C_{1212} \end{bmatrix} \begin{bmatrix} e_{11} \\ e_{22} \\ e_{33} \\ e_{23} \\ e_{13} \\ e_{12} \end{bmatrix}. \quad (1.22)
$$

The six columns of the apparent elastic tensor can be calculated by independently applying six orthogonal macroscopic deformation states **e** on V (e.g., three pure longitudinal and three pure shear deformations). Thus, six independent simulations are required to find the complete stiffness tensor. To compute straightforwardly one (or a set of) desired property(s), one can choose fewer deformation states depending on the desired property(s) and macroscopic symmetry of the composite (e.g. see Kanit *et al.* (2003)).

1.2.2 RVE determination

Numerous studies were devoted to the definition of the RVE (Hill, 1963; Sab, 1992; Drugan and Willis, 1996; Ostoja-Starzewski, 2006). The suggested definitions are generally based on the representativeness of either the structure of the volume element or its physical behavior, or both. Depending on the RVE application domain, the RVE definitions may be different. In the framework of homogenization, the aim is to obtain accurate effective properties. Thus, homogenization works as in those of Kanit *et al.* (2003); Kari *et al.* (2007); Barello and Lévesque (2008); Ghossein and Lévesque (2012) have most often adopted the *physical RVE* (Böhm, 2013) concept defined by *a volume element that computes the same target property as the bulk material* (Gusev, 1997).

Theoretically, a Volume Element (VE) is exactly representative of a random media when it contains an infinite number of heterogeneities (Ostoja-Starzewski, 2002). For finite volumes, the RVE of a random medium cannot be reached exactly but with a predefined error tolerance. In this regard, Kanit *et al.* (2003) defined quantitative RVE, which is not necessarily characterized by a single finite volume but by an ensemble of N_R realizations, each containing N_{RVE} heterogeneities. Realizations of a microstructure are randomly generated VEs containing randomly distributed heterogeneities with the same microstructural properties (i.e. volume fraction, aspect ratio, phase properties and volume size). Ensembles smaller than the RVE ensemble are characterized by n_R realizations and n_{VE} heterogeneities. The volume size of a VE is also defined by the number of its heterogeneities n_{VE}. Accurate effective properties, within a tolerance, are obtained by averaging apparent properties over all generated realizations. Kanit *et al.* (2003) observed a bias for results obtained with very small size volume elements. Therefore, quantitative RVE acceptation criteria are needed to determine the volume size and the number of realizations that define a RVE large enough to compute accurate estimations of the effective properties within a tolerance.

To determine the number of required realizations N_R, Kanit *et al.* (2003) proposed a criterion based on the confidence interval of the apparent properties as:

$$\text{Criterion for } N_R \text{ a): } \quad \frac{\epsilon_{\text{CI}}}{\tilde{Z}} \leq \delta_0, \tag{1.23}$$

where $\tilde{Z}$ refers to the ensemble average of the desired physical property Z over all realizations, ϵ_{CI} is the size of confidence interval of $\tilde{Z}$ and δ_0 is a given tolerance.

Several criteria have been proposed to estimate N_{RVE} based on the statistics of the apparent properties computed under different sets of BC (Gusev, 1997; Ostoja-Starzewski, 1999; Terada *et al.*, 2000; Kanit *et al.*, 2003; Ostoja-Starzewski, 2006; Stroeven *et al.*, 2004; Trias

et al., 2006; Ghossein and Lévesque, 2012; Moussaddy, 2013). One of the most commonly used criteria (Gusev, 1997; Kanit *et al.*, 2003; Ghossein and Lévesque, 2012) is *stability criterion*, which is based on the stability of the ensemble average of the desired property over increments of n_{VE} (Gusev, 1997):

$$\text{Criterion for } N_{RVE} \text{ a):} \quad \frac{|\tilde{Z}^{(i)} - \tilde{Z}^{(i-1)}|}{\tilde{Z}^{(i)}} \leq \delta_1, \tag{1.24}$$

where δ_1 is a given tolerance and superscripts (i) and $(i-1)$ refer to two successive ensembles with different n_{VE}. The suited BC set for the stability criteria is PBC. Figure 1.5 presents the convergence of the bulk modulus of random realizations of a voronoï mosaic microstructure under PBC, uniform displacement and traction BC (Kanit *et al.*, 2003). It is observed that the apparent properties have converged towards the effective properties for significantly smaller volumes under PBC than uniform BC.

Moussaddy (2013) propsed an *averaging variations criterion* in which the arithmetic and harmonic means of the stiffness tensor are used to set a criterion to determine N_{RVE}:

$$\overline{\mathbf{C}} = \frac{1}{r} \sum_{i=1}^{r} \mathbf{C}_i, \tag{1.25a}$$

$$\underline{\mathbf{C}} = \left(\frac{1}{r} \sum_{i=1}^{r} \mathbf{C}_i^{-1} \right)^{-1}, \tag{1.25b}$$

where $\mathbf{C}_i$ is the apparent elastic tensor of the ith realization. The focus of the study of Moussaddy (2013) was on isotropic composites so they dealt with bulk modulus as:

$$\bar{k} = \frac{\overline{\mathbf{C}}_{iijj}}{9}, \tag{1.26a}$$

$$\underline{\bar{k}} = \frac{\underline{\mathbf{C}}_{iijj}}{9}. \tag{1.26b}$$

It is worth mentioning that the result of Equation (1.26a) is equivalent to the arithmetic mean of $\tilde{k}$ evaluated by $\left[\frac{1}{r} \sum_{i=1}^{r} \tilde{k}^i \right]$. However, Equation (1.26b) is different than the harmonic mean of $\tilde{k}$ evaluated by $\left[\frac{r}{\sum_{i=1}^{r} \frac{1}{\tilde{k}^i}} \right]$. The average properties is then estimated by the average of both means:

$$\widehat{k}^r = \frac{\overline{k}^r + \underline{\overline{k}}^r}{2}, \tag{1.27}$$

and ,

$$\underline{\overline{k}}^r \leq \widehat{k}^r \leq \overline{k}^r. \tag{1.28}$$
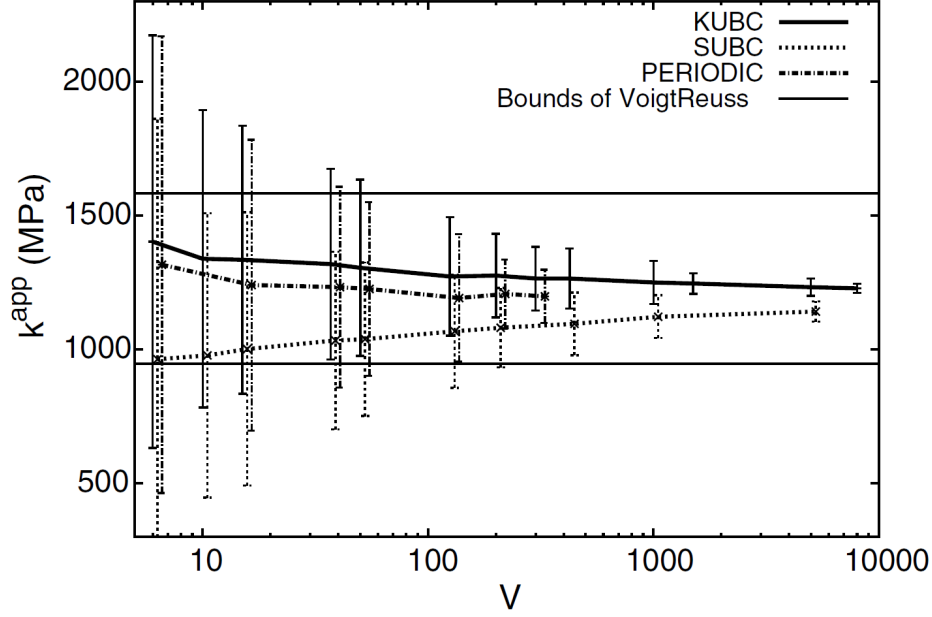
Figure 1.5 Mean bulk modulus of a voronoï mosaic composite as a function of volume size V (= the number of grains included). Three different types of boundary conditions were enforced: Kinematic Uniform Boundary Conditions (KUBC), Static Uniform Boundary Conditions (SUBC) and PERIODIC boundary conditions. For clarity, the errorbars were slightly shifted around each studied volume size V (Kanit *et al.*, 2003).

Equality in Equation (1.28) can only be obtained for ensemble of ideal RVEs. The difference between the ensemble average properties $\widehat{k}^r$ and any of $\overline{k}^r$ or $\overline{\overline{k}}^r$ was used to set a new criterion as:

$$\text{Criterion for } N_{RVE} \text{ b):} \quad \left(\frac{\widehat{k}^r - \overline{\overline{k}}^r}{\widehat{k}^r}\right) = \left(\frac{\widehat{k}^r - \overline{k}^r}{\widehat{k}^r}\right) \leq \delta_1. \tag{1.29}$$

1.3   Works on homogenization of PCN

1.3.1   Analytical works

In PCN, the well-defined concepts of matrix and reinforcement in conventional two-phase composites are no longer valid due to the multi-layered structure of the reinforcing particles and/or the presence of other phases such as interphase. This phenomenon makes the analytical studies to be generally categorized in one- and two- step models. In two-step methods,

two-phase conventional composite models are used after homogenizing the reinforcing particles through the *effective particle (EP)* concept (Sheng *et al.*, 2004; Luo and Daniel, 2003). The idea behind the effective particle concept is to have a single homogeneous phase as the reinforcement, the same as in conventional composites.

Sheng *et al.* (2004) used EP concept combined with micromechanical models (MT, Halpin-Tsai and FE) to predict the dependence of the PCN stiffness on the nanoclay and polymer properties. Molecular dynamics results obtained by Manevitch and Rutledge (2004) were used to find the nanoclay properties, i.e. thickness and modulus of nanoclay as a pair. The EPs were assumed to be all aligned and isotropic.

Figiel and Buckley (Figiel and Buckley, 2009) investigated the influence of employing isotropic EPs. They showed that the deviations obtained by the isotropic EPs are especially pronounced in the prediction of the transverse and shear moduli of PCN, even with fully aligned effective particles. They also extended the methodology proposed by Sheng *et al.* (2004) to misaligned cases by averaging the elasticity tensor over all possible orientations. Using the averaging method introduced by (Schjodt-Thomsen and Pyrz, 2001), their composite elasticity tensor calculated by the MT model was diagonally symmetric.

Mesbah *et al.* (2009) also used the EP concept for intercalated PCN. They used a simplified IDI model as the second homogenization step. The second step model had three phases: the EP, interphase surrounding the EP, and the polymer matrix. They found that analytical predictions considering aligned particles overestimate the experimental data and only the predictions with randomly oriented particles provide reasonable estimates (Figure 1.6).

Due to their generally multi-phase microstructures, one-step models for PCN refer to multi-phase models. These models have been mostly employed for exfoliated PCN in the presence of interphase (Mesbah *et al.*, 2009; Anoukou *et al.*, 2011). However, no one-step study has been performed so far for intercalated composites and, more importantly, no evaluation studies have been performed to assess the range of validity and time-efficiency of two- and one- step models.

1.3.2 Numerical works and validation of analytical models

Gusev (2001) simulated 3D periodic FE models consisting of different particles including nonoverlapping identical parallel discs. The models were generated by a Monte-Carlo method. He also performed convergence studies to determine the physical RVEs. A range of composite material properties including the dimensional stability of platelet-reinforced polymers were modeled. They found that the Halpin-Tsai (Halpin and Kardos, 1969, 1976) model considerably overestimated the dimensional stability.

VanEs (2001) validated the MT model with results of 3D periodic FE models generated by
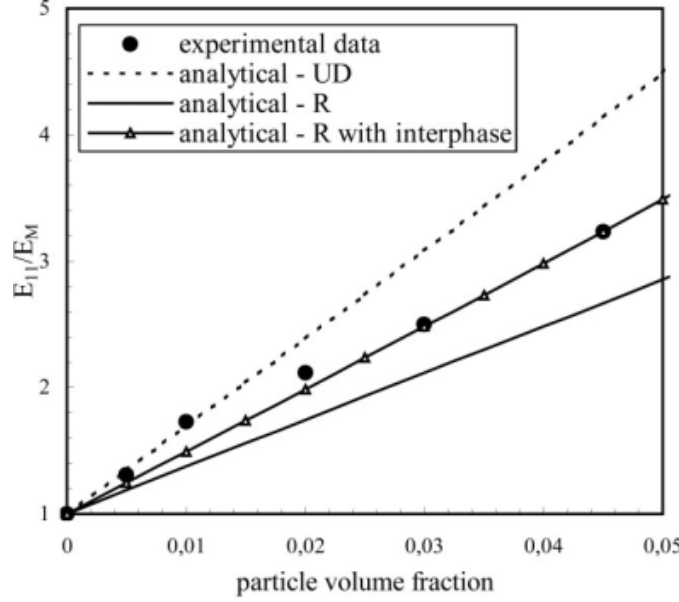
Figure 1.6 Comparison between analytical predictions and experimental data (Tyan *et al.*, 2000) for the effective Young's modulus of polyimide clay nanocomposite (Mesbah *et al.*, 2009).

a program called Palmyra for exfoliated Polypropylene talc composites. No study investigated the representativeness of the VEs. The aspect ratio of the particles was limited to 50 to reduce the computational time. An energy minimization approach was used to calculate physical properties like Young's modulus. They found that the MT model delivered reliable predictions for the stiffness of PCN.

Sheng *et al.* (2004) used also FE to predict the stiffness of PCN and also to validate their analytical model. A 2D plane strain model was developed for completely aligned effective particles. The structure of PCNs was assumed to be periodic in the direction of particle alignment. Three different models for the particles (Figure 1.7) in intercalated PCN were applied to the same VE and, despite the differences, the predicted effective stiffness E_{11}/E_m for these three cases were close.

Hbaieb *et al.* (2007) worked on both 2D and 3D FE models to account for random dispersion of aligned and randomly oriented nanoclay platelets. For the 3D modeling, they used symmetrical boundary conditions to avoid the difficulties of periodic boundary conditions. They found that the 2D FE results were consistently lower than those of 3D FE for both aligned and randomly oriented platelets. The MT model was found to deliver reasonably accurate predictions for the stiffness of PCN with aligned particles at volume fractions less than 5%, while underestimating at higher volume fractions. For randomly oriented particles, the MT model was found to overestimates the PCN stiffness at volume fractions higher than
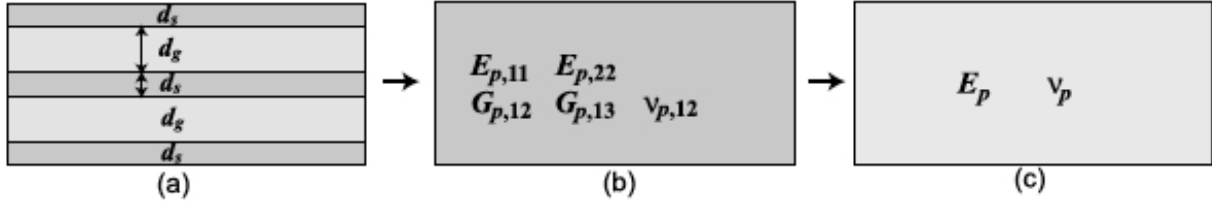
Figure 1.7 Structural models of the clay particle: (a) discrete stack; (b) anisotropic effective particle; (c) isotropic effective particle (Sheng *et al.*, 2004).

1%. For both 2D and 3D simulations, the results were insensitive to the VE size, provided that more than 30 particles were represented.

Figiel and Buckley (2009) also used a 2D plane strain FE model for intercalated PCN. They simulated both aligned and randomly oriented EPs in periodic models. Their models with aligned particles were the unit cells with columnar arrangement of particles. Only 6 platelets were included in each model. They found that the MT model slightly overestimates the FE results, where the difference were attributed to the differences in problem dimensionalities (2D in the FE versus 3D in the analytical model). They showed that, provided that the anisotropy of EPs was considered, close agreement could be found between results obtained by modeling the separate platelets and those calculated using the EP concept. As for the randomly oriented EPs, they used a Monte-Carlo methodology to generate the VEs. They found that MT overestimates the FE results for randomly oriented particles.

Cricri *et al.* (2011) employed a 3D periodic FE model to study hybrid PCN with a mixed intercalated-exfoliated nanostructure. An algorithm generated randomly positioned nanoclays, whereas their orientation was defined according to the distribution of the angles, experimentally evaluated, and reasonably approximated by a standard Gaussian distribution. The criterion to find the RVE size was an isotropy criterion. No convergence study was performed to determine the sufficient number of realizations to obtain statistically significant properties. For their randomly oriented hybrids, they found that MT model slightly overestimates FE results, in agreement with previous simulations reported in literature (Hbaieb *et al.*, 2007; Figiel and Buckley, 2009). They also found that the fraction of completely exfoliated clay particles is the most effective parameter in enhancing the stiffness of the hybrids.

The ranges of microstructural properties for composites studied in the above-mentioned works along with the RVE used to obtain their numerical results are listed in the Table 1.1.

Table 1.1 The ranges of microstructural properties for composites studied in different numerical works along with the RVE used to obtain their numerical results.

Cited work	Aspect ratio a_p	Volume fraction c_p	Rigidity contrast (E_p/E_m)	Realizations number	Volume size	Orientation of particles
Gusev (2001)	10-200	5-10%	NA	3	9	aligned
VanEs (2001)	50	5-15%	100	7	20	aligned
Sheng *et al.* (2004)	25-400	1-5%	0-600	10	50-100	aligned
Hbaieb *et al.* (2007)	50	1-10%	100	9-10	50-100	aligned/randomly
Figiel and Buckley (2009)	≈ 11	5%	≈ 35	5	30	random
Cricri *et al.* (2011)	≈ 55	3-6%	$\approx 90 - 135$	5	30	random

It is clear from analyzing the literature that most of numerical studies have been reported without a thorough determination of the appropriate RVE due its computational burden, which can raise questions about the accuracy of the reference data used for the comparisons. In addition, very few works have addressed the interphase effects, especially in 3D. As for the validation of analytical models against rigorous numerical results, no comprehensive evaluation study has been performed, yet, to examine and compare the validity range of different analytical models (one- and two- step models) for the microstructural features (i.e. modulus contrast, aspect ratio of the reinforcing phase and its volume fraction) associated to PCN.

1.4   PCN in experimental works

Numerous experimental works on PCN with different type of polymers and clays have been reported in the literature (Kojima *et al.*, 1993; Messersmith and Giannelis, 1994; Okada and Usuki, 1995; Giannelis, 1996; Fornes *et al.*, 2001; Sheng *et al.*, 2004). Fornes *et al.* (2001) worked on Nylon6-Montmorillonite PCN and produced well exfoliated structures (Figure 1.8). Sheng *et al.* (2004) produced intercalated MXD6 Nylon-clay nanocomposites (Figure 1.9). Figures 1.8 and 1.9 show the good degree of alignment found between the reinforcing stacks. The nanoclays, generally considered as straight platelets, are shown in the figures to exhibit wavy shapes. Moreover, they are not perfectly uniformly distributed.
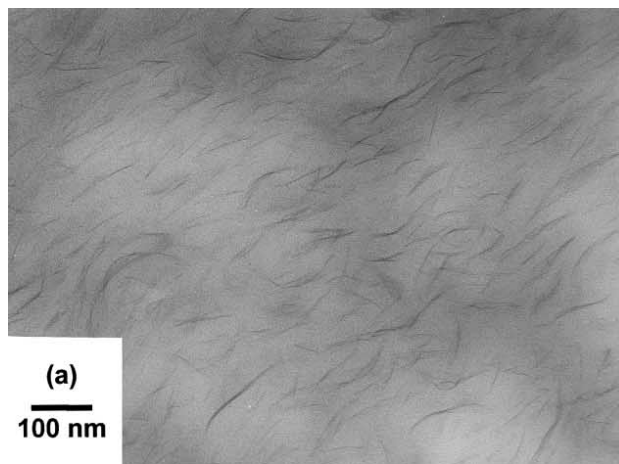
Figure 1.8 TEM image of PCN containing 3 wt% montmorillonite based on high molecular weight Nylon6 Fornes *et al.* (2001).
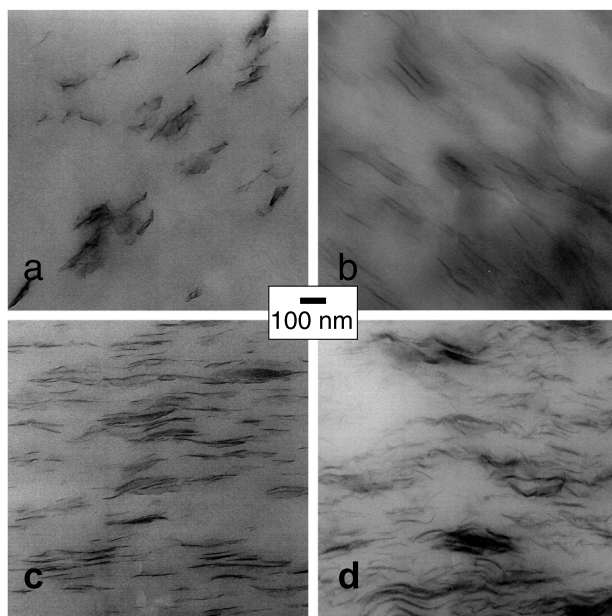
Figure 1.9 TEMs of MXD6 nylon/clay nanocomposite with various clay contents: a) 1.1 wt%, b) 3.67 wt%, c) 4.17 wt% and d) 5.27 wt% Sheng *et al.* (2004).

CHAPTER 2

OBJECTIVES AND SCIENTIFIC APPROACH

2.1   Rationale of the thesis

Based on the literature survey, the rationale of the project can be explained as follow:

1. Several analytical models exist for predicting the elastic properties of PCN, ranging from simplified two-step models to more complex one-step methods. However, no thorough study has yet evaluated the influence of simplifying assumptions such as use of EP concept, limitations on the aspect ratio and isotropic particles. In addition, the estimates of none of the models have been rigorously verified, especially for the range of microstructural properties typical of PCN. Thorough assessment of analytical models is required for quick and accurate predictions of PCN properties. Assessment of analytical models is usually performed by comparison with numerical homogenization of the RVE.

2. Very few one-step analytical models taking explicitly into account all the constituent phases encountered in PNC have been reported.

3. Numerical models are still far from modeling the real PCN microstructure reported in the literature. For example, most of the models have failed to model the detailed 3D microstructure considering the randomly positioned reinforcing particles, the nanoclays with large aspect ratios, the explicit incorporation of the constituent phases and applying appropriate boundary conditions. Moreover, the influence of the EP concept that has been used to perform FE modeling more efficiently has not been rigorously verified, yet.

4. Most of numerical studies have been reported without a thorough determination of the appropriate RVE due its computational burden, resulting in benchmark results of questionable exactitude.

5. No comparative study has been performed to assess the range of accuracy and time-efficiency of two- and one- step models.

2.2   Objectives

The general objective of this research was to model the elastic behavior, particularly the stiffness, of nanoclay nanocomposites using analytical and numerical tools. This work was

divided into two specific objectives:

1. **Assessment of analytical homogenization methods against a 3D FE model**

   The first specific objective of this thesis aimed at validating commonly used analytical micromechanical models for the prediction of PCN elastic properties with the help of 3D FE simulations based on the following sub-objectives:

   - To incorporate the interphase effect in a two-step homogenization procedure;

   - To validate different micromechanical models commonly used in two-step approaches against results of 3D FE simulations;

   - To determine the RVEs in numerical models.

2. **Assessment of two- and one- step homogenization methods, analytical as well numerical**

   The second objective of this thesis was to study the estimates of two- and one- step models based on the following sub-objectives:

   - To adopt and employ one-step analytical models for predicting the elastic properties of PCN, especially for intercalated morphologies with multi-layer microstructure;

   - To compare the predictions of one- and two- step analytical homogenization models to the results of 3D FE simulations of PCN layered microstructures;

   - To assess the influence of the EP concept on the accuracy of numerical homogenization models;

   - To determine the RVEs.

   In the all studied models, the polymer matrix and particles were assumed to be linearly elastic. Particles were assumed to have identical shapes, perfectly bonded to the matrix, aligned and randomly distributed.

2.3   Scientific approach

Two research papers were prepared in order to achieve the above-mentioned objectives. The following describes each article as well as its context with respect to the two specific objectives.

2.3.1   Article 1: Prediction of Elastic Properties in Polymer-Clay Nanocomposites: Analytical Homogenization Methods and 3D Finite Element Modeling

The first paper presents a rigorous evaluation of the performance of commonly used analytical models that predict stiffness of exfoliated PCN with aligned particles. The influence

of the interphase on the effective properties was taken into account by a two-step homogenization procedure relying on the EP concept. The validity of different analytical micromechanical models, used as the second step of homogenization, was studied with the help of 3D FE simulations. An elaborate series of FE simulations was performed to determine the RVE. A simplified procedure to guide the determination of the RVE based on statistical and material symmetry criteria on the desired property was developed. Numerical results were also compared to the experimental data extracted from the literature. This study covered rigidity contrasts of 10 to 64 between the Young' modulus of polymer and that of reinforcing particles. The volume fraction of effective particles varied in the range of 1-44%.

The main findings of this paper are:

1. It was found that the MT model was the most reliable method to be used for the possible ranges of modulus contrasts, aspect ratios and volume fractions typical of exfoliated PCN. Lielens's model may improve on the MT model at high volume fractions when the rigidity contrast between reinforcing particle and polymer is also high. The SC scheme overstimates the axial Young's modulus for all studied cases of PCN.

2. The properties and the thickness of the interphase were estimated from comparison between the numerical parametric study and experimental results.

3. The importance of incorporating the interphase was highlighted, which can lead to 13% of increase in axial Young's modulus.

The manuscript of this article was accepted in "Computational Materials Science" on June 10th, 2013. This journal publishes original contributions on the computational modelling of materials properties. This article was written almost entirely by the author of this thesis.

2.3.2 Article 2: Numerical and Analytical Modeling of the Stiffness of Polymer-Caly Nanocomposites: One- and Two-Step Methods

This paper extends the evaluation study to a wider class of homogenization methods. In particular, it examines the influence of the EP concept on numerical as well as analytical modeling and seeks other modeling alternatives. Analytical one-step models have been adopted and employed for intercalated composites as well as exfoliated morphologies in the presence of interphase. The predictions of analytical and simplified numerical homogenization models were compared against detailed 3D FE simulations where the PCN layered microstructure was explicitly simulated. The theoretical predictions were also compared to experimental data extracted from the literature. By comparison to existing works, the originality of this work lies in the fact that the RVE was established following the methodology presented in Article 1. Both analytical and numerical models did not rely on simplifying assumptions like

the EP concept or isotropic particle.

The main findings of this paper are:

1. Although both numerical and analytical two-step methods can deliver accurate predictions in some cases, they can significantly diverge from FE results of layered-microstructure models taking into account the details of the morphology.

2. Analytical multi-coated inclusions model require more efforts for its numerical implementation, but once implemented, can be run in a negligible time and deliver more reliable resutls than two-step methods.

3. The more the EP is different from the nanoclay, in terms of rigidity and aspect ratio, or the higher the volume fraction is, the more the accuracy of two-step numerical models is deteriorated.

4. Despite their higher computational costs, one-step FE models are necessary, depending on the PCN microstructure and desired accuracy.

5. Employing the transversely isotropic EP delivers more precise numerical results than the isotropic EP.

This article was submitted to "Computational Materials Science" on June 26$^{\text{th}}$, 2013. This article was written entirely by the author of this thesis.

CHAPTER 3

ARTICLE 1: Prediction of Elastic Properties in Polymer-Clay Nanocomposites: Analytical Homogenization Methods and 3D Finite Element Modeling

M. Pahlavan Pour, H. Moussaddy, E. Ghossein, P. Hubert, M. Lévesque (2013). Accepted in: "*Computational Materials Science*".

3.1   Abstract

Accurate predictive models can support the exploitation of Polymer-Clay Nanocomposites (PCN) in their evergrowing applications. The purpose of this paper is to validate commonly used analytical micromechanical models for the prediction of PCN elastic properties with the help of 3D periodic Finite Element (FE) simulations of the same microstructures, considered as reference data. The effect of the interphase was taken into account in a two-step homogenization procedure that exploits the effective particle concept. The predictions of a range of procedures relying on the different micromechanical models (i.e. Mori-Tanaka, self-consistent and Lielens's) were tested. Elaborate series of FE simulations were performed to determine Representative Volume Elements (RVEs). In addition, a simplified procedure to guide the definition of the RVE based on statistical and transverse isotropy symmetry criteria was developed. The predicted elastic properties of PCN were studied as a function of the thickness and the elastic properties of the formed interphase around the nanoclay platelets. It was found that the Mori-Tanaka model was the most reliable method for the simulated cases. Furthermore, numerical model predictions were compared with experimental results extracted from the literature for aligned exfoliated Nylon-6 Montmorillonite nanocomposites. Finally, a comparison between the parametric study results and the experimental data was used to estimate the properties and the thickness of the interphase.

3.2   Introduction

Polymer-Clay Nanocomposites (PCN) offer interesting opportunities to important industrial sectors (e.g. transportation, construction, packaging), even with modest amount of clay (Chen *et al.*, 2008). Establishing accurate predictive models for the physical properties of PCN is of considerable interest since such models can guide the elaboration of future materials and estimate the potential gains in terms of performance.

Clay minerals have a layered structure constituted of silicate platelets of nano thickness, referred herein as nanoclays. Three types of morphologies exist for polymer-clay systems: exfoliated, intercalated, and agglomerated (non-intercalated), depending on the degree of separation and polymer penetration between silicate layers. Exfoliated morphology occurs when separated single nanolayers of silicate are dispersed in a polymer matrix. The intercalated morphology is resulted from the penetration of polymer chains between the silicate nanolayers that remain in parallel stacks. Interactions at the interface between the nanoclay and polymer matrix result in the formation of a modified polymer, called interphase hereinafter, that has a thickness of a few nm.

Finite Element (FE) methods have been used by several researchers (Hbaieb *et al.*, 2007; Sheng *et al.*, 2004; Figiel and Buckley, 2009; Mesbah *et al.*, 2009; Cricri *et al.*, 2011) to predict the elastic properties of PCN. Hbaieb *et al.* (2007) worked on both two-dimensional (2D) and three-dimensional (3D) FE models to account for random dispersion of aligned and randomly oriented clay platelets. One of their findings is that 2D models cannot predict accurately the effective properties of such materials. Cricri *et al.* (2011) used a 3D periodic FE model to study the elastic properties of PCN. Mesbah *et al.* (2009) considered the interphase effect but in a 2D plane strain simulation. Although studies have shown the existence and importance of interphase effect (Chen *et al.*, 2008; Kojima *et al.*, 1993; Shelley *et al.*, 2001; Xu *et al.*, 2012), none of the mentioned works took into account the interphase effect in 3D. Moreover, none of the previous FE studies on PCN calculated the overall properties from rigorously determined Representative Volume Elements (RVEs), resulting in benchmark results of questionable exactitude.

A number of research works have also been devoted to the analytical modeling of PCN. Models like the rule of mixtures (Kojima *et al.*, 1993), Mori-Tanaka (Luo and Daniel, 2003; Sheng *et al.*, 2004; Wang and Pyrz, 2004) and the self-consistent schemes (Mesbah *et al.*, 2009; Anoukou *et al.*, 2011) have been used. A comparative study on the performance and validity ranges of these analytical models may avoid their inappropriate use. For example, Tucker and Liang (1999) conducted a validation study for short-fiber composite micromechanical models. In their work, they assessed analytical models by comparing their results to 3D FE calculations of periodic arrays of fibers and also to the Ingber and Papathanasiou's boundary element results for randomly positioned aligned fibers (Ingber and Papathanasiou, 1997). However, the validations were mostly performed against results of models with regularly arranged fibers. Furthermore, their conclusions are valid for a limited range of aspect ratios ($lenght/diameter \approx 1 - 50$) and fiber/matrix rigidity contrasts (≈ 30). Thus, their findings cannot be extended to PCN where the reinforcements have typically very high aspect ratios ($diameter/length \approx 100$), as well as high rigidity contrasts (Young's modulus of nanoclay

/ Young's modulus of matrix $\approx 50 - 90$ for typical PCN). Ghossein and Lévesque (2012) performed a thorough validation of analytical homogenization models for composites with spherical particles, for a broad range of phases mechanical properties contrasts and volume fractions. However, no comprehensive evaluations have been performed, yet, to examine and compare the validity range of analytical models for the microstructural features associated to PCN (i.e. modulus contrast, aspect ratio of the reinforcing phase and its volume fraction).

The principal objective of this work was to evaluate the performance of commonly used analytical models that predict the elastic properties of exfoliated PCN with aligned particles. The influence of the interphase on the effective properties was taken into account by a two-step homogenization procedure relying on the effective particle concept. The validity of different analytical micromechanical models, to be used as the second step of homogenization, was studied with the help of 3D FE simulations of detailed microstructures. An elaborate series of FE simulations was performed to determine the RVE based on statistical and transverse isotropy symmetry criteria. A parametric study was performed on the influence of the thickness and the elastic properties of the interphase on the PCN effective properties. Comparisons between the numerical results and experimental data extracted from the literature for Nylon-6 Montmorillonite nanocomposite was used to estimate the elastic property and thickness of interphase, as well as validating the overall numerical modeling method.

3.3   Background

3.3.1   PCN: Properties and Challenges

Nanoclay platelets have a thickness of about 1 nm and their lateral dimensions may vary from 30 nm to several microns (Ray and Okamoto, 2003). In exfoliated morphology, an interphase region forms around each nanoclay platelet (Figure 3.1). When compared to intercalated PCN, the volume of the interphase is larger in exfoliated PCN since each layer of nanoclay has two layers of interphase. Thus, the exfoliated morphology may show more pronounced dependence on interphase property and structure. In addition, for the same clay loading, an exfoliated PCN is usually preferred since it exhibits a higher tensile strength and elastic modulus (Chen *et al.*, 2008; Pinnavaia and Beall, 2000).

The interphase has the same length-scale as that of the nanoclay and its properties were reported to be different (mostly higher) from those of the bulk polymer matrix (Chen *et al.*, 2008; Shelley *et al.*, 2001; Sheng *et al.*, 2004; Xu *et al.*, 2012; Kojima *et al.*, 1993; Sikdar *et al.*, 2008). The increase in stiffness was found to be due to changes in the mobility of polymer chains adjacent to nanoclays, and also to changes in crystallinity in semicrystalline polymers like Nylon-6 (Chen *et al.*, 2008). A variety of methods has been used to measure
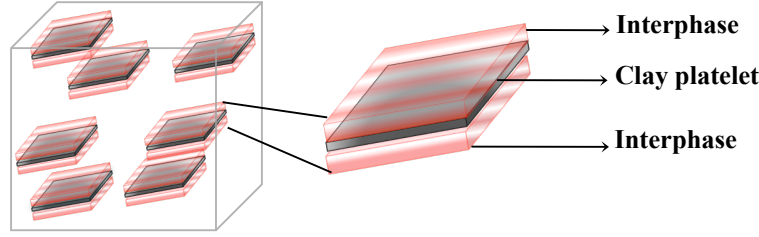
Figure 3.1 Three-layer reinforcing stacks in exfoliated composites.

the interphase properties for Nylon-6/Montmorillonite (MMT) PCN. The results of some of these studies are summarized in Table 3.1.

3.3.2 Modeling of PCN

Luo and Daniel (2003) considered intercalated composites as two-phase composites by replacing the intercalated stacks of nanoclays by an equivalent homogenized particle. Equivalent homogenized particles were also used by Sheng *et al.* (2004) and were named "effective particles". This concept was then used by other researchers for intercalated nanocomposites (Mesbah *et al.*, 2009; Figiel and Buckley, 2009) where the homogenized anisotropic properties of the layered particles were computed from the rule of mixtures. Both analytical and numerical micromechanical models were subsequently used to calculate the mechanical properties of the nanocomposite (Sheng *et al.*, 2004; Mesbah *et al.*, 2009; Figiel and Buckley, 2009; Luo and Daniel, 2003).

Analytical homogenization models, like Mori-Tanaka (MT) model (Mori and Tanaka, 1973; Benveniste, 1987), the Self-Consistent (SC) scheme (Hill, 1965; Budiansky, 1965) and Lielens's model (Lielens, 1999) have been used for predicting the response of short fiber composites. Tucker and Liang (1999) reported that SC model overestimates the axial modulus at high volume fractions but the MT model delivers the best results for large aspect ratio fillers for short-fiber composites. These two modes were also used widely for PCN. Lielens's model may improve on the MT model for higher fiber volume fractions or rigidity contrasts (Tucker and Liang, 1999).

3.3.3 Numerical micromechanical models

Homogenization problems can also be addressed by numerical methods such as FE (Gusev, 1997; Segurado and LLorca, 2002; Barello and Lévesque, 2008). Let's define a Volume Element (VE) as a volume containing a certain number of heterogeneities (reinforcements,

Table 3.1 Summary of previous works on the interphase properties and thickness for Nylon-6/ MMT PCN. E, ν, d and f denote Young's modulus, Poisson's ratio, thickness and volume fraction, respectively. Subscripts I, m and p refer to interphase, matrix/bulk polymer and effective particle, respectively.

Cited work	Young's modulus Method	Interphase thickness Method
Shelley *et al.* (2001)	$E_I = 10\,E_m$ Power law mixing rule, fitting experimental data	$d_I \approx 8.5$ nm, equivalent to the reported $f_I = 30\%$ Loss and storage moduli data
Sikdar *et al.* (2008)	$E_I = (4 \sim 5)\,E_m$ Nano-indentation tests	$d_I = 2.5$ nm Atomic force microscopy
Xu *et al.* (2012)	$E_p = 36.8$ GPa Molecular Dynamics	$d_I = 3$ nm Molecular Dynamics
Mesbah *et al.* (2009)	$E_m < E_I < 5\,E_m$ Fitting experimental data to analytical model results	$d_I = 2 \sim 3$ nm Dynamic mechanical analyses, differential scanning calorimetry
Tzika *et al.* (2000) * & Sheng *et al.* (2004)	$E_I = 1.25\,E_m$, $\nu_I = 0.53$ Orthotropic single crystal	NA

* The interphase in that study was transversely isotropic.

grains, etc.). One of the key issues in numerical homogenization problems is to find a Representative Volume Element (RVE) among a number of VEs. The size of a VE is typically characterized by the number of represented heterogeneities. The RVE is typically defined as a VE for which increasing the number of represented heterogeneities does not alter the computed effective properties. Moreover, the smallest RVE is usually sought in order to limit the computational costs of numerical simulations. Numerical homogenization therefore requires a procedure for establishing the RVE, means to generate VEs and methods for computing the overall properties.

Generation of Volume Elements

Molecular Dynamics (MD) approaches (Lubachevsky *et al.*, 1991; Ghossein and Lévesque, 2012) can deliver high volume fractions, for a large number of represented heterogeneities in a very short computational time. In MD simulations, the reinforcements are all created at once in the VE, but with a null volume. They are then put in motion and the volume of each reinforcement progressively increases. Collision detection and post-collision algorithms must

be developed and the computations end when the target volume fraction is reached.

Determination of the RVE

One approach to identify the size of RVE is the concept of "physical RVE" (Böhm, 2008) where the statistical variability of a physical property is used as criterion. For example, Kanit *et al.* (2003) used the statistical dispersion of the predicted overall modulus to define their RVEs for two-phase 3D Voronoï mosaics. Their approach consisted in generating a family of different realizations of VE, called ensemble of VEs herein. Realizations in the ensemble consisted of randomly distributed constituents with the same microstructural properties (i.e. volume fraction, aspect ratio, phase properties and VE size). The number of realizations in an ensemble was increased so that the desired confidence interval width was achieved on the ensemble average for the desired property. They observed a bias for very small size VEs and they assumed that all VEs larger size than the smallest size VE for which the bias could be neglected was a RVE, provided that sufficient number of realizations were simulated to reach the desired accuracy on the average of the ensemble (Kanit *et al.*, 2003).

Boundary conditions on Volume Elements

Different types of boundary conditions (uniform displacements, uniform tractions, etc.) lead to different effective properties for the same VE (Kanit *et al.*, 2003). Moreover, it has been exemplified by Kanit *et al.* (2003) that uniform boundary conditions tend to converge much slower to the RVE than Periodic Boundary Conditions (PBC). PBC can be enforced following the method explained by Barello and Lévesque (2008). If FE is used to compute the local fields, the nodal positions also should be periodic, i.e. exactly homologous nodes should be located at each two opposite faces. This requirement makes the FE meshing procedure difficult and requires the VE to also be periodic.

3.4 The proposed multiscale modeling strategy

The multiscale modeling strategy used herein consisted of a two-step homogenization (Figure 3.2). Step I aimed at computing the effective properties of the stack of nanoclay platelet surrounded by its interface. This allowed computing the effective particle properties. The effective particles were then considered as inclusions in Step II where different analytical and numerical homogenization models were used to obtain the overall properties.
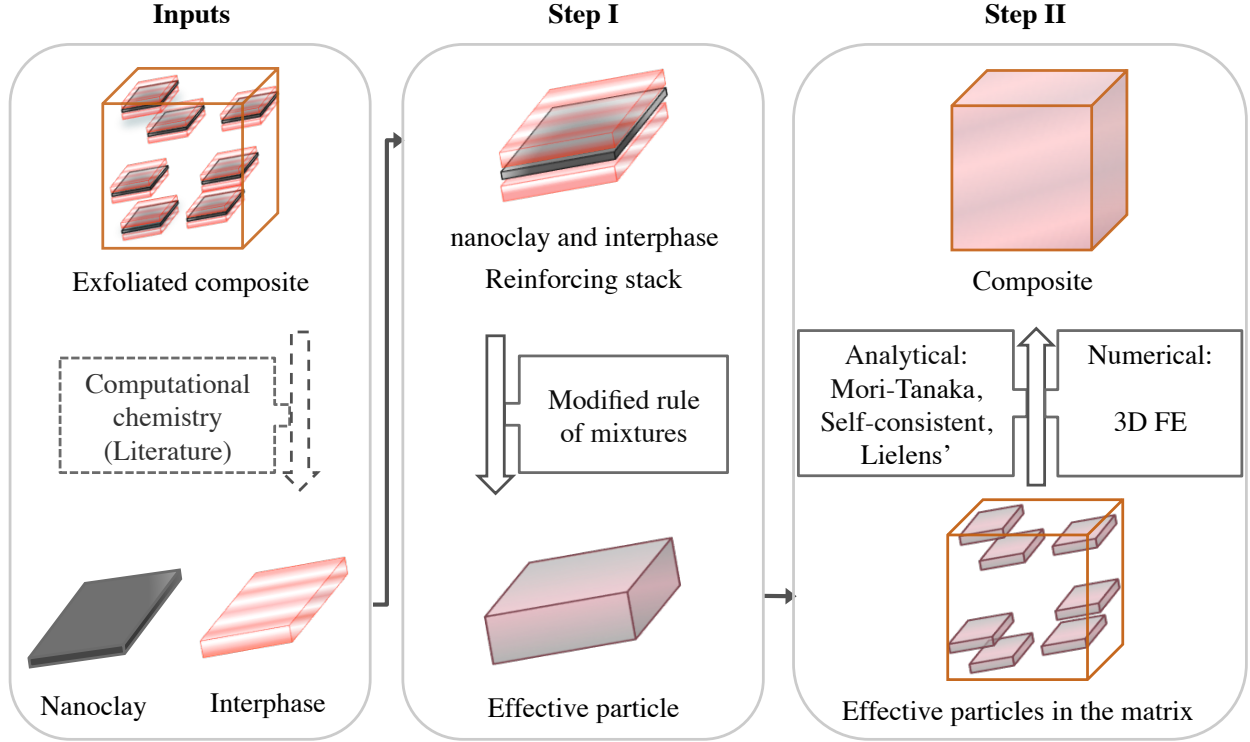
Figure 3.2 Two-step modeling strategy. Modeling inputs were obtained from the literature. In the first step, the properties of effective particles were calculated from a modified rule of mixtures. In the second homogenization step, the overall properties for the PCN were calculated using both numerical and analytical models.

3.4.1 Step I : Effective particle for exfoliated PCN

As a first approximation, the reinforcing particle in an exfoliated PCN was considered as a stack containing a nanoclay platelet surrounded by two layers of interphase (Figure 3.1). Since the thickness of each platelet is small, it was assumed that the interphase lied only on the nanoclay platelet top and bottom surfaces. Therefore, the thickness of the effective particle was obtained from:

$$d_\mathrm{p} = d_\mathrm{s} + 2d_\mathrm{I}, \tag{3.1}$$

where d refers to the thickness and subscripts s, p and I refer to the silicate layer, the effective particle and the interphase, respectively. The elastic properties of the effective particle (Young's modulus (E), Poisson's ratio (ν) and shear modulus (G)) were computed

as per the modified rule of mixtures by Tsai and Hahn (1980) as:

$$E_{p,11} = E_{p,33} = \chi E_s + (1 - \chi)E_I, \tag{3.2}$$

$$\nu_{p,12} = \nu_{p,32} = \chi \nu_I + (1 - \chi)\nu_s, \tag{3.3}$$

$$E_{p,22} = \frac{E_s E_I}{\chi E_I + (1 - \chi)E_s - \chi(1 - \chi)\beta E_I E_s}, \tag{3.4}$$

$$\nu_{p,13} = \frac{\chi \nu_s E_s(1 - \nu_I^2) + (1 - \chi)\nu_I E_I(1 - \nu_s^2)}{\chi E_s(1 - \nu_I^2) + (1 - \chi)\nu_I E_I(1 - \nu_s^2)}, \tag{3.5}$$

$$G_{p,12} = G_{p,32} = \frac{G_s G_I}{\chi G_I + (1 - \chi)G_s - \chi(1 - \chi)\eta G_I G_s}, \tag{3.6}$$

$$G_{p,13} = \frac{E_{p,11}}{2(1 + \nu_{p,13})}, \tag{3.7}$$

where subscripts 1, 2 and 3 correspond to the principal axes shown in Figure 3.3. χ is the silicate volume fraction in the effective particle, defined as:

$$\chi = \frac{V_s}{V_p} = \frac{d_s}{d_p}, \tag{3.8}$$

in which V_s is the volume of the silicate in the effective particle and V_p is the volume of the effective particle. β and η are defined as:

$$\beta = \frac{\nu_s^2 E_I/E_s + \nu_I^2 E_s/E_I - 2\nu_s \nu_I}{\chi E_s + (1 - \chi)E_I},$$

$$\eta = \frac{\nu_s^2 G_I/G_s + \nu_I^2 G_s/G_I - 2\nu_s \nu_I}{\chi G_s + (1 - \chi)G_I}. \tag{3.9}$$

For an exfoliated PCN the relationship between the total volume of interphase, $V_{I(tot)}$, and total volume of the silicate in the whole composite, $V_{s(tot)}$, is:

$$\frac{V_{I(tot)}}{V_{s(tot)}} = \frac{2d_I}{d_s}. \tag{3.10}$$

The volume fraction of the silicate phase in the composite, f_s, is then expressed as:

$$f_s = \frac{V_{s(tot)}}{V_c}, \tag{3.11}$$

where V_c is the whole volume of the composite. Therefore, the volume fraction of the effective particle, f_p, is given by:

$$f_p = f_s \left(1 + \frac{2d_I}{d_s} \right). \tag{3.12}$$

In this study, the particles were assumed to be aligned and had their thickness axis parallel to axis 2, as shown in Figure 3.3. The focus of the present work is on loadings along direction 1. Consequently, the effect of particle anisotropy was neglected (Sheng et $al.$, 2004). However, one should expect a slightly stiffer response when compared to the case where the particle anisotropy is considered (Figiel and Buckley, 2009). The two required independent constants, E_p and ν_p, were approximated by $E_{p,11}$ and $\nu_{p,12}$ (Equations (3.2) and (3.3), respectively).

3.4.2 Step II: Micro-scale models

In the second homogenization step, the effective particle properties, as well as those of the polymer matrix, were used as input parameters in three analytical homogenization models: the MT model, the SC scheme and that of Lielens. The effective particle properties were also used for the reinforcements of the numerical models.

The assumption in both numerical and analytical models is that the distributed effective particles and the matrix are isotropic, linearly elastic and perfectly bonded at their interface. Although this assumption is not fully realistic, it shall not affect the validity of the results since the main objective of the present work was to assess the validity of analytical models against numerical simulations based on the same assumptions.
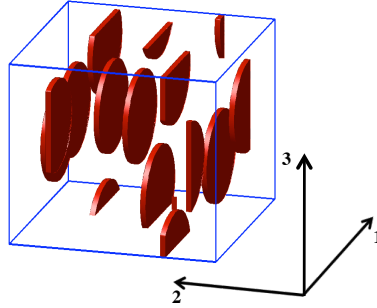
Figure 3.3 Periodic volume element with disc-shaped particles aligned perpendicular to the axis 2.

3.5   Numerical model

3.5.1   Generation of volume elements and retrieving desired properties

Randomly distributed aligned disc-shaped effective particles were generated in periodic VEs, Figure 3.3, with an algorithm implemented in MATLAB software. The algorithm is based on MD simulations and is elaborated in (Ghossein and Lévesque, 2012) for the case of microstructures with spherical particles. The algorithm was adapted to disc shaped particles and the modifications to the original algorithm are listed in Appendix A (Section 3.10). In order to avoid meshing problems, criteria were defined to accept or reject a generated VE based on the minimum distance between particles, as well as the minimum size of divided particles at the periodic boundaries.

The geometries were then exactly replicated in ANSYS FE package. Particular attention was paid to the generation of identical geometries at opposite faces, especially, where particles intersected with the cube faces. In this regard, only one of the particles in each pair was transfered in ANSYS and was then copied to its analogous position on the opposite cube face to generate its twin. Copying periodic particles and applying the divide command in ANSYS solved the problem of having identical surfaces on opposite faces. Moreover, identical meshes on opposite faces were obtained with the MSHCOPY command and MESH200 elements on the opposite faces of the cubic volume. MESH200 is a "mesh-only" element and does not contribute to the solution. Element SOLID92 was chosen for meshing of the cubic volume and particles. Meshing was completely performed in ANSYS package.

PBC were applied. Six sets of displacement boundary conditions were applied separately on a single volume, leading to six different analyses. Specifically, three uniaxial tensile displacements in the direction of the normal axes, 1, 2 and 3, and three shear displacements in the three orthogonal planes, 23, 13 and 12, were applied to obtain columns 1- 6 of the stiffness tensor $\mathbf{C}$, respectively. Components of $\mathbf{C}$, for each realization, were calculated from the following relation:

$$C_{ijkl} = \frac{<\sigma_{ij}>}{<\varepsilon_{kl}>} = \frac{<\sigma_{ij}>}{e_{kl}}, \qquad (3.13)$$

where σ and ε are the stress and strain tensors, respectively, and $<\,.\,>$ denotes volume averaging over all elements within the volume. Calculations on 4th order tensors were performed according to the modified Voigt notation. Young's modulus, E_{11}, was calculated from the compliance tensor, $\mathbf{S}$, as:

$$E_{11} = \frac{1}{S_{11}}. \qquad (3.14)$$

3.5.2 Procedure for determining the ensemble of RVEs

For given constituent properties and volume fraction, an ensemble of VEs is characterized by two quantities: the VE size, n_{VE}, and the number of realizations per ensemble, n_{R}, referred to as the ensemble size. A first study was performed to study the convergence of the desired property as a function of n_{R} (Figure 3.4). This convergence study was based on the statistical methodology of Kanit *et al.* (2003). Furthermore, an a priori formula was proposed to estimate the converged N_{R}, hence reducing the number of numerical evaluations in the overall process. Another convergence study was also performed with respect to n_{VE} (Figure 3.4). The RVE was reached when the effective properties converged with respect to both n_{VE} and n_{R}.
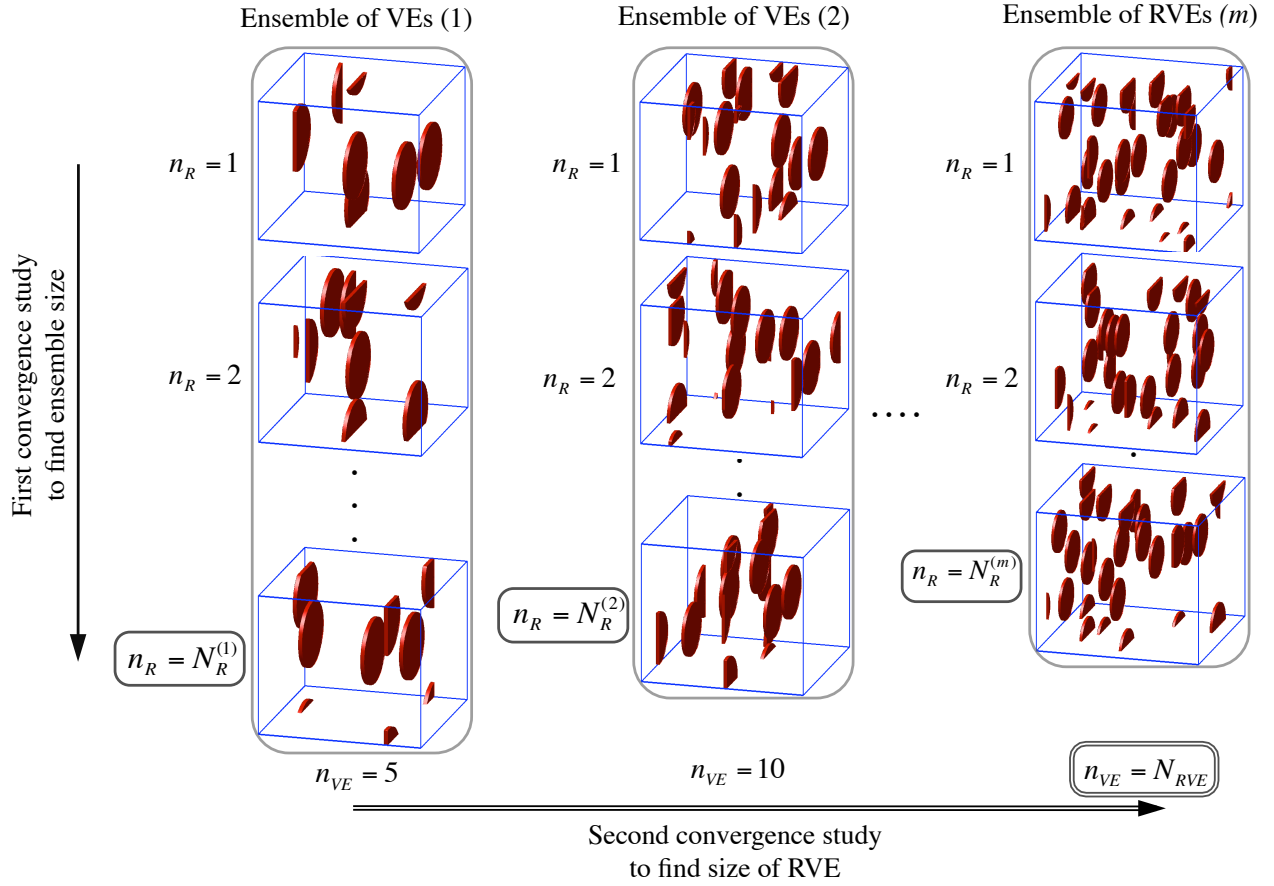
Figure 3.4 Illustration of two-fold convergence study to characterize the ensemble of RVEs in numerical simulations.

Convergence study on n_R

Let Z be the effective property of a given realization and $\tilde{Z}$ the average of that property over all the VEs of the ensemble. For each ensemble, the converged size N_R was found so that the normalized width of the confidence interval on $\tilde{Z}$, for a confidence level of 95%, was smaller than a given threshold δ_0, such that:

$$\text{CR. I:} \quad \epsilon_{rel} = \frac{\epsilon_\text{CI}}{\tilde{Z}} \leq \delta_0, \tag{3.15}$$

where

$$\epsilon_\text{CI} = \frac{P_{n_\text{R}} s}{\sqrt{n_\text{R}}}, \tag{3.16}$$

is the size of the confidence interval, s is the standard deviation of the n_R desired moduli and P_{n_R} denotes the 97.5$^\text{th}$ percentile of Z probability distribution. Z was assumed to have the student's t-distribution. In this study, E_{11} was the sought property.

The simulated microstructures herein contained parallel reinforcing platelets and the stiffness tensor was expected to be transversely isotropic. After a sufficient number of realizations, one should have:

$$\tilde{E}_{11} \approx \tilde{E}_{33}, \tag{3.17}$$

(see Figure 3.3). Although the effective moduli $\tilde{E}_{11}$ and $\tilde{E}_{33}$ were calculated from the same ensemble, they can be seen as two evaluations of $\tilde{E}_{11}$ from two different ensembles. Therefore, it follows from Equations (3.15) and (3.17) that:

$$\text{CR. II:} \quad \frac{|\tilde{E}_{33} - \tilde{E}_{11}|}{\tilde{E}_{11}} \leq \delta_0. \tag{3.18}$$

The value $\delta_0 = 0.01$ was used in this study.

An initial estimate of ensemble size could largely accelerate the convergence analysis. Consider two ensembles of VEs with the same volume fraction and constituent properties, but with different VE sizes. Let ensemble 1 be the ensemble with smaller VE size, i.e. $n_\text{VE}^{(2)} > n_\text{VE}^{(1)}$. If the same confidence interval width is sought, then

$$\epsilon_\text{CI}^{(1)} = \epsilon_\text{CI}^{(2)}, \tag{3.19}$$

which is expanded to the following relation using Equation (3.16) and supposing there is no

bias for neither of the ensembles, i.e. $\tilde{Z}^{(1)} \approx \tilde{Z}^{(2)}$:

$$\frac{p_{N_R}^{(1)} s^{(1)}}{\sqrt{N_R^{(1)}}} = \frac{p_{N_R}^{(2)} s^{(2)}}{\sqrt{N_R^{(2)}}}, \tag{3.20}$$

in which the superscript parentheses (1) and (2) refer to ensemble labels.

Using the power law proposed by Kanit *et al.* (2003) and Cailletaud *et al.* (1994), for a given volume fraction and constituent properties, the standard deviation could be related to the VE size by the following relation:

$$s^2 = B \left(\frac{1}{n_{VE}} \right)^{\alpha}, \tag{3.21}$$

where α is an empirical parameter that depends only on the geometry of the reinforcements. B is a constant for a fixed volume fraction and constituent properties. Thus, Equation (3.20) can be recast as:

$$\frac{p_{N_R}^{(1)})(n_{VE}^{(2)})^{\alpha/2}}{\sqrt{N_R^{(1)}}} = \frac{p_{N_R}^{(2)})(n_{VE}^{(1)})^{\alpha/2}}{\sqrt{N_R^{(2)}}}, \tag{3.22}$$

from which the initial estimate of the required size of ensemble (2) can be obtained as:

$$N_R^{(2)} = N_R^{(1)} \left(\frac{p_{N_R}^{(2)}}{p_{N_R}^{(1)}} \right)^2 \left(\frac{n_{VE}^{(1)}}{n_{VE}^{(2)}} \right)^{\alpha}. \tag{3.23}$$

In this paper, the value of $\alpha = 1$ was used (see also Section 3.7).

Convergence study on n_{VE}

The averaged property $\tilde{E}_{11}$ for each ensemble of VEs varies with n_{VE} and converges to an asymptote for fixed volume fraction and aspect ratio. The value of n_{VE} at which the asymptote is approximately reached is called the RVE size and is denoted by N_{RVE}.

The criterion to determine the RVE size was defined as:

$$\text{CR. III:} \quad \epsilon_{REL} = \frac{|\tilde{E}_{11}^{(i)} - \tilde{E}_{11}^{(i-1)}|}{\tilde{E}_{11}^{(i)}} \leq \delta_1, \tag{3.24}$$

where superscripts (i) and $(i-1)$ refer to two successive ensembles with different n_{VE}. CR. III imposes the stability of $\tilde{E}_{11}$ over the increase of n_{VE}. The value $\delta_1 = 0.01$ was used in this work. It can be seen in the literature that higher contrast of properties or increase in volume fraction leads to both higher N_R and N_{RVE} (Kanit *et al.*, 2003, 2006). It was therefore

assumed that, if the RVE is already reached for a higher volume fraction of effective particles (a denser PCN), it can also be used for PCN with lower volume fractions, provided that all other parameters remained constant. Similarly, if the RVE is reached for a PCN with higher contrast of rigidity between its phases, it can also be used as representative ensemble for composites containing phases with lower rigidity contrast and where all other parameters are kept constant. Both of these two conditions are combined as:

$$
\begin{cases}
(N_{\mathrm{R}},\ N_{\mathrm{RVE}}) \leftarrow (N_{\mathrm{R}},\ N_{\mathrm{RVE}})^{denser} \\
or \\
(N_{\mathrm{R}},\ N_{\mathrm{RVE}}) \leftarrow (N_{\mathrm{R}},\ N_{\mathrm{RVE}})^{higher\,contrast}
\end{cases}
\tag{3.25}
$$

Finally, the whole process of characterizing the ensemble of RVEs was implemented according to Algorithm 1 in Appendix B (Section 3.11).

3.6   Methodology for quantitative analyses and experimental validation

Properties from the literature (Xu *et al.*, 2012; Shelley *et al.*, 2001; Sheng *et al.*, 2004; Tzika *et al.*, 2000; Mesbah *et al.*, 2009; Kojima *et al.*, 1993; Sikdar *et al.*, 2008; Ji *et al.*, 2002; Chen *et al.*, 2008) were assigned to the studied PCN constituting phases. Three different thicknesses, namely 0, 3 (Xu *et al.*, 2012; Mesbah *et al.*, 2009; Sikdar *et al.*, 2008) and 5 nm were assigned to the interphase (Case I). Since the morphology was exfoliated, the distance between separated platelets was assumed to be 10 nm. It was also assumed that all the interlayer space between these separated platelets was filled with interphase. Hence, a maximum interphase thickness of 5 nm was considered for each platelet. For Case II, three different rough elastic moduli, $0.5\,E_{\mathrm{m}}$, E_{m}, $5\,E_{\mathrm{m}}$ (Kojima *et al.*, 1993; Sikdar *et al.*, 2008; Mesbah *et al.*, 2009) were assigned for the interphase (Table 3.2). The thickness of interphase was considered to be 3 nm in this case. Case III (a) was inspired by work of Tzika *et al.* (2000) (see Table 3.1) and was also used by Sheng *et al.* (2004), although their interphase was transversely isotropic. The properties of the silicate layers were taken from the results of computational chemistry simulations available in the literature (Chen *et al.*, 2008). The properties for the matrix and nanoclay are also given in Table 3.2.

Last part of Table 3.2 presents the properties of the effective particle after the first step of homogenization (the values were obtained with Equations (3.1 - 3.3, 3.8) and the properties listed on the top of the Table). For all listed configurations in Case I and Case II, the numerical results of FE were compared with analytical predictions. In both numerical and

Table 3.2 Property of phases in the exfoliated PCN. Property of the effective particle is found after first step of homogenization.

			Young's modulus E (GPa)	Poisson's ratio ν	Thickness d (nm)
Matrix (Nylon-6) (Sheng *et al.*, 2004)			2.8	0.35	NA
Nanoclay (MMT) (Chen *et al.*, 2008)			178	0.28	1*
	Case I	(a)	-	-	0
		(b)	13	0.35	3
		(c)	13	0.35	5
Interphase	Case II	(a)	1.3	0.35	3
		(b)	2.8	0.35	3
		(c)	13	0.35	3
	Case III	(a)	2.8	0.5	3
	Case I	(a)	178	0.28	1
		(b)	36.6	0.34	7
		(c)	28	0.34	11
Effective Particle	Case II	(a)	26.5	0.34	7
		(b)	27.82	0.34	7
		(c)	36.6	0.34	7
	Case III	(a)	27.82	0.47	7

* Nanoclay lateral dimension was considered as 100 nm in all configurations.

analytical models, the aspect ratio of the effective particle a_{p} was defined as

$$a_{\mathrm{p}} = \frac{d_{\mathrm{p}}}{\ell}, \tag{3.26}$$

where ℓ is the length of the nanoclay platelet.

The predictions obtained with the different interphases listed in Table 3.2 were compared against the Young's moduli obtained from experiments on Nylon-6/MMT nanocomposites by Fornes *et al.* (2001). They claimed nearly complete exfoliation and good particle alignment with clay contents varying from 1.6 to 7.2 wt % (Fornes *et al.*, 2001). The relation to convert the nanoclay weight fraction, w_{s}, to its volume fraction, f_{s}, is linearized as Sheng *et al.* (2004)

$$f_{\mathrm{s}} \approx \frac{\rho_{\mathrm{m}}}{\rho_{\mathrm{s}}} w_{\mathrm{s}}, \tag{3.27}$$

where ρ is the density of each phase and subscript m refers to the matrix. A density value of $\rho_{\mathrm{m}} = 1080 \ kgm^{-3}$ was assigned to the matrix (Chen *et al.*, 2008; Fornes *et al.*, 2002). The density of clay platelets, according to Chen *et al.* (2008) was considered as 3067 kgm^{-3}.

3.7 Results and discussion

3.7.1 Convergence studies on ensemble of VEs

For illustration purposes, Figure 3.5 shows the convergence of n_{VE} for Case II (a) of Table 3.2. It also shows that generally the converged ensemble size, N_R, decreases with increasing n_{VE}. Figure 3.6 shows the converged values of n_R for different n_{VE}, target accuracy of ϵ_{rel} and
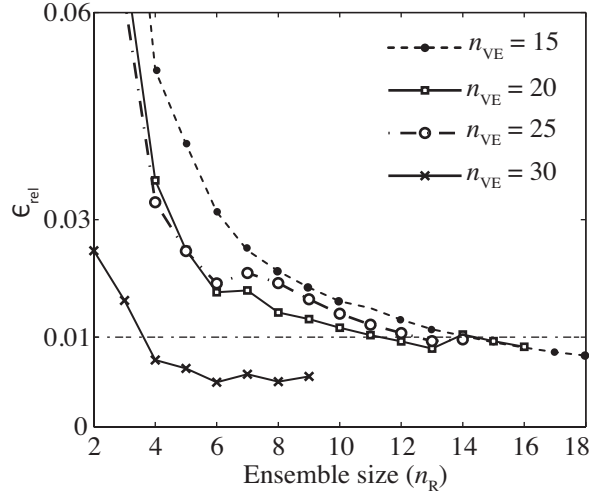
Figure 3.5 Convergence of the number of realizations for a target precision of ϵ_{rel}, $\delta_0 = 0.01$ and different volume sizes (n_{VE}) to find the ensemble sizes. Case II (a), effective particle volume fraction $f_p = 28\%$.

the cases listed in Table 3.2. It also shows the estimations of Equation (3.23) for $\alpha = 1$ and where the base ensemble, labeled as (1) in Equation (3.23), is that containing the smallest VE size (VE sizes of 10 and 15). This value is different from that obtained by Cailletaud et al. (1994) ($\alpha = 0.7$) for Boolean cylinder microstructures. Figure 3.7 shows the evolution of E_{11} as a function of n_{VE}. It reveals that E_{11} exhibits higher variations as a function of n_{VE} at higher volume fractions. This could be attributed to the effect of particle interactions.

The effect of modulus contrast on the required size of RVE is shown in Figures 3.8(a) and 3.8(b). It is shown that larger RVEs are required for higher contrast of rigidity. These observations in Figures 3.7 and 3.8(a) provide confirmations to relations in Equation (3.25).

The reached ensembles of RVEs for each of the studied cases, following the process explained in Algorithm 1, are listed in Table 3.3. According to Equation (3.25) the ensembles reached for stiffer or denser material systems were used also for softer or lower volume fraction PCN, respectively.
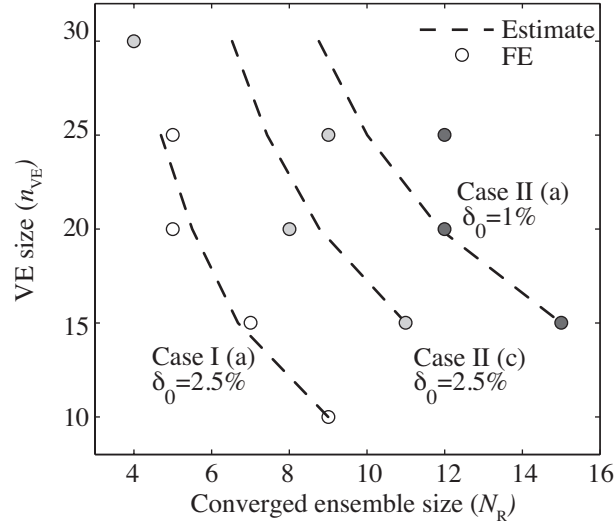
Figure 3.6 Converged ensemble size (N_{R}) by estimate of Equation (3.23) and by FE simulations. Nanoclay volume fraction = 4%.
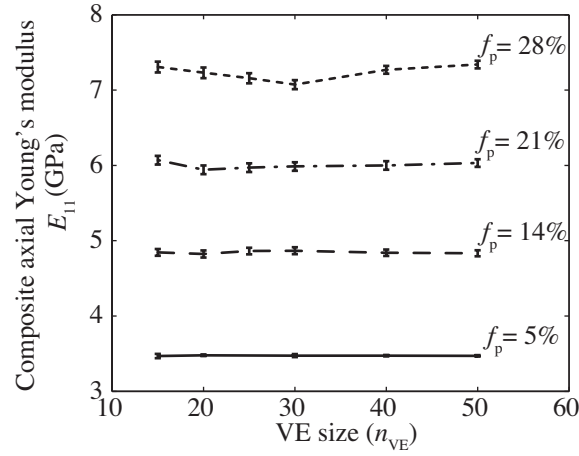
Figure 3.7 Evolution of E_{11} as a function of VE size for different effective particle volume fractions. The bars correspond to confidence intervals on the average level of 95%. Case III (a).
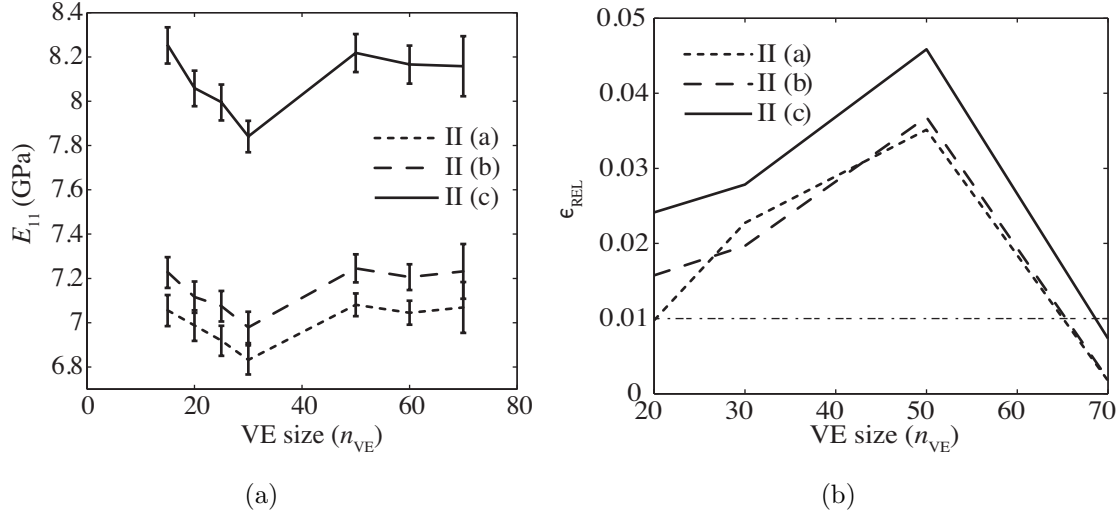
Figure 3.8 Determination of the RVE size. a) Averaged Young's modulus ; b) Relative error of Young's modulus; f_p=28% and a_p=0.07. The bars in (a) correspond to confidence intervals on the average level of 95%.

3.7.2 Parametric study

Effect of interphase thickness

Predictions of the analytical and numerical models for Case I are shown in (Figure 3.9). In the absence of interphase, where the contrast of rigidity is high, at all tested volume fractions (=< 4%), the differences between predictions of MT and Lielens's model are very small (Figure 3.9, Case I(a)). With 3 nm of interphase, both MT and Lielens's models provide acceptable results, but MT model delivers the most accurate predictions (Figure 3.9 - Case I (b)). It is interesting to note that for Case I (b) at high volume fractions ($\approx$ 4%), Lielens's model also delivers accurate predictions. For Case I (c) with an interphase thickness of 5 nm, the best model is again the MT model. For this case where the rigidity contrast is not so high (= 10) and even for very high volume fractions (e.g. 44%), the MT model is more accurate than Lielens's model. On the other hand, the results show that Lielens's model may improve on the MT model at high volume fractions ($\approx$> 30%) only when the rigidity contrast is also high (=> 13) (e.g., Case Ib, refer to Table 3.3 for rigidity contrasts and volume fractions). These conclusions are somewhat different from those obtained by Tucker and Liang (1999) for short fiber composites. In all studied cases, the SC approach tends to generally overestimate the axial Young's modulus, not only at high volume fractions, as reported by Tucker and Liang (1999), but also at low volume fractions (e.g. Figure 3.9, Case I (a)). Divergence between MT and SC models results in case I (c) above 2% clay loading

Table 3.3 Reached ensemble of RVEs, (N_R and N_{RVE}), for different material cases.

	volume fraction highest (f_p)	Rigidity contrast E_p/E_m	N_R	N_{RVE}
Case I (a)	4%	63.6	7	35
Case I (b)	28%	13	13	50
Case I (c)	44%	10	5	50
Case II (a)	28%	9.5	same as Case I (b)	
Case II (b)	28%	9.9	same as Case I (b)	
Case II (c)	28%	13	same as Case I (b)	
Case III (a)	28%	9.9	9	50
		$\nu_p/\nu_m = 1.35$		

(Figure 3.9) might be due to the high volume fraction of the effective particle (22% for a clay volume fraction of 2%). In the case of short fiber composites with very high contrast of rigidity ($= 10^6$), this divergence happens at almost 5% of fiber loading (Tucker and Liang, 1999).

According to Figure 3.9, the effect of the interphase is quite pronounced, especially for high volume fractions of nanoclay. This effect can increase E_{11} by 13% when 2 nm is added to the thickness of the interphase (when comparing Case I (b) to Case I (c) at 4% of nanoclay loading).

For more clarifications on numerical homogenization calculations, two examples of calculated stiffness tensors for Case I (b) are presented in the Appendix II at the end of this thesis.

Effect of interphase properties

For Case II, the parametric study was conducted on interphase elastic moduli (Figures 3.10(a) and 3.10(b)). At 4% of nanoclay loading, a 10 times stiffer interphase leads to an increase of 14% for the stiffness (Figure 3.10(a)). MT model reproduces very well the FE results for all the three cases. For case II (c) at 4% of nanoclay loading, MT and Lielens's models deliver predictions of similar accuracy. For volume fractions higher than 3.5%, the FE results diverge from the MT results and converge toward Lielens's predictions. Although more extended study is required, one may expect that Lielens's model improves on MT model at higher volume fraction ($> 28\%$ of effective particle for a 4% of nanoclay) while the contrast of rigidity is also high.
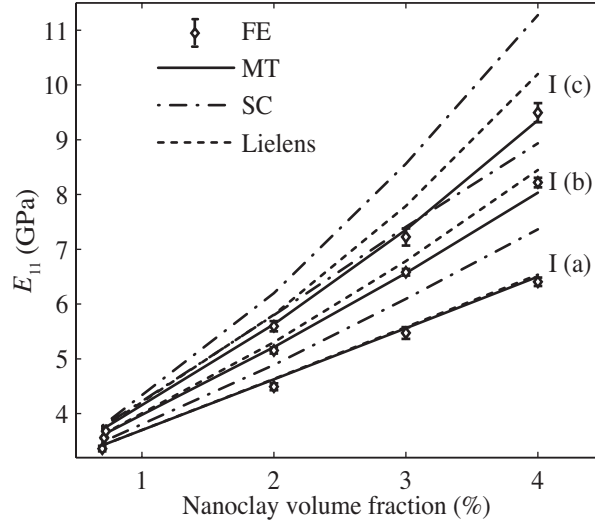
Figure 3.9 Effect of interphase thickness on the prediction of the composite axial Young's modulus as a function of f_s. The effective particle volume fractions for each of the three cases are different and can be calculated according to Equation (3.12). $d_s = 1$nm. $d_I = 0$, 3 and 5nm for cases I (a), (b) and (c), respectively. The bars correspond to confidence intervals on the average level of 95%.
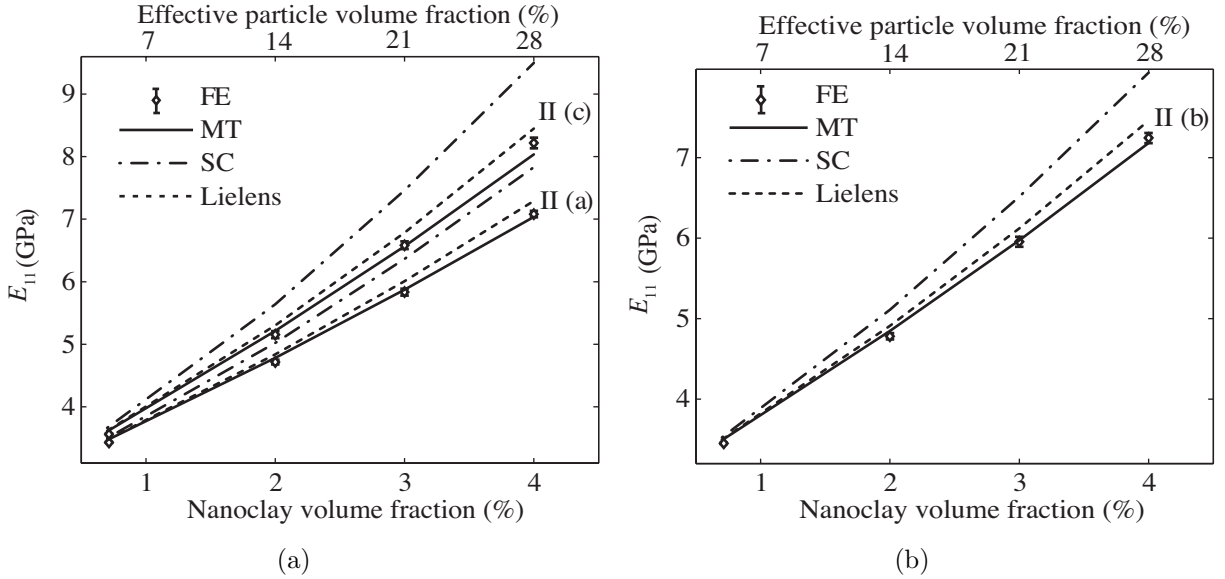
Figure 3.10 Effect of interphase elastic modulus on the predictions of PCN axial Young's modulus, E_{11}. a) Case II (a) and Case II (c); b) Case II (b). The bars correspond to confidence intervals on the average level of 95%.

3.7.3 Comparison with experimental results from the literature

Case I (b) is the case whose numerical results best fit the experimental results (Figure 3.11). This suggests that an interphase of 3 nm with a modulus about 5 times stiffer than that of the matrix provides good description of the interphase in Nylon-6/MMT nanocomposites. This finding is in good concordance with results obtained by Xu *et al.* (2012), Mesbah *et al.* (2009) and Sikdar *et al.* (2008) (refer to Table 3.1 for reported values and employed methods). The $E_{\mathrm{p}} = 36.8$ GPa obtained by Xu et al. Xu *et al.* (2012) for Young's modulus of effective particle is in good agreement with assigned $E_{\mathrm{p}} = 36.6$ GPa in Table 3.2. As mentioned in Section 3.6, Case III (a) was inspired by studies of Tzika et al. Tzika *et al.* (2000) and Sheng *et al.* (2004) (see Table 3.1). As it is shown in Figure 3.11, the interphase described by Case I (b) delivers closer results to those of experiments than Case III (a).
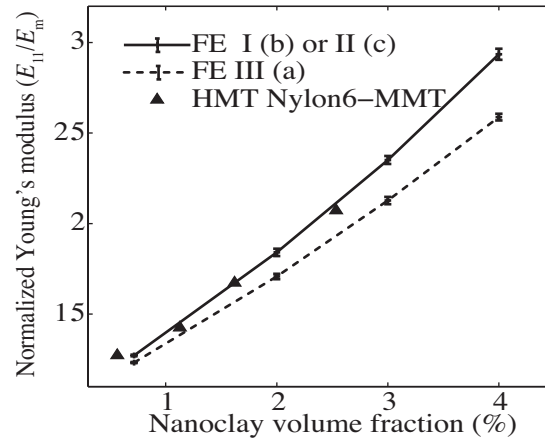
Figure 3.11 Comparison between numerical predictions and experimental data (Fornes *et al.*, 2001) of the overall Young's modulus of Nylon-6/MMT nanocomposites. The bars correspond to confidence intervals on the average level of 95%.

3.8 Conclusions

Three analytical micromechanical models, namely, Mori-Tanaka, self-consistent and Lielens's model were evaluated by 3D FE simulations. All analytical and numerical models were developed using the effective particle concept. A parametric study on elastic properties and thickness of interphase was conducted to find the range of validity and exactitude of analytical models. This study covered rigidity contrasts of 10 to 64 between the Young's modulus

of polymer and that of effective particles. The volume fraction of effective particles varied in the range of $1-44\%$. Results of comparisons between analytical and 3D FE simulations revealed that the MT model is the most reliable method to be used for the possible ranges of modulus contrast, aspect ratio and volume fraction that may happen in exfoliated PCN. Lielens's model may improve on the MT model at high volume fractions when the rigidity contrast between effective particle and polymer is also high. The SC scheme overstimates the axial Young's modulus for all studied cases of PCN.

Experimental verification with data extracted from the literature for Nylon-6/MMT nanocomposite was then used to estimate the elastic property and thickness of the interphase. It was found that the thickness of the interphase for Nylon-6/MMT nanocomposites is about $3\,\mathrm{nm}$ with Young's modulus of about $13\,\mathrm{GPa}$ ($\approx 5\,E_\mathrm{m}$). Considering these properties for the interphase for Nylon-6/MMT nanocomposites, the numerical results, as well as those of Mori-Tanaka model, very well reproduce the experimental data.

The importance of incorporating the interphase was once more highlighted considering the effect of the evaluated interphase that may be up to 13% of increase in axial Young's modulus, when compared to the case without interphase.

3.9   Acknowledgments

3.10   Appendix A

The algorithm for generating parallel disc-shaped particles based on molecular dynamics is a multiple-step procedure. At each step of the simulation, two types of events must be checked: binary collision between two discs and collision between a disc and a cube face. If a binary collision occurs, the velocity vector of each disc must be updated according to the kinetic energy principle. The discs are generated in a cube of side L oriented along the axes 1, 2 and 3. It is assumed that the discs remain parallel during the simulation and their normal axis is oriented along the 2-axis. At each step of the simulation, each disc k has the following parameters: a position vector ($\mathbf{r}^k$), a velocity vector ($\mathbf{v^k}$), a radius (R^k) and its growth rate (a^k), and finally a thickness (d^k) and its growth rate (b^k). t also denotes time.

Computation of binary collisions

Let k and l be two discs in space. Two types of binary collision can occur: an out-of-plane collision, i.e. along the 2-axis (see Figure 3.3), and an in-plane collision, i.e. in the 13-plane. Two parameters must be computed. The first, δ_2 is the distance between the two discs in the 13-plane and is calculated as follows:

$$\mathbf{D}^r = \mathbf{r}^k - \mathbf{r}^l, \tag{3.28a}$$

$$\mathbf{D}^v = \mathbf{v}^k - \mathbf{v}^l,$$

$$\delta_2(t) = \sqrt{\left(D_1^r + t\, D_1^v\right)^2 + \left(D_3^r + t\, D_3^v\right)^2}$$
$$- \left(R^k + R^l + \left(a^k + a^l\right)t\right). \tag{3.28b}$$

δ_3 represents the distance between the two discs along axis 2 and is given by:

$$\delta_3(t) = \left|D_2^r + t\, D_2^v\right| - \left(\frac{d^k + d^l + \left(b^k + b^l\right)t}{2}\right) \tag{3.28c}$$

The next collision time between the discs k and l is the smallest positive value t_c such that $\delta_2(t_c) \leq 0$ and $\delta_3(t_c) \leq 0$. To find the time t_c, the roots of $\delta_2(t)$ and $\delta_3(t)$ should be computed first, i.e. find t_1 and t_2 such that $\delta_2(t_1) = 0$ and $\delta_3(t_2) = 0$. If the quadratic equation $\delta_2(t_1) = 0$ has no solution, there will never be a collision between the two discs. Otherwise, if t_1 exists, three cases must be considered. If $t_1 > t_2$ and $\delta_3(t_1) \leq 0$, an in-plane collision occurs at time $t_c = t_1$. If $t_1 \leq t_2$ and $\delta_2(t_2) \leq 0$, an out-of-plane collision occurs at time $t_c = t_2$. In all other cases, there is no collision between the discs.

The procedure is repeated for each pair of discs and the next binary collision time is the smallest time obtained among all pairs of discs.

Computation of collisions with the cube cell faces

For each disc k, a collision time with each cube face should be calculated. The collision time were obtained as follows:

$$
T_{km} = \begin{cases}
\left(r^k_{(2m-1)} - R^k\right)\left(a^k - v^k_{(2m-1)}\right)^{-1} \\
\qquad \text{for} \quad m = \{1, 2\} \quad @x = 0 \ \& \ z = 0 \\[2ex]
\left(L - r^k_{(2m-5)} - R^k\right)\left(a^k + v^k_{(2m-5)}\right)^{-1} \\
\qquad \text{for} \quad m = \{3, 4\} \quad @x = L \ \& \ z = L \\[2ex]
\left(r^k_2 - d^k/2\right)\left(b^k/2 - v^k_2\right)^{-1} \\
\qquad \text{for} \quad m = 5 \quad @y = 0 \\[2ex]
\left(L - r^k_2 - d^k/2\right)\left(b^k/2 + v^k_2\right)^{-1} \\
\qquad \text{for} \quad m = 6 \quad @y = L
\end{cases}
\tag{3.29}
$$

T_{km} is a $n \times 6$ matrix, where n is the number of discs. The next collision time with a cube face is obtained by finding the minimum of T_{km}.

Velocities update after binary collisions

The update of velocities depends on the type of collision. If an in-plane collision occurs, the velocities update procedure is the same as for a collision between two circles or spheres (see Algorithm 4 in (Ghossein and Lévesque, 2012) for more details). If an out-of-plane collision occurs, only the y-component of the velocities is affected. The respective y-components of the two discs are exchanged while considering the thickness growth rate. The computation of the post-collision velocities is performed as follows:

$$
(v^k_2)^+ = (v^l_2)^- + \left(\frac{b^k + b^l}{2}\right) u,
\tag{3.30a}
$$

$$
(v^l_2)^+ = (v^k_2)^- - \left(\frac{b^k + b^l}{2}\right) u,
\tag{3.30b}
$$

where

$$
u = \frac{r^k_2 - r^l_2}{\left| r^k_2 - r^l_2 \right|} = 1 \ \text{or} \ -1.
\tag{3.31}
$$

It should be noted that $(\mathbf{v})^-$ and $(\mathbf{v})^+$ denote respectively the velocities before and after the binary collision.

3.11 Appendix B

Following algorithm was used to characterize the ensemble of RVEs:

Algorithm 1 Characterize ensemble of RVEs, $(N_\mathrm{R}, N_\mathrm{RVE})$

Input: volume fraction, aspect ratio, elastic properties
Output: size of RVE (N_RVE), size of ensemble (N_R)

1: Initialize VE size, n_VE
2: Assign ensemble lable $i \leftarrow 1$
3: **while** CR. III is not met **do**
4:     **if** $i > 1$ **then**
5:         Estimate size of ensemble, N_R, from Equation (3.23), $n_\mathrm{R} \leftarrow N_\mathrm{R}$
6:     **else**
7:         Initialize size of ensemble, n_R
8:     **end if**
9:     **while** CR. I and CR. II are not met **do**
10:         Total of n_R generated realizations needed
11:         Retrieve desired property, Z, from FE analyses
12:         $n_\mathrm{R} \leftarrow n_\mathrm{R} + 1$
13:     **end while**
14:     $N_\mathrm{R} \leftarrow n_\mathrm{R}$
15:     Calculate ensemble average of Z, $\tilde{Z} \leftarrow \frac{\sum Z}{N_\mathrm{R}}$
16:     $i \leftarrow i + 1$
17:     $N_\mathrm{RVE} \leftarrow n_\mathrm{VE}$
18:     increase n_VE
19: **end while**
20: **return** $(N_\mathrm{R}, N_\mathrm{RVE})$

CHAPTER 4

ARTICLE 2: Numerical and Analytical Modeling of the Stiffness of Polymer-Clay Nanocomposites: One- and Two-Step Methods

M. Pahlavan Pour, P. Hubert, M. Lévesque (2013). Submitted to: "*Computational Materials Science*".

4.1 abstract

This paper studies one- and two- step homogenization models for predicting the stiffness of Polymer-Clay Nanocomposites (PCN). In particular, the influence of the Effective Particle (EP) concept central to two-step models is assessed for numerical as well as analytical modeling. This study covers intercalated PCN, as well as exfoliated morphologies in the presence of interphase. The predictions of analytical and simplified numerical homogenization models were compared against detailed 3D Finite Element (FE) simulations where the PCN layered microstructure is explicitly simulated. The Representative Volume Element (RVE) was rigorously determined. The theoretical predictions were also compared against experimental data extracted from the literature. It was found that both numerical and analytical two-step methods may significantly diverge from the FE simulations of the detailed microstructures. In general, the analytical multi-coated inclusions model delivers more reliable results than two-step methods. Despite their higher computational costs, one-step FE models are necessary, depending on the PCN microstructure and the desired accuracy. It was also found that the more the EP is different from the nanoclay, in terms of rigidity and aspect ratio, or the higher the volume fraction is, the more the accuracy of two-step numerical models is deteriorated.

4.2 Introduction

Polymer-Clay Nanocomposites (PCN) are used in various sectors like packaging, transportation and construction. Clays, in their natural form, are stacks of parallel nanoclay platelets. Depending on the degree of separation and polymer penetration between the nanoclays, three different morphologies for clay-polymer systems can be found: intercalated, exfoliated and aggregates. Exfoliated morphology occurs when completely separated single nanoclays are dispersed in the polymer matrix. The intercalated morphology results from the

penetration of polymer chains between parallel nanoclays. At the molecular level, the inter-actions at the interface between the nanoclay and the polymer matrix result in the formation of an interphase with a thickness of a few nm.

Numerous studies have been devoted to the mechanical behavior prediction of interca-lated and exfoliated PCN (Luo and Daniel, 2003; Sheng *et al.*, 2004; Figiel and Buckley, 2009; Mesbah *et al.*, 2009; Anoukou *et al.*, 2011; Hbaieb *et al.*, 2007; Cricri *et al.*, 2011). However, only a limited number of such studies have taken into account the interphase ef-fects (Sheng *et al.*, 2004; Mesbah *et al.*, 2009; Anoukou *et al.*, 2011). Analytical studies can be generally categorized in one- and two-step homogenization models. Two-step models rely on the *Effective Particle* concept (Sheng *et al.*, 2004; Luo and Daniel, 2003) as a first ho-mogenization step. This concept homogenizes the multiphase layered particle (the exfoliated nanoclay surrounded by the interphase or the intercalated stacks) into a single phase, the Effective Particle (EP). The second step then computes the overall properties of the simpli-fied two-phase composite (i.e. distributed EPs in a uniform matrix). The EP concept has simplified the homogenization problem but its accuracy has not been rigorously evaluated, yet. One-step models have been mostly applied to exfoliated PCN, with or without incorpo-rating the interphase (Mesbah *et al.*, 2009; Anoukou *et al.*, 2011). However, to the authors' best knowledge, no one-step study has been performed for intercalated composites. More importantly, no comparative studies have been performed to assess the range of validity and time-efficiency of two- and one-step models.

The numerical modeling of PCN has also been the subject of numerous works. The devel-oped models range from simplified 2D (Hbaieb *et al.*, 2007; Sheng *et al.*, 2004; Mesbah *et al.*, 2009; Figiel and Buckley, 2009) to more complex 3D Finite Element (FE) models (Hbaieb *et al.*, 2007; Cricri *et al.*, 2011). In most of the numerical works, the representativeness of the analyzed models was not verified, which can raise questions about the accuracy of the reference data used for the comparisons. The EP concept has been also used in numerical models (Sheng *et al.*, 2004; Figiel and Buckley, 2009; Mesbah *et al.*, 2009; Pahlavanpour *et al.*, 2013). Figiel and Buckley (2009) examined the EP concept in a 2D FE study by comparing the predictions of their model constituted of EPs against those of detailed layered microstruc-tures. They have shown that the concept could lead to accurate predictions, provided that the anisotropy of the EPs was taken into account. However, no accurate numerical study has yet dealt with the 3D explicit representation of the different phases.

The purpose of this work was to study further the relevance and accuracy of the EP con-cept in two-step numerical, as well as analytical, modeling. Two analytical one-step models have been adopted to predict elastic properties of PCN. The predictions of analytical homog-enization models were compared to 3D FE simulations of PCN detailed microstructures for

intercalated and exfoliated microstructures. The effect of the interphase was explicitly incorporated in numerical as well as in analytical modeling. The originality of the present work lies in the fact that the Representative Volume Element (RVE) was rigorously established and that neither analytical nor numerical models were limited by simplifying assumptions such as isotropic particles and the EP concept. To the best of the authors' knowledge, their 3D FE models in which the interface is explicitly represented are the most representative FE model published so far for the studied microstructures. Furthermore, numerical results were compared to experimental data extracted from the literature for exfoliated Nylon-6/Montmorillonite (MMT) and intercalated MXD6 Nylon/MMT nanocomposites.

The paper is organized as follows: Section 4.3 presents a brief background on PCN and the modeling methods. Section 4.4 discusses the proposed modeling strategy. The properties of the constituent phases for the studied PCN are presented in Section 4.5. Section 4.6 presents the performance evaluation of the various models by comparing their predictions against benchmark numerical and experimental data published in the literature. Finally, Section 6 concludes this work.

4.3 Background

4.3.1 Polymer-Clay Nanocomposites

Nanoclay platelets have a thickness of about 1 nm and their lateral dimensions may vary from 30 nm to several microns (Ray and Okamoto, 2003). In an exfoliated morphology, an interphase region forms around each nanoclay platelet (Figure 4.1(a)). The thickness of the interface in intercalated morphologies can be negligible, when compared to that of the intercalated stack (Chen *et al.*, 2008; Mesbah *et al.*, 2009). Therefore, the properties of the intercalated PCN are not affected in the presence of interphase as much as those of exfoliated case (Mesbah *et al.*, 2009). In an intercalated morphology, an interlayer space, called *gallery*, separates the nanoclays. The distance between the central planes of two consecutive nanoclays is denoted by $d_{(001)}$ (Figure 4.1(b)).

4.3.2 Two-step homogenization models

Two-step models based on the EP concept were initially developed for intercalated PCN (Luo and Daniel, 2003; Sheng *et al.*, 2004). They were later used for exfoliated nanoclays with interphase (Pahlavanpour *et al.*, 2013). For the intercalated morphology, the EPs were mechanically equivalent to layered reinforcing stacks consisting of nanoclays and galleries (Figure 4.1(b)). For exfoliated morphologies, given the small nanoclay thickness, it was

(a)

(b)
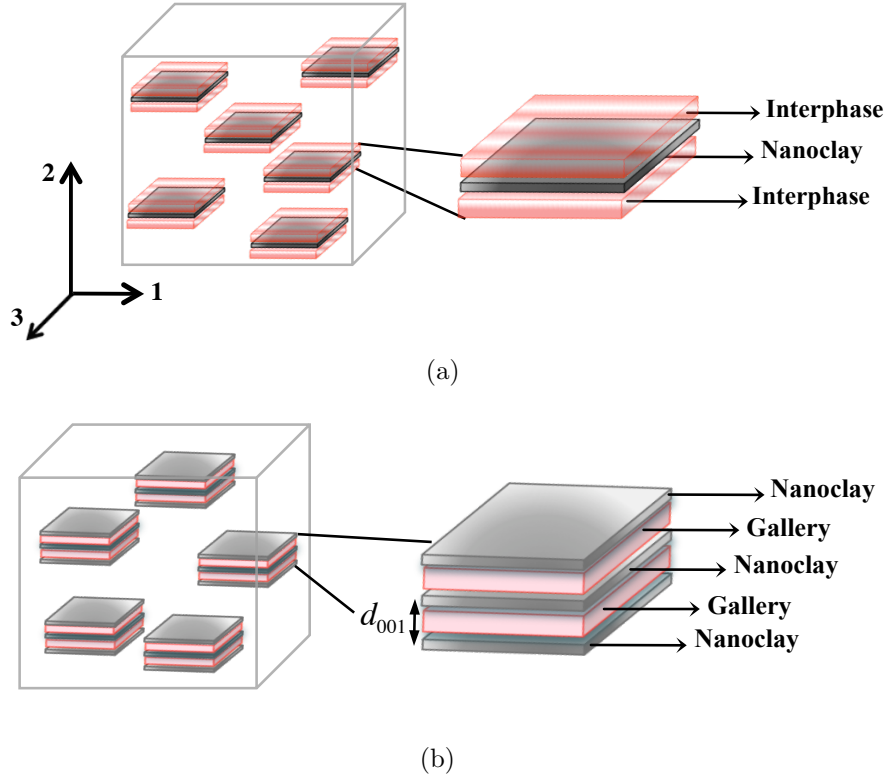
Figure 4.1 Layered structure of reinforcing stacks in a) exfoliated PCN b) intercalated PCN. The interphase is not considered for the intercalated morphology.

assumed that the interphase lied only on the top and bottom faces of the nanoclay, leading to a three-layer reinforcing stack (Figure 4.1(a)).

First step

In the works of Mesbah *et al.* (2009) and Pahlavanpour *et al.* (2013), the properties of the EPs were computed as per the modified rule of mixtures (Tsai and Hahn, 1980) as:

$$E_{p,11} = E_{p,33} = \chi E_s + (1-\chi)E_t, \tag{4.1}$$

$$\nu_{p,12} = \nu_{p,32} = \chi\nu_t + (1-\chi)\nu_s, \tag{4.2}$$

$$E_{p,22} = \frac{E_s E_t}{\chi E_t + (1-\chi)E_s - \chi(1-\chi)\beta E_t E_s}, \tag{4.3}$$

$$\nu_{p,13} = \frac{\chi\nu_s E_s(1-\nu_t^2) + (1-\chi)\nu_t E_t(1-\nu_s^2)}{\chi E_s(1-\nu_t^2) + (1-\chi)\nu_t E_t(1-\nu_s^2)}, \tag{4.4}$$

$$G_{p,12} = G_{p,32} = \frac{G_s G_t}{\chi G_t + (1 - \chi)G_s - \chi(1 - \chi)\eta G_t G_s}, \tag{4.5}$$

$$G_{p,13} = \frac{E_{p,11}}{2(1 + \nu_{p,13})}, \tag{4.6}$$

where E, ν and G denote the Young's modulus, the Poisson's ratio and the shear modulus, respectively. Subscripts 1, 2 and 3 correspond to the principal axes shown in Figure 4.1 (i.e. the platelets have their thickness along axis 2). Subscripts s, p and t refer to the nanoclay, the EP and the third phase (interphase in the exfoliated or gallery in the intercalated morphology), respectively. β and η were defined as:

$$\beta = \frac{\nu_s^2 E_t/E_s + \nu_t^2 E_s/E_t - 2\nu_s\nu_t}{\chi E_s + (1 - \chi)E_t},$$
$$\eta = \frac{\nu_s^2 G_t/G_s + \nu_t^2 G_s/G_t - 2\nu_s\nu_t}{\chi G_s + (1 - \chi)G_t}, \tag{4.7}$$

where χ denotes the nanoclay volume fraction in the EP and was computed from:

$$\chi = \frac{N\, d_s}{d_p}, \tag{4.8}$$

where d refers to the thickness. N denotes the number of nanoclays in each stack. In the above equations, the nanoclay was assumed to be isotropic and the material symmetry of the third phase was either isotropic or cubic. Equations (4.1-4.6) deliver the properties of a Transversely Isotropic (TIso) EP. Also, the volume fraction of the EPs f_p was obtained knowing the nanoclay volume fraction f_s in the composite and by the following relation:

$$f_p = \frac{f_s}{\chi}. \tag{4.9}$$

The aspect ratio of the EP, a_p, was defined as

$$a_p = \frac{d_p}{\ell}, \tag{4.10}$$

where ℓ denotes the length of the nanoclay platelet. Finally, the thickness of the EP can be obtained from:

$$d_p = d_s + 2d_I + (N - 1)d_{(001)}, \tag{4.11}$$

where subscript I refers to the interphase.

Second step

Both analytical (e.g., Mori-Tanaka (MT) model (Mori and Tanaka, 1973; Benveniste, 1987), Self-Consistent (SC) scheme Hill (1965); Budiansky (1965) and Lielens's model (Lielens, 1999)) and numerical micromechanical models can be subsequently used in a second step to calculate the effective mechanical properties of the nanocomposite (Sheng *et al.*, 2004; Mesbah *et al.*, 2009; Figiel and Buckley, 2009; Luo and Daniel, 2003; Pahlavanpour *et al.*, 2013). Pahlavanpour *et al.* (2013) evaluated the performance of commonly used homogenization models for the stiffness prediction of exfoliated PCN by comparing their predictions to those of 3D FE simulations relying on the EP concept. They found that the MT model was the most reliable method for the range of property contrasts and morphologies encountered in exfoliated PCN. They also reported that the SC scheme generally overestimates the axial Young's modulus of exfoliated PCN.

4.3.3   One-step analytical homogenization models

The one-step analytical models used in this paper are the models developed for predicting the properties of composites reinforced by coated particles. The double-inclusion model of Hori and Nemat-Nasser (1993) was developped for an ellipsoidal inclusion surrounded by single ellipsoidal coating layer. The coated inclusion is further embedded in an infinitely extended homogeneous medium (Figure 4.2(a)). The shape and orientation of the inclusion and the coating, as well as the elastic properties of the three phases can be set arbitrarily. Ju and Chen (1994) reported that the model of Hori and Nemat-Nasser is a noninteracting solution that does not take into account the interactions between particles. In the same work (Ju and Chen, 1994), they derived the general governing equations for composites containing aligned particles by incorporating the effects of particle-particle interactions. More recently, Liu and Sun (2005) derived the effective stiffness tensor equations for three-phase composites containing randomly distributed, yet aligned, spheroidal particles with interphase. This model is referred herein as *Interacting Double-Inclusion (IDI)* approach. The formulation for the IDI model is presented in Appendix A (Section 4.9).

Lipinski *et al.* (2006) developed a one-step model for linearly elastic ellipsoids coated by n concentric layers (Figure 4.2(b)), called *multi-coated* model hereinafter. The model relies on a combination of Green's function techniques with interface operators, capturing the stress and strain jump conditions at the interfaces between two adjacent coatings. The derivation of the stiffness tensor for the multi-coated model is presented in Appendix B (Section 4.10).
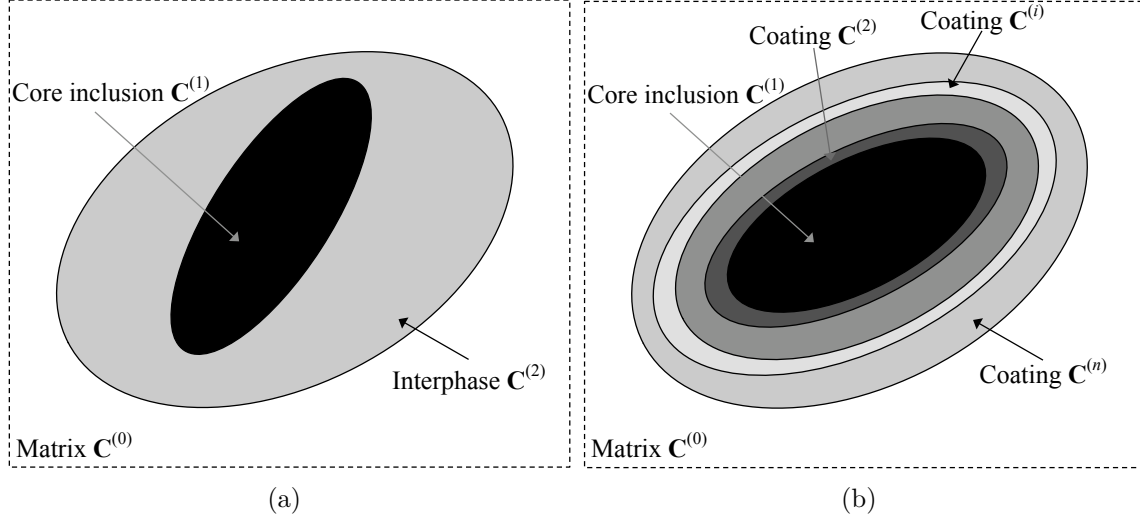
Figure 4.2 a) Double Inclusion (Hori and Nemat-Nasser, 1993) and b) n-layer inclusion composed of n concentric ellipsoids, embedded in Matrix (Lipinski *et al.*, 2006). $\mathbf{C}$ is the stiffness tensor and the superscript (i) refers to the phase i.

4.3.4 Numerical model and RVE determination

In numerical modeling, the Volume Element (VE) is a volume containing a certain number of heterogeneities distributed in the uniform matrix. Herein, the size of a VE is characterized by the number of represented heterogeneities. The RVE is typically defined as a VE for which increasing number of represented heterogeneities does not alter the computed effective properties. Moreover, the smallest RVE is usually sought in order to limit the computational costs. Numerical homogenization therefore requires means to generate VEs and a procedure for establishing the RVE. In this study, FE was used as the numerical homogenization tool.

Molecular Dynamics (MD) approaches can be used to generated randomly positioned particles in a VE (Lubachevsky *et al.*, 1991; Ghossein and Lévesque, 2012; Pahlavanpour *et al.*, 2013). MD delivers high volume fractions, for a large number of represented heterogeneities in a very short computational time. In MD simulations, the particles are all created at once in the VE, but with a null volume. They are then put in motion and the volume of each particle progressively increases. Collisions are checked after each step of volume increase until the desired volume fraction is reached.

Periodic Boundary Conditions (PBC) were shown by (Gusev, 1997; Kanit *et al.*, 2003) to yield smaller RVEs when compared to the cases where uniform boundary conditions are applied. PBC can be enforced through Multiple Point Constraints (MPC) following the method explained by Barello and Lévesque (2008). In FE modeling, applying PBC necessitates a periodic geometry, as well as a periodic mesh (Pahlavanpour *et al.*, 2013).

Kanit *et al.* (2003) and Pahlavanpour *et al.* (2013) (among many others) used the statistical dispersion of the predicted overall modulus to define their RVEs. Their approach consisted in generating a family of different VE realizations, called ensemble of VEs herein. Each realization in the ensemble was a VE constituted of a randomly distributed constituents with the same microstructural properties (i.e. volume fraction, aspect ratio, phase properties and VE size). The number of realizations in an ensemble (n_{VE}) was increased so that the desired confidence interval width was achieved on the average property of the ensemble (Kanit *et al.*, 2003). Pahlavanpour *et al.* (2013) added an additional tolerance on the material symmetry that led to the following criteria for establishing the converged number of realizations N_{R} :

$$\text{Criteria for } N_{\mathrm{R}} : \begin{cases} \dfrac{\epsilon_{\mathrm{CI}}}{\tilde{E}_{11}} \leq \delta_0 \quad and \\[2mm] \dfrac{|\tilde{E}_{33} - \tilde{E}_{11}|}{\tilde{E}_{11}} \leq \delta_0, \end{cases} \tag{4.12}$$

where E_{11} refers to the axial Young's modulus (the desired property in this study) of a given realization (please refer to Figure 4.1 for the coordinate system), the tilde symbol in $\tilde{E}_{11}$ denotes the ensemble average of that property and δ_0 is a given threshold. ϵ_{CI} is the half-width of a two-tailed 95% confidence interval. The second constraint of Equation 4.12 enforces the transverse isotropy symmetry of the obtained results for PCN reinforced with aligned particles. One of the most commonly used criteria (Gusev, 1997; Kanit *et al.*, 2003; Ghossein and Lévesque, 2012; Pahlavanpour *et al.*, 2013) to determine the size of RVE N_{RVE} is the stability criterion, which is based on the stability of the ensemble average of the desired property over VE size (n_{VE}) increments:

$$\text{Criterion for } N_{RVE} : \quad \frac{|\tilde{E}_{11}^{(i)} - \tilde{E}_{11}^{(i-1)}|}{\tilde{E}_{11}^{(i)}} \leq \delta_1, \tag{4.13}$$

where superscripts (i) and $(i-1)$ refer to two successive ensembles, for which N_R has converged, with different VE sizes and δ_1 is a given threshold. Figure 4.3 schematically depicts the determination procedure of the converged values for N_{R} and N_{RVE}.

4.4 The modeling strategy

The modeling strategy consisted of both two-step and one-step homogenizations (Figure 4.4). In two-step models, Step I computed the EP properties for both exfoliated and intercalated morphologies. The EPs were then considered as inclusions in Step II where different
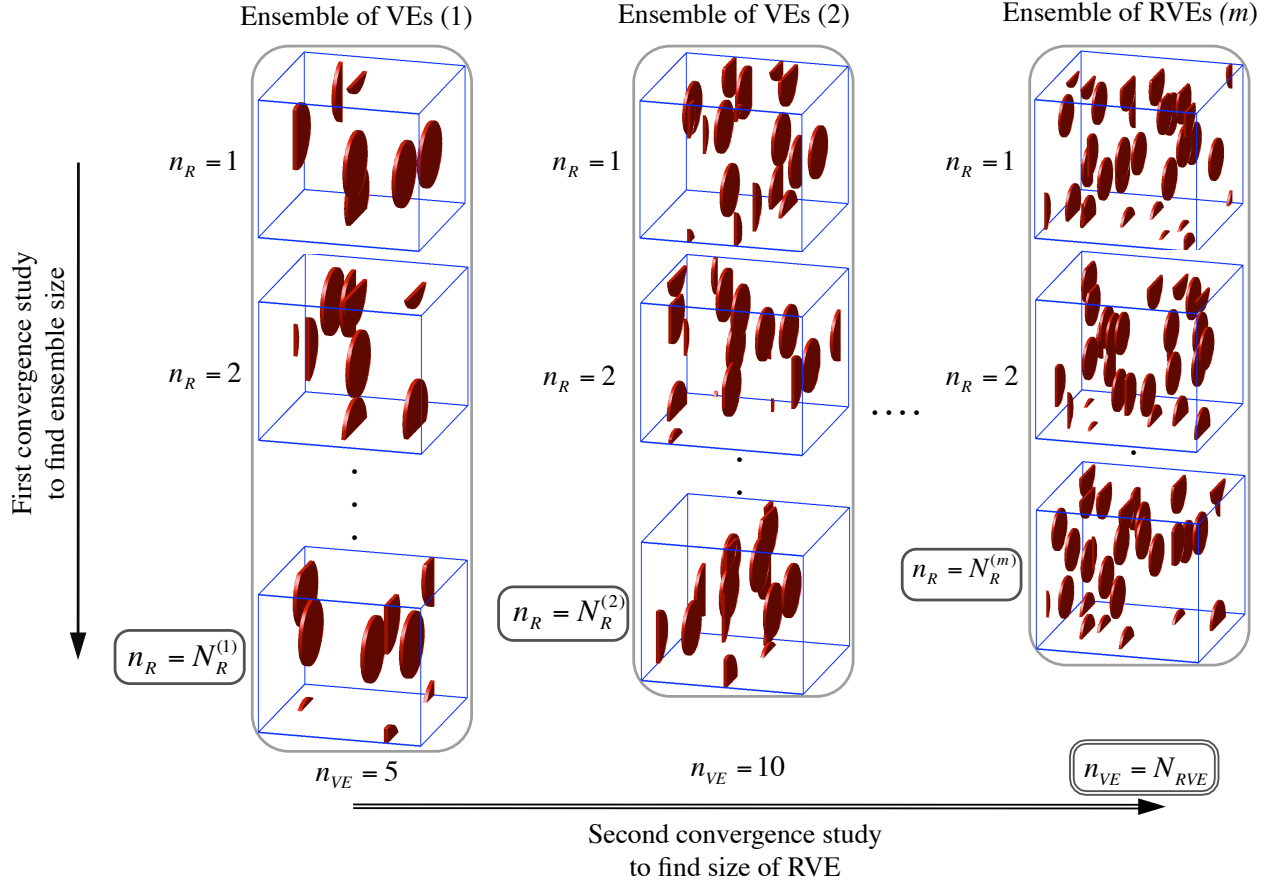
Figure 4.3 Illustration of two-fold convergence study to determine the ensemble of RVEs in numerical simulations (Pahlavanpour *et al.*, 2013).

analytical models (i.e. MT and Lielens's model)[1] and numerical homogenization models were used to obtain the overall properties of PCN. In the sequel, the two-step homogenization procedures are referred to as Step II/Step I (e.g. MT/EP, Lielens/EP), where the EP concept was employed as Step I. For the simplified Isotropic (Iso) EP, only two independent constants, E_p and ν_p, were required, which were approximated by $E_{p,11}$ and $\nu_{p,12}$ (Equations (4.1) and (4.2), respectively).

Both IDI and multi-coated models were used for exfoliated morphologies. For the intercalated morphology, the multi-layer disc-shaped stack (Figure 4.5(a)) was modeled as a multi-coated ellipsoid (Figure 4.5(b)) having the same volume and aspect ratio as the disc-shaped stacks. This approximation (Figure 4.5(c)) was deemed reasonable, considering the

---

1. The SC model was not considered since it has been shown to overestimate the axial Young's modulus (Pahlavanpour *et al.*, 2013).

Two-step models

Step I

Step II

Inputs

Composite

Literature
(Computational
chemistry, …)

Nanoclay

Interphase

Gallery

Polymer matrix

Reinforcing stack

Modified rule
of mixtures

Effective Particle

Composite

Analytical:		Numerical:
Mori-Tanaka, Lielens's		3D FE

Effective particles in the matrix

Analytical: Multi-coating, IDI, simplified IDI	
Numerical: Layered Particle 3D FE	

reinforcing stacks in polymer

Composite

One-step models

Figure 4.4 One and two- step modeling strategies. Modeling inputs were obtained from the literature. In two-step strategy, Step I computed the properties of effective particles by a modified rule of mixtures. In Step II, the overall properties for the PCN were calculated using both numerical and analytical models. In one-step models, the overall properties for the PCN were calculated directly from the microstructures reinforced by layered particles.

high aspect ratio of the stacks.

Layered Particles (LPs), as well as the EPs (Figures 4.6(a) and 4.6(b)) were simulated in the detailed microstructure FE models following the methodology explained in (Pahlavanpour *et al.*, 2013). Randomly positioned aligned disc-shaped particles were generated in 3D periodic VEs using MD simulations. The RVE was determined through the two-fold convergence procedure depicted in Figure 4.3. Thresholds of $\delta_0 = \delta_1 = 0.01$ were considered.

All the constituent phases were assumed to be linearly elastic and perfectly bonded to their neighbors.

4.5   Studied morphologies: properties of the constituent phases

The properties of the nanoclay layers were taken from the results of computational chemistry simulations available in the literature (Chen *et al.*, 2008). The relation to convert the nanoclay weight fraction w_s to its volume fraction f_s was linearized as (Sheng *et al.*, 2004):

$$f_s \approx \frac{\rho_m}{\rho_s} \frac{1}{\psi} w_s, \tag{4.14}$$

where ρ denotes the density of each phase, subscript m refers to the matrix and

$$\psi = \frac{1}{\left(1 - \frac{1}{N}\right)\left(\frac{d_{(001)}}{d_s}\right) + \frac{1}{N}}. \tag{4.15}$$

A density value of $\rho_m = 1000$ kgm^{-3} was assigned to the matrix (Sheng *et al.*, 2004). The density of nanoclay platelets was set to 3067 kgm^{-3} (Chen *et al.*, 2008).

4.5.1   Exfoliated morphology

The constituent phase properties and material symmetries for the studied exfoliated Nylon-6/MMT nanocomposite are listed in Table 4.1. The properties of the interphase, Case I, were obtained from (Xu *et al.*, 2012; Pahlavanpour *et al.*, 2013). For comparison purposes, another case with an imaginary interphase, Case II, was also introduced in Table 4.1. Table 4.1 also lists the EP properties obtained for both Cases I and II.

Experimental data on Nylon-6/MMT nanocomposites by Fornes *et al.* (2001) was used as a comparison basis. They claimed nearly complete exfoliation and good particle alignment with clay content varying from 1.6 to 7.2 wt% (Fornes *et al.*, 2001).
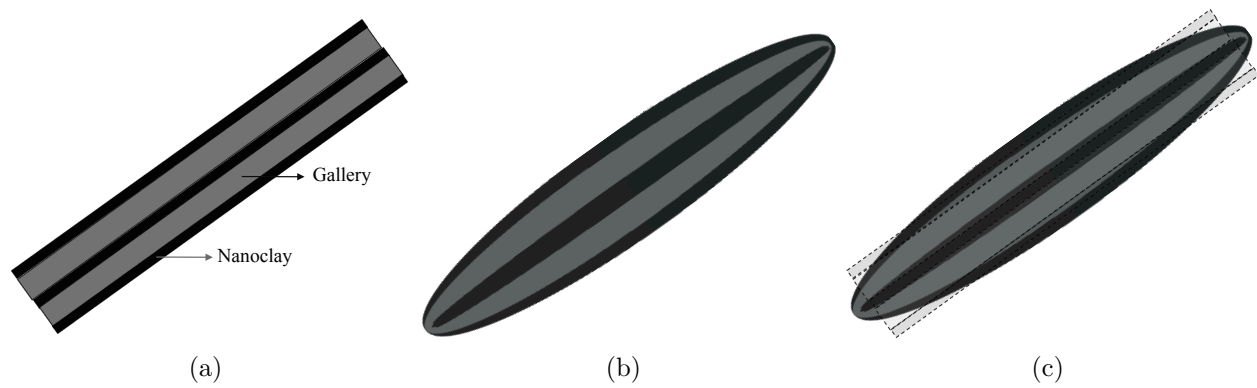
Figure 4.5 Schematic cross-section of the reinforcing stack in a) an idealized intercalated morphology reinforced with multi-layer discs b) the analytical modeling for composites reinforced by multi-coated ellipsoids. c) Approximating the multi-layer disc by a multi-coated ellipsoid of identical volume and aspect ratio.
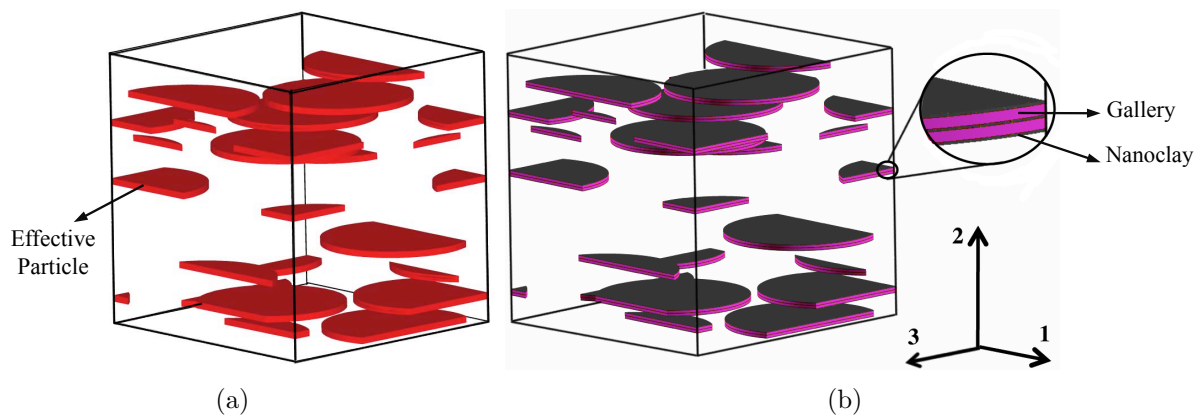
Figure 4.6 Randomly positioned aligned disc-shaped particles in 3D periodic volume elements. a) Effective particles in a two-step FE model b) Layered particles in a one-step FE model.

4.5.2   Intercalated morphology

The constituent phases of the studied intercalated PCN were those of the MXD6 Nylon/MMT nanocomposite, presented in Table 4.2 along with those of the EPs. The cubic symmetry of the gallery was taken into account in the TIso EP by using three independent E, ν and G for the galley in Equations (4.1-4.6). The interphase was not assumed for the intercalated morphology since the experimental data was for an amorphous polymer (Nylon MXD6) in which there is no possibility of change in crystallinity (Sheng *et al.*, 2004; Chen *et al.*, 2008).

Experimental data on MXD6 Nylon/MMT nanocomposites by Sheng *et al.* (2004), with clay content varying from 1.1 to 5.27 wt%, was used for comparison purposes. Intercalated multi-layered stacks were observed to be well aligned and the structure of intercalated clay stacks was seen to be independent of clay content. The number of nanoclays in each stack N was 3 and the average interlayer space $d_{(001)}$ was 4.1 nm (Sheng *et al.*, 2004).

Table 4.1 Property of phases in the exfoliated PCN.

		Material symmetry	Young's modulus E (GPa)	Poisson ratio ν	Thickness d (nm)
Matrix (Nylon-6) (Fornes *et al.*, 2001)		Isotropic	2.8	0.35	NA
Nanoclay (MMT) (Chen *et al.*, 2008)		Isotropic	178	0.28	1*
Interphase	Case I	Isotropic	13	0.35	3
	Case II	Isotropic	2.8	0.35	3
	Case I	Isotropic	36.6	0.34	7
Effective Particle		Transversely isotropic	$E_{11} = E_{33} = 36.6$ $E_{22} = 16.2$ $(G_{12} = G_{32} = 6.01,$	$\nu_{12} = \nu_{32} = 0.34$ $\nu_{13} = 0.38$ $G_{13} = 13.25)$	7
	Case II	Isotropic	27.82	0.34	7
		Transversely isotropic	$E_{11} = E_{33} = 27.82$ $E_{22} = 3.65$ $(G_{12} = G_{32} = 1.35,$	$\nu_{12} = \nu_{32} = 0.34$ $\nu_{13} = 0.3$ $G_{13} = 10.66\ )$	7

* Nanoclay aspect ratio was reported to be 0.01 for the exfoliated morphology (Fornes *et al.*, 2001; Sheng *et al.*, 2004).

Table 4.2 Property of phases in the intercalated PCN.

	Material symmetry	Young's modulus E (GPa)	Poisson's ratio ν	Thickness d (nm)
Matrix (MXD6 Nylon) (Sheng *et al.*, 2004)	Isotropic	4.14	0.35	NA
Nanoclay (MMT) (Chen *et al.*, 2008)	Isotropic	178	0.28	1*
Gallery (Sheng *et al.*, 2004)	Cubic	4.14	0.35	3.1
	$(G = 0.015\,\text{GPa})$			
Effective Particle	Isotropic	60.83	0.33	9.2
	Transversely isotropic	$E_{11} = E_{33} = 60.83$ $E_{22} = 6.83$ $(G_{12} = G_{32} = 0.025,$	$\nu_{12} = \nu_{32} = 0.33$ $\nu_{13} = 0.3$ $G_{13} = 23.53)$	9.2

* Nanoclay aspect ratio was reported to be 0.005 for the intercalated morphology (Sheng *et al.*, 2004).

4.6 Results and discussion

All the presented results were normalized with respect to the Young's modulus of the matrix E_m for the sake of clarity.

4.6.1 Numerical models : Bias induced by two-step models

A simple case that may clearly reveal the possible biases induced by two-step models is the case of exfoliated morphology with imaginary interphase having the same properties as the bulk polymer (Case II in Table 1). Figure 4.7 shows the numerical results for Case II with both two-step and one-step methods. Although the results of these two methods should be theoretically identical, Iso EP for a nanoclay volume fraction of 4% leads to an E_{11} 13% stiffer than that predicted from the one-step model. The figure reveals that, even when considering transverse isotropy effects, the fact of assuming an EP can induce discrepancies in the order of 10%. The representativeness of the EP concept for the exfoliated PCN with real interphase is investigated in Figure 4.8. The figure shows that Iso EP and TIso EP overestimate E_{11} by 5% and 3.5%, respectively. The representativeness of the EP concept was also studied for intercalated morphologies and the results are shown in Figure 4.9. It can be seen that Iso EP overstimates E_{11} by 3% where TIso EP agrees very well with the one-step (LP) results. The analysis of Figures 4.7-4.9 reveals that the volume fraction of nanoclay (f_s), the rigidity contrast between the nanoclay and the EP (E_s/E_p) and the inverse of their aspect ratios[2] (a_p/a_s) have direct impacts on the error induced by the EP concept. In other words, the more the EP differs from the nanoclay, in terms of rigidity and aspect ratio, the more the

---

2. The aspect ratio of the nanoclay in the studied intercalated and exfoliated morphologies was reported to be different. In addition, the thickness of the reinforcing stacks in these two morphologies is different, leading to different aspect ratios. Please refer to Tables 4.1, 4.2 and 4.3 for more details.

Figure 4.7 Axial Young's modulus predictions of one-step (LP) and two-step (Iso EP and TIso EP) FE models for the exfoliated morphology with the imaginary interphase. Results obtained from 4-10 realizations, each containing 50 reinforcing stacks. The bars correspond to confidence intervals on the average level of 95%.
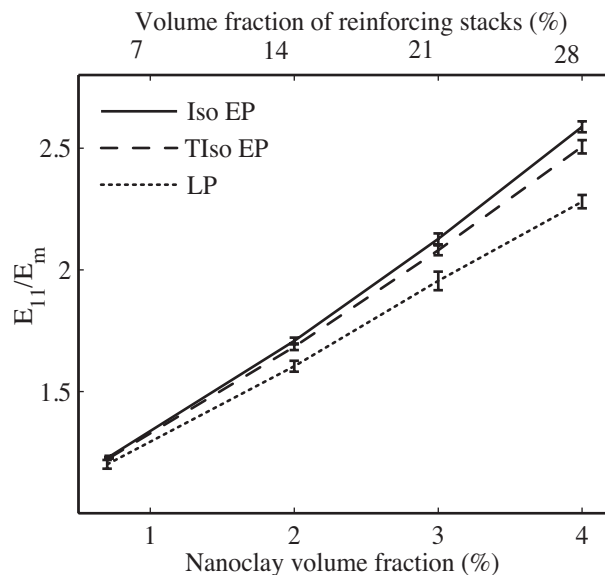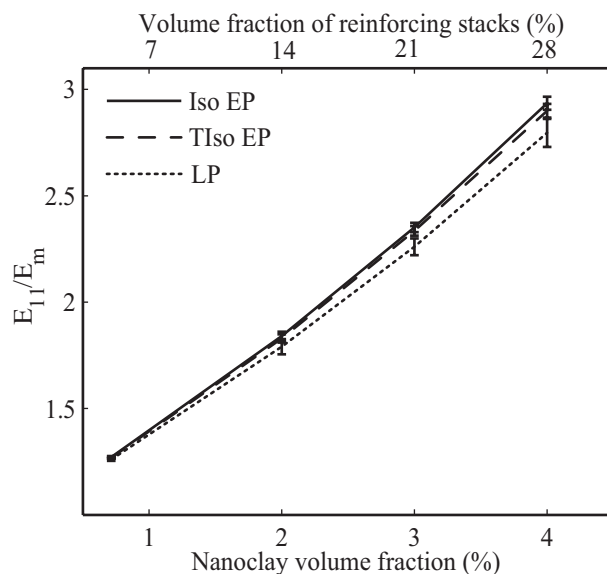

Figure 4.8 Axial Young's modulus predictions of one-step (LP) and two-step (Iso EP and TIso EP) FE models for the exfoliated morphology with the real interphase. Results obtained from 5-14 realizations, each containing 50 reinforcing stacks. The bars correspond to confidence intervals on the average level of 95%.
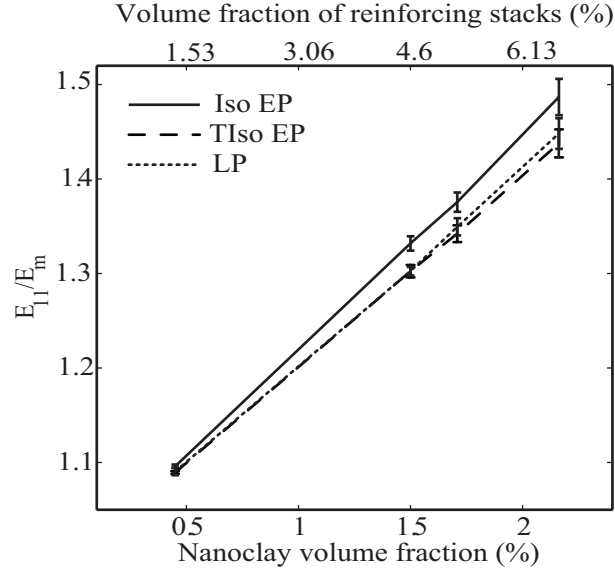
Figure 4.9 Axial Young's modulus predictions of one-step (LP) and two-step (Iso EP and TIso EP) FE models for the intercalated morphology. Results obtained from 4-12 realizations, each containing 10 reinforcing stacks. The bars correspond to confidence intervals on the average level of 95%.

accuracy of two-step models is deteriorated. Table 4.3 lists the influence of rigidity contrast and aspect ratio for the three studied cases for a constant volume fraction.

The computational burden associated with one-step numerical models is much more important than that of two-step models due to the fine mesh required to adequately represent each layer of the reinforcing stacks. For the studied cases, fully detailed models required at least 5 times more elements that those relying on the EP concept. Considering the much lower computational cost associated with the solution of the two-step numerical models, one may conclude that the error induced by EP concept can be acceptable (at least for the range of parameters tested in this study), depending on the application of the results. However, when it comes to set the numerical results as benchmark to validate the analytical models, any initial error reduces the accuracy of the evaluation.

4.6.2 Comparison with experimental databases

Figures 4.10 and 4.11 compare the numerical predictions to experimental results obtained from the literature, for both morphologies. The figures reveal that the numerical models reproduce well the experimental results, especially for the exfoliated morphology.

Figure 4.10 Experimental validation of one-step FE (LP) model for the exfoliated morphology, Case I. Results obtained from 5-10 realizations, each containing 50 reinforcing stacks. The bars correspond to confidence intervals on the average level of 95%.

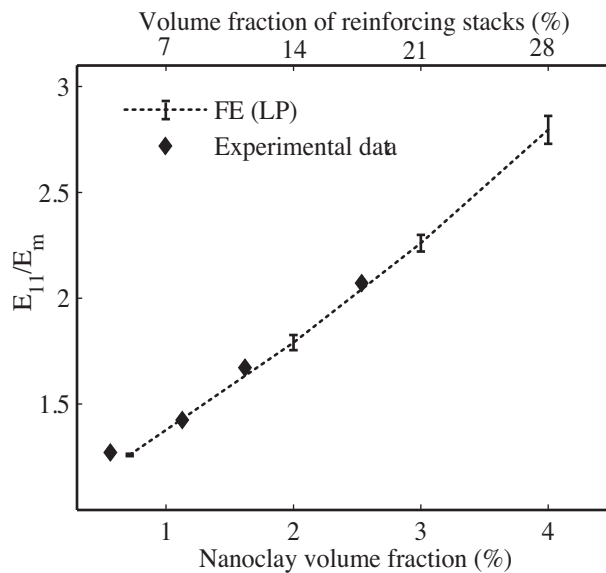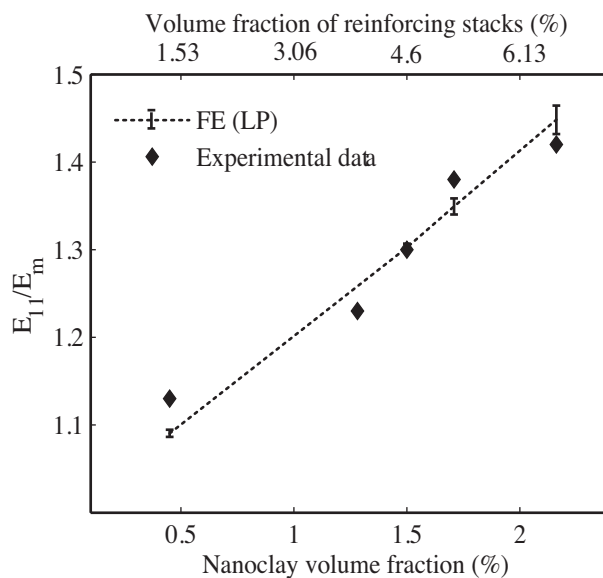Figure 4.11 Experimental validation of one-step FE (LP) model for the intercalated morphology. Results obtained from 4-10 realizations, each containing 10 reinforcing stacks. The bars correspond to confidence intervals on the average level of 95%.

Table 4.3 The influence of rigidity contrast and aspect ratio on the bias induced by two-step numerical models.

	E_s/E_p	a_p/a_s	Error*
Intercalated PCN	2.93	9.2	2.18%
Exfoliated (Case I)	4.86	7	2.82%
Exfoliated (Case II)	6.4	7	6.47%

* The error is calculated between the Iso EP and LP models.
$f_s = 2\%$ for all the three cases.

4.6.3 Analytical models

The predictions of the analytical models were compared to those of the numerical simulations in Figure 4.12. Simplified IDI is the less accurate of all models, inducing discrepancies as high as 15%. All the other models delivered similarly accurate predictions, the one-step IDI model being slightly more accurate than the others (for the cases studied in this work).

Figure 4.13 shows the analytical and numerical predictions for the intercalated case. It can be seen that the most accurate predictions were delivered by the one-step multi-coated model and they lied within 1% of the numerical simulations. All the other analytical models overestimate the axial Young's modulus, inducing discrepancies as high as 5%. These results show the superiority of the multi-coated approach and, although it required a more delicate numerical implementation and more computational time, it should be the model to be used to represent such multilayer microstructures.

4.7 Conclusions

Although both numerical and analytical two-step methods can deliver accurate predictions in some cases, it was shown that they can significantly diverge from detailed microstructures taking into account the details of the morphology. The analytical multi-coated inclusions model requires more efforts for its numerical implementation, but once implemented, can be run in a negligible time and deliver more reliable resutls than two-step methods. Also, IDI model is recommended for PCN containing three-layer reinforcing stacks.

In the numerical modeling, it was found that the more the EP is different from the nanoclay, in terms of rigidity and aspect ratio, or the higher the volume fraction is, the more the accuracy of two-step numerical models is deteriorated. Considering the much lower computational cost of two-step numerical models, the error induced by EP concept can be acceptable depending on the application of the results. However, when the numerical
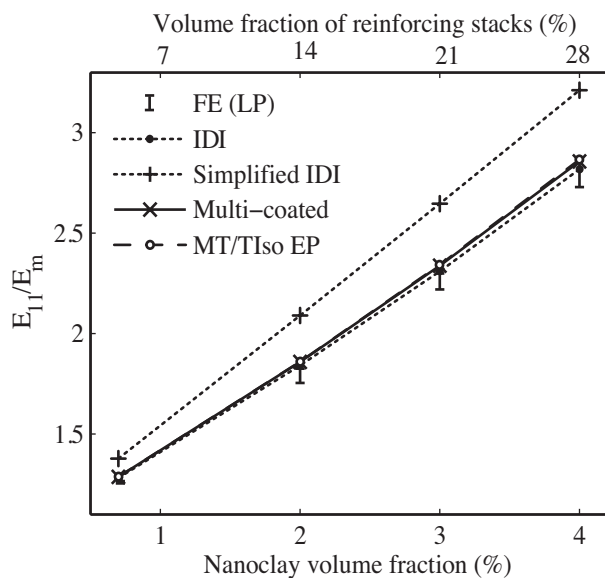
Figure 4.12 Evaluation of one-step (Multi-coated, IDI, simplified IDI) and two-step (MT/TIso EP) analytical models against one-step FE (LP) model. Exfoliated morphology, Case I. Results obtained from 5-10 realizations, each containing 50 reinforcing stacks. The bars correspond to confidence intervals on the average level of 95%.
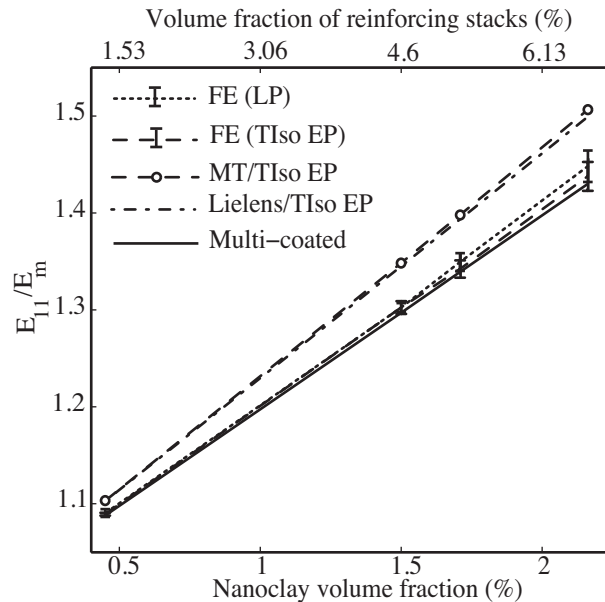

Figure 4.13 Evaluation of one-step (Multi-coated) and two-step (MT/TIso EP, Lielens's/TIso EP) analytical models against one-step (LP) and two-step (TIso EP) numerical models. Intercalated morphology. Results obtained from 4-10 realizations, each containing 10 reinforcing stacks. The bars correspond to confidence intervals on the average level of 95%.

simulations are to be used as validation means, whose accuracy should be unquestionable, the use of one-step FE models is highly recommended. Although the TIso EP reduces the discrepancies induced by two-step numerical models when compared to the Iso EP, it has a negligible effect on the analytical predictions for the axial Young's modulus.

4.8   Acknowledgments

4.9   Appendix A

The effective stiffness tensor $\mathbf{C}^{\text{eff}}$ equation for IDI approach is (Liu and Sun, 2005; Ju and Chen, 1994) :

$$\mathbf{C}^{\text{eff}} = \mathbf{C}^{(0)} : [\mathbf{I} - \Phi_{(\Omega)}\mathbf{T}^{(\Omega)} : (\Phi_{(\Omega)}\mathbf{S}^{(\Omega)} + \mathbf{I})^{-1}], \tag{4.16}$$

where $\mathbf{C}^{(0)}$ denotes the matrix stiffness tensor, $\mathbf{I}$ refers to the fourth-order identity tensor, $\Phi_{(\Omega)}$ is the volume fraction of the coated inclusion Ω (i.e. ellipsoidal core particle + interphase) in the composite and $\mathbf{T}^{(\Omega)}$ is a fourth-order tensor given by:

$$\mathbf{T}^{(\Omega)} = \phi_{(1)}\mathbf{T}^{(1)} + \phi_{(2)}\mathbf{T}^{(2)}, \tag{4.17}$$

where scripts (1) and (2) refer to the core particle and interphase, respectively (Figure 4.2(a)). $\mathbf{T}^{(1)}$ and $\mathbf{T}^{(2)}$ are two fourth-order tensors defined by

$$\mathbf{T}^{(1)} = -\big[(\mathbf{S}^{(1)} + \mathbf{A}^{(1)}) + \Delta\mathbf{S} : \big(\mathbf{S}^{(1)} - \phi_{(1)}/\phi_{(2)}\Delta\mathbf{S} + \mathbf{A}^{(2)}\big)^{-1}$$
$$: \big(\mathbf{S}^{(1)} - \phi_{(1)}/\phi_{(2)}\Delta\mathbf{S} + \mathbf{A}^{(1)}\big)\big]^{-1}, \tag{4.18a}$$

$$\mathbf{T}^{(2)} = -\big[\Delta\mathbf{S} + (\mathbf{S}^{(1)} + \mathbf{A}^{(1)}) : \big(\mathbf{S}^{(1)} - \phi_{(1)}/\phi_{(2)}\Delta\mathbf{S} + \mathbf{A}^{(1)}\big)^{-1}$$
$$: \big(\mathbf{S}^{(1)} - \phi_{(1)}/\phi_{(2)}\Delta\mathbf{S} + \mathbf{A}^{(2)}\big)\big]^{-1}, \tag{4.18b}$$

where $\phi_{(1)}$ and $\phi_{(2)}$ refer to the particle and interphase volume fraction inside the coated inclusion Ω, respectively. $\Delta\mathbf{S} = \mathbf{S}^{(\Omega)} - \mathbf{S}^{(1)}$ where $\mathbf{S}^{(\Omega)}$ and $\mathbf{S}^{(1)}$ are Eshelby's tensors (Eshelby, 1957) when the infinite media is the matrix and the inclusion is the coated particle and the ellipsoidal core, respectively. $\mathbf{A}^{(1)}$ and $\mathbf{A}^{(2)}$ are two mismatch material property fourth-order

tensors for domain (1) and (2) expressed by

$$\mathbf{A}^{(1)} = (\mathbf{C}^{(1)} - \mathbf{C}^{(0)})^{-1} : \mathbf{C}^{(0)}, \qquad \mathbf{A}^{(2)} = (\mathbf{C}^{(2)} - \mathbf{C}^{(0)})^{-1} : \mathbf{C}^{(0)}. \tag{4.19}$$

In a simplified version of this model (e.g., in (Mesbah *et al.*, 2009)), called *simplified IDI* hereinafter, it was assumed that the interphase around the particle had the same aspect ratio as that of the particle, which leads to $\mathbf{S}^{(\Omega)} = \mathbf{S}^{(1)}$ and $\Delta\mathbf{S} = 0$. Consequently, Equations (4.18a) and (4.18b) become much simpler.

4.10 Appendix B

The stiffness tensor of the composite reinforced with aligned n-layer inclusions $\Omega_{(n)}$, was calculated as (Lipinski *et al.*, 2006):

$$\mathbf{C}^{\text{eff}} = \mathbf{C}^{(0)} + \sum_{j=1}^{n} \Phi_{(j)}(\mathbf{C}^{(j)} - \mathbf{C}^{(0)}) : \mathbf{A}^{(j)}, \tag{4.20}$$

where j denotes the different phases (i.e., $j = 0$, $j = 1$ and $j > 1$ represent the matrix, the core particle and coating layers, respectively (Figure 4.2(b)) and $\Phi_{(j)}$ refers to the volume fraction of the phase j in the whole composite. The fourth-order strain concentration tensors $\mathbf{A}^{(j)}$, determinated by the generalized self-consistent scheme, take the form $\mathbf{A}^{(j)} = \boldsymbol{\alpha}^{(j)} : \mathbf{A}$ where

$$\mathbf{A} = \left[\mathbf{I} + \mathbf{T}^{\Omega_{(n)}}(\mathbf{C}^{\text{eff}}) : \left(\sum_{j=0}^{n} \Phi_{(j)} \Delta\mathbf{C}^{(j/\text{eff})} : \boldsymbol{\alpha}^{(j)} \right) \right]^{-1}, \tag{4.21}$$

and $\Delta\mathbf{C}^{(j/\text{eff})} = \mathbf{C}^{(j)} - \mathbf{C}^{\text{eff}}$. The fourth-order $\mathbf{T}^{\Omega_n}(\mathbf{C}^{\text{eff}})$ is such that

$$\mathbf{T}^{\Omega_{(n)}}(\mathbf{C}^{\text{eff}}) = \mathbf{S}^{\Omega_{(n)}}(\mathbf{C}^{\text{eff}}) : (\mathbf{C}^{\text{eff}})^{-1}, \tag{4.22}$$

in which $\mathbf{S}^{\Omega_{(n)}}(\mathbf{C}^{\text{eff}})$ is the well-known Eshelby tensor depending on the matrix $\mathbf{C}^{\text{eff}}$ elastic properties and aspect ratio of the $\Omega_{(n)}$. The fourth-order concentration operators $\boldsymbol{\alpha}^{(j)}$ are

$$\boldsymbol{\alpha}^{(1)} = \left(\sum_{j=0}^{n} \Phi_{(j)} \mathbf{w}^{(j)} \right)^{-1}, \tag{4.23a}$$

$$\boldsymbol{\alpha}^{(j+1)} = \mathbf{w}^{(j+1)} : \boldsymbol{\alpha}^{(1)}, \tag{4.23b}$$

$$\boldsymbol{\alpha}^{(0)} = \boldsymbol{\alpha}^{(n+1)} = \mathbf{w}^{(n)} : \boldsymbol{\alpha}^{(1)}, \tag{4.23c}$$

where the tensors $\mathbf{w}^j$ are defined such that

$$\mathbf{w}^{(1)} = \mathbf{I}, \quad \mathbf{w}^{(2)} = \boldsymbol{\omega}^{(2/1)}, \tag{4.24a}$$

$$\mathbf{w}^{(j+1)} = \frac{\sum\limits_{k=1}^{j} \left(\Phi_{(k)} \boldsymbol{\omega}^{(j+1/k)} : \mathbf{w}^{(k)} \right)}{\sum\limits_{k=1}^{j} \Phi_{(k)}}. \tag{4.24b}$$

$\boldsymbol{\omega}^{(j+1/k)}$ is the concentration tensor describing the jump of average strains between the layer $j+1$ and layer k. The expressions below define the general form of this tensor

$$\boldsymbol{\omega}^{(j+1/k)} = \mathbf{I} - \left[\mathbf{T}^{\Omega_{(j)}}(\mathbf{C}^{(j+1)}) - \frac{\sum\limits_{l=1}^{j} \Phi_{(l)}}{\Phi_{(j+1)}} (\mathbf{T}^{\Omega_{(j+1)}}(\mathbf{C}^{(j+1)}) - \right.$$

$$\left. \mathbf{T}^{\Omega_{(j)}}(\mathbf{C}^{(j+1)})) \right] : \Delta\mathbf{C}^{(j+1/k)}$$

$$\text{for} \quad k = 1, .., j \tag{4.25}$$

where $\Delta\mathbf{C}^{(j+1/k)} = \mathbf{C}^{(j+1)} - \mathbf{C}^{(k)}$ and the composite inclusion $\Omega_{(j+1)}$ consists of phases from 1 to $j+1$. Because of the numerical calculations of the Eshelby's tensor and required calculations for every coating layer at each iteration, the computational time of this model is higher than the other analytical models explained in this paper.

CHAPTER 5

GENERAL DISCUSSION

5.1 General remarks

This study presented a comprehensive evaluation on the performance of analytical models, with special focus on the microstructural features associated to PCN. For example, for low volume fractions and very low aspect ratios (typical of PCN), the axial Young's modulus is slightly overestimated by Lielens's model (Figure 1.2, curve of $E^\perp$ at volume fraction of 5%). The MT model delivers slightly lower predictions for this range of properties. Therefore, similarly to what was concluded in the first article (Section 3), for this particular range of aspect ratios, rigidity contrasts and volume fractions the general conclusion of Pierard *et al.* (2004) is not applicable and it is the MT model that delivers the most accurate results.

The results obtained in this thesis highlighted the fact that analytical models are fast predictive tools, but are not accurate for all ranges of aspect ratios, rigidity contrasts and volume fractions. For example, it was shown in Section 4 that the simplified IDI model overestimates the stiffness of exfoliated PCN in the presence of interphase. This model was employed as the analytical model by Mesbah *et al.* (2009) (Figure 1.6). The overestimation of this analytical model thus casts doubts on the accuracy of the concluded interphase properties or particle orientation in (Mesbah *et al.*, 2009).

This thesis is also the first to systematically reveal the bias induced by two-step models, which is discussed more in the following.

5.2 Complementary works

The underlying reason for the observed bias in the results of two-step models may be explored by comparing the general equations given by the multi-coated model, as the most accurate analytical model, and the two-step MT/EP model. To this end one may write the composite stiffness tensor by the MT/EP model in the following form (see the Appendix):

$$\mathbf{C}^{\mathrm{MT/EP}} = \mathbf{C}^{(0)} + \left[\sum_{j=1}^{n} \Phi_{(j)}(\mathbf{C}^{(j)} - \mathbf{C}^{(0)})\right] : \mathbf{A}^{\mathrm{MT}}. \tag{5.1}$$

Composite stiffness tensor by the multi-coated model as presented in Section 4 is:

$$\mathbf{C}^{\text{multi-coated}} = \mathbf{C}^{(0)} + \sum_{j=1}^{n} \Phi_{(j)}(\mathbf{C}^{(j)} - \mathbf{C}^{(0)}) : \mathbf{A}^{(j)}. \tag{5.2}$$

The comparison of Equations (5.1) and (5.2) reveals that the induced error is mainly due to the assumptions regarding the strain concentration tensors at each layer of the coated inclusion. The two-setp model uses a single strain concentration tensor whose properties were calculated from the EP homogenized properties. On the other hand, the multi-coated model is able to capture the strain and stress jumps at each layer. Equation (5.2) also shows that the effect of these jumps on the final stiffness tensor depends not only on the phase stiffness tensor but also on its volume fraction. It is also worth mentioning that the calculations of the $\mathbf{A}$ tensors in these two models are based on two different concepts. The MT model considers the EPs embedded in the matrix, whereas in the multi-coated model the coated particles are first assumed to be surrounded by a layer of matrix and then embedded in the composite whose effective properties are yet unknown .

To demonstrate the EP effect on numerical models, a simple case with an imaginary interphase was simulated with both layered and isotropic effective particles (Figure 5.1). An axial displacement was applied to the periodic models and the results for axial stress (along the direction x) are shown in Figures 5.1 and 5.2. For the EP model, the axial stresses in the EPs are quite lower than those in the nanoclays for the LP model. The EP model clearly dose not capture the stress jumps in the reinforcing stacks (Figure 5.1). Larger fraction of the matrix is affected in the presence of EPs but with lower stresses, when compared with the LP model (Figure 5.2). In summary, the EP concept clearly disturbs the real stress and strain fields in the composite.

Furthermore, the influence of the EP material symmetry on the obtained results was investigated for different analytical models. It was shown in Section 4 that the TIso EP can reduce the induced bias in numerical results. Here, the results of different analytical models with Iso and TIso EPs are listed in Table 5.1. It was found that the EP anisotropy had a very insignificant effect on analytical results for axial Young's modulus, when compared with its effect on numerical results (the numerical results were presented in Section 4). The SC scheme and the Lielens's model are relatively more sensitive to the anisotropy of the reinforcement than the MT model since they can take into account the Eshelby's tensor of the composite and the reinforcement, respectively.
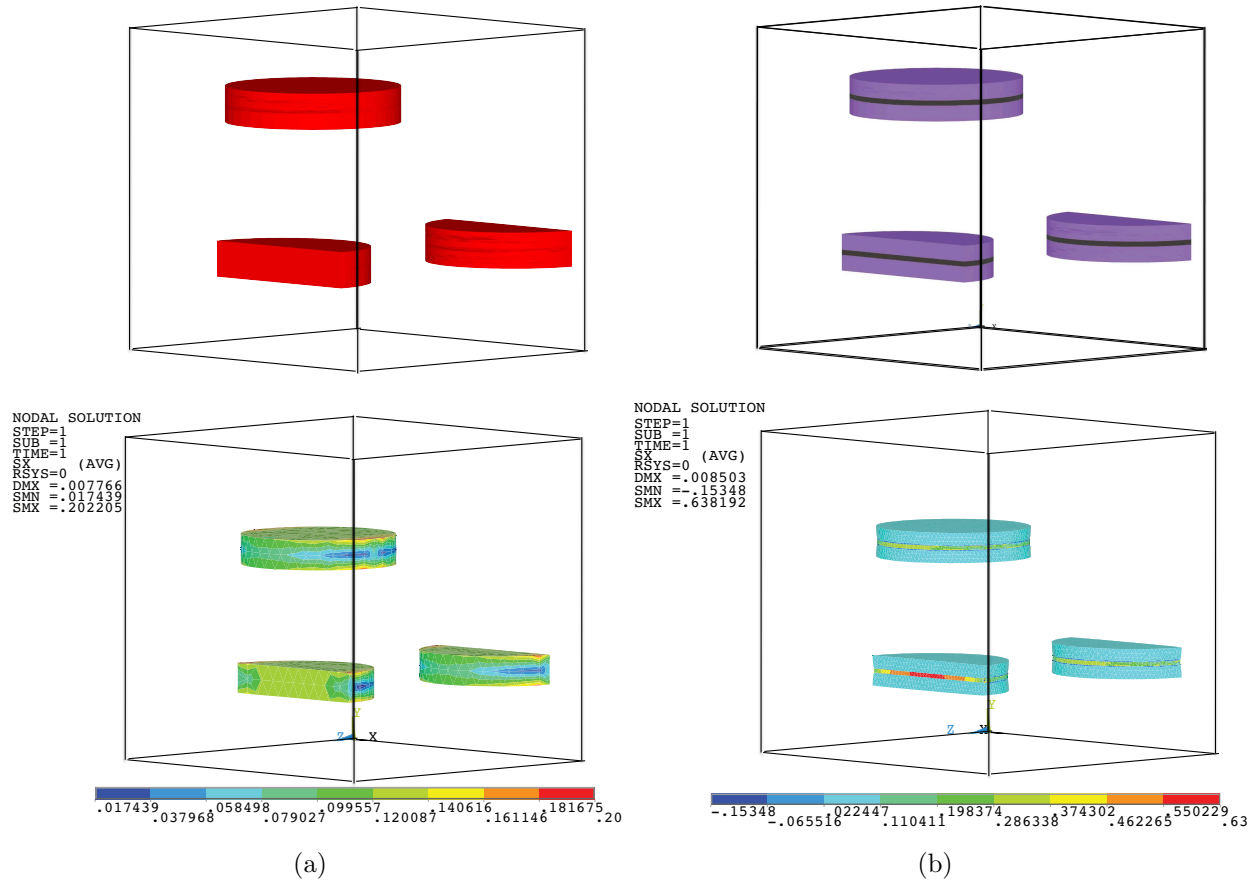
Figure 5.1 Numerical models with a) Effective particles (EPs) and b) Layered particles (LPs) consisting of nanoclays coated by imaginary interphase. Results are for the axial stress calculated under axial displacement.
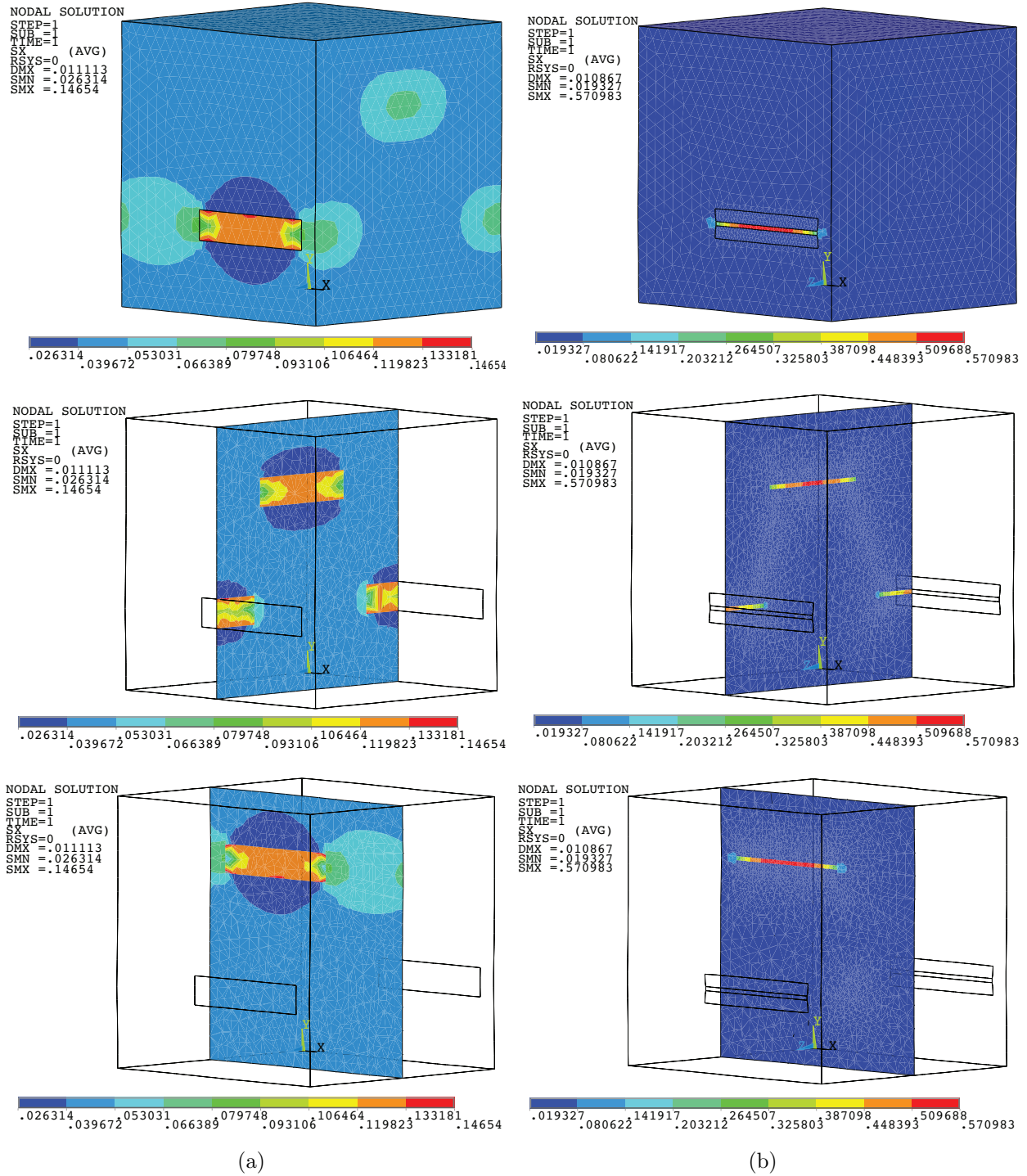
Figure 5.2 FE results for models with a) Effective particles (EPs) and b) Layered particles (LPs) consisting of nanoclays coated by imaginary interphase. Results are for the axial stress calculated under axial displacement.

Table 5.1 Estimations of axial Young's modulus (E/E_m) by different analytical models based on Iso and TIso EP concept. The volume fraction of reinforcing stack is 28% and 6% for exfoliated and intercalated cases, respectively.

		MT	SC	Lielens
Exfoliated PCN	Iso EP	2.869	3.392	2.907
(Case I)	TIso EP	2.867	3.387	2.877
Intercalated PCN	Iso EP	1.454	1.495	1.454
	TIso EP	1.455	1.450	1.449

CONCLUSION

In this thesis, a thorough evaluation study was performed to examine the performance of different homogenization methods for predicting the mechanical behavior of nanoclay nanocomposites using analytical and numerical approaches.

The evaluations was first performed on two-step procedures based on the EP concept. The validity of commonly used analytical micromechanical models, as the second homogenization step, for the prediction of exfoliated PCN elastic properties was examined with the help of 3D FE simulations. In particular, special attention was devoted to the interphase around the nanoclays. To obtain accurate FE results, the RVE was determined. In addition, a simplified procedure to guide the determination of the RVE based on statistical and material symmetry criteria on the desired property was developed. The theoretical results were validated further against experimental data extracted from the literature. It was found that the MT model was the most reliable method to be used in two-step models for the possible ranges of modulus contrast, aspect ratio and volume fraction that may occur in exfoliated PCN. Lielens's model may improve on the MT model at high volume fractions when the rigidity contrast between the EP and the polymer is also high. In addition, the SC scheme was shown to overestimate the axial Young's modulus for all studied cases. The properties and the thickness of the interphase were also estimated from comparison between the numerical parametric study and experimental results. The incorporation of the interphase was shown to increase the estimated axial Young's modulus by up to 13%.

The evaluation was then extended to a wider class of models, two- and one -step methods. Analytical models were adopted to explicitly model the interphase in exfoliated nanocomposites, as well as the layered structure of intercalated morphology. Detailed 3D FE simulations of PCN layered microstructures were performed to provide benchmark results using well established RVEs. The theoretical predictions were also compared to experimental data extracted from the literature. It was found that the results of EP-based models not explicitly considering all constituent phases may significantly diverge from those of FE layered-microstructure models. However, despite some lack of rigor and accuracy, there are circumstances in which two-step models such as explicit MT/EP model or efficient EP-based FE models are useful. The maximum bias of two-step methods found in this study was less than 15%, which can be regarded as acceptable for certain applications. On the other hand, the use of detailed layered FE models may be inevitable, despite their high computational cost, depending on the desired accuracy and the PCN morphology. The more the EP is different from the nanoclay, in terms of rigidity and aspect ratio, or the higher the volume fraction is,

the more the bias of two-step numerical models is pronounced. Employing the transversely isotropic EP can reduce the bias in numerical modeling. As far as analytical modeling is concerned, the one-step multi-coated inclusions model requires more efforts for its numerical implementation, but once implemented, can be run in a negligible time and deliver more reliable resutls than two-step methods. Introducing multi-coated inclusions model for predicting PCN properties offers a new class of analytical models to the exploration of these materials. High accuracy along with the vast number of modeling parameters make this model a perfect and rigorous tool for predicting a wide range of PCN in terms of morphology and mechanical properties. However, the accuracy of this model is only verified for a small range of properties in this thesis, which was very promising, and it needs to be evaluated more for wider ranges of geometrical and mechanical properties of constituent phases.

The main contribution of this thesis was in exploring the better suited models for predicting the mechanical behavior of PCN based on the performed evaluations on the accuracy of different homogenization models. The evaluations were performed using 3D FE simulations of detailed RVEs. The originality of the present work lies in the fact that the RVE was established and that neither analytical nor numerical models were limited by simplifying assumptions common in most of modeling approaches such as ignoring constituent phases, EP concept, isotropic particles or limitations on aspect ratio.

Recommendations for future studies

- **Extension to other morphologies:** The presented modeling strategy was developed for PCN with aligned reinforcing stacks. However, the analytical model can be simply extended to the randomly (or partially randomly) oriented particles by averaging the effective stiffness tensor over all possible orientations using distribution orientation functions (Schjodt-Thomsen and Pyrz, 2001; Figiel and Buckley, 2009; Pierard *et al.*, 2004). On the other hand, the generation of numerical models consisting of randomly oriented particles requires new codes able to deal with particles with high aspect ratio and to efficiently generate high number of realizations required to perform the RVE studies. In addition, the PCN have been found to be mostly partially intercalated-exfoliated, especially at high nanoclay loadings. Moreover, experimental literature also reports the presence of agglomerates and large particles in PCN. The presented methodology needs to be extended to be able to predict the behavior of composites with such hybrid morphologies. The generation of numerical models for such morphologies requires the statistical distribution functions. The analytical modeling for multi-phase composites with different aspect ratios and mechanical properties can be easily performed by two-

or multi -step models, but a rigorous evaluation of their accuracy will be essential.

- **Optimized implementation of numerical homogenization**: Lower cost alternative methods are highly desired for different steps of the numerical homogenization process. For example:

  1. Numerical resolution techniques: FE is the most popular numerical method for computing accurate local stress and strain fields within heterogeneous materials. However, the discretization of microstructures with heterogeneities of high aspect ratios largely increases the computation time and memory. Mesh-free methods (Belytschko *et al.*, 1996; Li and Liu, 2002), as alternatives to the FE method, have shown a promising potential and have consequently found applications in various numerical problems including homogenization of composite materials (Li *et al.*, 2011). Basically, such methods include shape functions describing the microstructure in the original analytical formulation. Efforts needs to be devoted in exploring the efficiency and applicability of mesh-free techniques to nanocomposites such as PCN.

  2. Boundary conditions: Interpolated PBC proposed by Nguyen *et al.* (2012) does not require periodic meshing and periodic geometries. It thus can simplify the microstructure generation and meshing procedures. The implementation of such PBC needs to be studied for modeling of PCN.

  3. Assessment of new RVE quantitative definitions: Employing the methodologies developed by Moussaddy (2013) may accelerate the RVE determination process. In their work, it was demonstrated that new quantitative definitions can determine accurate effective properties for smaller material volumes. Particularly, the arithmetic and harmonic means of apparent elasticity tensors have collectively delivered a good estimate of the effective properties. Their definition of RVE for volumes containing aligned high aspect ratio discs needs to be assessed.

- **Extension to other elastic properties:** Given the interest of experimental works, the focus of the present study was mainly on the axial Young's modulus. The same methodology can be employed to study other elastic properties. For all the studied cases, the whole stiffness tensor were found and saved in a database and can be thus used for any future studies. Homogenization models may behave quite differently in predicting different elastic properties (Tucker and Liang, 1999). In addition, effect of different modeling parameters, such as the anisotropy of particles, on different desired properties may be very dissimilar (Figiel and Buckley, 2009).

- **Exploitation of the multi-coated model:** The multi-coated model offers a fast and reliable predictive tool applicable to a vast PCN morphologies from the exfoliated

nanocomposites to intercalated morphologies in the presence of interphase. The interphase was not considered for the intercalated morphology in the present study but it can be easily incorporated by the multi-coated model. Moreover, morphologies with higher number of layers in each stack, with different mechanical properties and material symmetries can also be predicted by this rigor model. However, this work only evaluated the validity of this model for a limited range of material properties and more assessments are required for other morphologies. Furthermore, efforts should be made to find the range of aspect ratios for which the assumption of modeling the multi-layer disc-shaped particles as multi-layer coated inclusions is reasonable. There should be no problem in terms of the aspect ratio and the volume fraction of each phase, since they have been entered correctly in the analytical model, but in terms of the arrangement of the phases. For very thick particles, difference in the phase arrangements of numerical and multi-coated models may lead to different local stress and strain fields, and consequently to different effective properties.

- **Extension to thermal and barrier properties:** PCN have found numerous applications in industrial sectors requiring high thermal and barrier properties. There have been numerous work devoted to these studies (Osman *et al.*, 2004; Sheng, 2006; Minelli *et al.*, 2009; Xiao *et al.*, 2010) but the evaluation of different models by a rigorous detailed numerical model is still missing.

REFERENCES

ALEXANDRE, M. and DUBOIS, P. (2000). Polymer-layered silicate nanocomposites: preparation, properties and uses of a new class of materials. *Materials Science and Engineering: R: Reports*, <u>28</u>, 1 – 63.

ALTENDORF, H. and JEULIN, D. (2011a). Random-walk-based stochastic modeling of three-dimensional fiber systems. *Physical Review E*, <u>83</u>, 041804.

ALTENDORF, H. and JEULIN, D. (2011b). Stochastic modeling of a glass fiber reinforced polymer. P. Soille, M. Pesaresi and G. Ouzounis, editors, *Mathematical Morphology and Its Applications to Image and Signal Processing*, Springer, vol. 6671. 439–450.

ANOUKOU, K., ZAïRI, F., NAïT-ABDELAZIZ, M., ZAOUI, A., MESSAGER, T. and GLOAGUEN, J. (2011). On the overall elastic moduli of polymer–clay nanocomposite materials using a self-consistent approach. part i: Theory. *Composites Science and Technology*, <u>71</u>, 197–205.

BARELLO, R. B. and LÉVESQUE, M. (2008). Comparison between the relaxation spectra obtained from homogenization models and finite elements simulation for the same composite. *International Journal of Solids and Structures*, <u>45</u>, 850–867.

BELYTSCHKO, T., KRONGAUZ, Y., ORGAN, D. and FLEMING, M. (1996). Meshless methods: An overview and recent developments. *Computer Methods in Applied Mechanics and Engineering*, 3–47.

BENVENISTE, Y. (1987). A new approach to the application of mori-tanaka's theory in composite materials. *Mechanics of Materials*, <u>6</u>, 147–157.

BERRYMAN, J. G. and BERGE, P. A. (1996). Critique of two explicit schemes for estimating elastic properties of multiphase composites. *Mechanics of Materials*, <u>22</u>, 149–164.

BHARADWAJ, R. K. (2001). Modeling the barrier properties of polymer-layered silicate nanocomposites. *Macromolecules*, <u>34</u>, 9189–9192.

BÖHM, H. J. (2008). A short intorduction to basic aspects of continuum micromechanics, Institute of Lightweight Design and Structural Biomechanics (ILSB), Vienna University of Technology.

BÖHM, H. J. (2013). *A short introduction to basic aspects of continuum micromechanics*.

BORNERT, M., BRETHEAU, T. and GILORMINI, P. (2001). *Homogénéisation en mécanique des matériaux*. Hermès, Paris.

BUDIANSKY, B. (1965). On the elastic moduli of some heterogeneous materials. *Journal of the Mechanics and Physics of Solids*, 13, 223–227.

CAILLETAUD, G., JEULIN, D. and ROLLAND, P. (1994). Size effect on elastic properties of random composites. *Engineering with Computers*, 11, 99–110.

CHEN, B., EVANSAND, J. R. G., GREENWELL, H. C., BOULET, P., COVENEY, P. V., BOWDENF, A. A. and WHITING, A. (2008). A critical appraisal of polymer–clay nanocomposites. *Chemical Society Reviews*, 37, 568–594.

CHRISTENSEN, R. M. and LO, K. H. (1979). Solutions for effective shear properties in three phase sphere and cylinder models. *Journal of the Mechanics and Physics of Solids*, 27, 315–330.

CRICRI, G., GAROFALO, E., NADDEO, F. and INCARNATO, L. (2011). Stiffness constants prediction of nanocomposites using a periodic 3d-fem model. *Journal of Polymer Science Part B: Polymer Physics*, 50, 207–220.

DRUGAN, W. and WILLIS, J. (1996). A micromechanics-based nonlocal constitutive equation and estimates of representative volume element size for elastic composites. *Journal of the Mechanics and Physics of Solids*, 44, 497–524.

DUNN, M. L. and LEDBETTER, H. (1995). Elastic moduli of composites reinforced by multiphase particles. *Journal of Applied Mechanics*.

ESHELBY, J. D. (1957). The determination of the elastic field of an ellipsoidal inclusion, and related problems. *Proceedings of the Royal Society of London*, A 241, 376–396.

FEDER, J. (1980). Random sequential adsorption. *Journal of Theoretical Biology*, 237–254.

FIGIEL, L. and BUCKLEY, C. P. (2009). Elastic constants for an intercalated layered-silicate/polymer nanocomposite using the effective particle concept - a parametric study using numerical and analytical continuum approaches. *Computational Materials Science*, 44, 1332 – 1343.

FORNES, T. D., YOON, P. J., HUNTER, D. L., KESKKULA, H. and PAUL, D. R. (2002). Effect of organoclay structure on nylon 6 nanocomposite morphology and properties. *Polymer*, 43, 5915–5933.

FORNES, T. D., YOON, P. J., KESKKULA, H. and PAUL, D. R. (2001). Nylon 6 nanocomposites: the effect of matrix molecular weight. *Polymer*, 42, 9929–9940.

GAVAZZI, A. C. and LAGOUDAS, D. C. (1990). On the numerical evaluation of eshelby's tensor and its application to elastoplastic fibrous composites. *Computational Mechanics*, 7, 13–19.

GHOSSEIN, E. and LÉVESQUE, M. (2012). A fully automated numerical tool for a comprehensive validation of homogenization models and its application to spherical particles reinforced composites. *International Journal of Solids and Structures*, 49, 1387–1398.

GIANNELIS, E. P. (1996). Polymer layered silicate nanocomposites. *Advanced Materials*, 29–35.

GILMAN, J. W. (1999). Flammability and thermal stability studies of polymer layered-silicate (clay) nanocomposites. *Applied Clay Science*, 15, 31–49.

GUSEV, A. A. (1997). Representative volume element size for elastic composites: a numerical study. *Journal of the Mechanics and Physics of Solids*, 45, 1449–1459.

GUSEV, A. A. (2001). Numerical identification of the potential of whisker- and platelet-filled polymers. *Macromolecules*, 34, 3081–3093.

HALPIN, J. C. and KARDOS, J. L. (1969). Stiffness and expansion estimates for oriented short fiber composites. *Journal of Composite Materials*, 3.

HALPIN, J. C. and KARDOS, J. L. (1976). The halpin-tsai equations: A review. *Polymer Engineering and Science*, 16, 344–352.

HBAIEB, K., WANG, Q., CHIA, Y. and COTTERELL, B. (2007). Modelling stiffness of polymer/clay nanocomposites. *Polymer*, 48, 901 – 909.

HERVÉ, E. and ZAOUI, A. (1993). n-layered inclusion-based micromechanical modelling. *International Journal of Engineering Science*, 31, 1–10.

HILL, R. (1963). Elastic properties of reinforced solids – some theoretical principles. *Journal of Mechanics and Physics of Solids*, 11, 357–372.

HILL, R. (1965). A self-consitent mechanics of composites materials. *J. Mech. Phys. Solids*, 13, 213–222.

HORI, M. and NEMAT-NASSER, S. (1993). Double-inclusion model and overall moduli of multi-phase composites. *Mechanics of materials*, 14, 189–206.

HU, G. K. and WENG, G. J. (2000). The connections between the double-inclusion model and the ponte castaneda-willis, mori-tanaka, and kuster-toksoz models. *Mechanics of Materials*, 32, 495–503.

HUANG, M. and LI, Y. (2013). X-ray tomography image-based reconstruction of microstructural finite element mesh models for heterogeneous materials. *Computational Materials Science*, 67, 63–72.

HUET, C. (1990). Application of variational concepts to size effects in elastic heterogeneous bodies. *Journal of the Mechanics and Physics of Solids*, 38, 813–841.

INGBER, M. S. and PAPATHANASIOU, T. D. (1997). A parallel-supercomputing investigation of the stiffness of aligned short-fiber-reinforced composites using the boundary element method. *international Journal of Numerical Methods in Engineering*, 3477–3491.

JI, X. L., JING, J. K., JIANG, W. and JIANG, B. Z. (2002). Tensile modulus of polymer nanocomposites. *Polymer Engineering and Science*, <u>42</u>, 983–993.

JU, J. W. and CHEN, T. M. (1994). Micromechanics and effective moduli of elastic composites containing randomly dispersed ellipsoidal inhomogeneities. *Acta Mechanica*, <u>103</u>, 103–121.

KANIT, T., FOREST, S., GALLIET, I., MOUNOURY, V. and JEULIN, D. (2003). Determination of the size of the representative volume element for random composites: statistical and numerical approach. *International Journal of Solids and Structures*, <u>40</u>, 3647–3679.

KANIT, T., NGUYEN, F., FOREST, S., JEULIN, D., REED, M. and SINGLETON, S. (2006). Apparent and effective physical properties of heterogeneous materials: Representativity of samples of two materials from food industry. *Comput. Methods Appl. Mech. Engrg.*, <u>195</u>, 3960–3982.

KARI, S., BERGER, H. and GABBERT, U. (2007). Numerical evaluation of effective material properties of randomly distributed short cylindrical fibre composites. *Computational Materials Science*, <u>39</u>, 198–204.

KOJIMA, Y., USUKI, A., KAWASUMI, M., OKADA, A., FUKUSHIMA, Y., KURAUCHI, T. and KAMAGAITO, O. (1993). Mechanical properties of nylon 6-clay hybrid. *J. Mater. Res.*, <u>8</u>, 1185–1189.

LI, L., WEN, P. and ALIABADI, M. (2011). Meshfree modeling and homogenization of 3d orthogonal woven composites. *Composites Science and Technology*, <u>71</u>.

LI, S. and LIU, W. K. (2002). Meshfree and particle methods and their applications. *Applied Mechanics Review*, <u>55</u>, 1–34.

LIELENS, G. (1999). *Micro-Macro Modeling of Structured Materials*, Universite Catholique de Louvain.

LIELENS, G., PIROTTE, P., COUNIOT, A., DUPRET, F. and KEUNINGS, R. (1997). Prediction of thermo-mechanical properties for compression-moulded composites. *Composites Part A: Applied Science and Manufacturing*, <u>29</u>, 63–70.

LIPINSKI, P., BARHDADI, E. H. and CHERKAOUI, M. (2006). Micromechanical modelling of an arbitrary ellipsoidal multi-coated inclusion. *Philosophical Magazine*, <u>86</u>, 1305–1326.

LIU, H. and SUN, L. (2005). Multi-scale modeling of elastoplastic deformation and strengthening mechanisms in aluminum-based amorphous nanocomposites. *Acta Materialia*, 53, 2693–2701.

LUBACHEVSKY, B. and STILLINGER, F. (1990). Geometric properties of random disk packings. *Journal of Statistical Physics*, 60, 561–583.

LUBACHEVSKY, B., STILLINGER, F. and PINSON, E. (1991). Disks vs. spheres : contrasting properties of random packings. *Journal of Statistical Physics*, 64, 501–523.

LUO, J.-J. and DANIEL, I. M. (2003). Characterization and modeling of mechanical behavior of polymer/clay nanocomposites. *Composites Science and Technology*, 63, 1607 – 1616.

LUSTI, H. R. and GUSEV, A. A. (2004). Finite element predictions for the thermoelastic properties of nanotube reinforced polymers. *Modelling and Simulation in Materials Science and Engineering*, 12, S107–S119.

MANEVITCH, O. L. and RUTLEDGE, G. C. (2004). Elastic properties of a single lamella of montmorillonite by molecular dynamics simulation. *J. Phys. Chem. B*, 108, 1428–1435.

MESBAH, A., ZAïRI, F., BOUTALEB, S., GLAOGUEN, J. M., NAïT-ABDELAZIZ, M., XIE, S., BOUKHAROUBA, T. and LEFEBVRE, J. M. (2009). Experimental characterization and modeling stiffness of polymer/clay nanocomposites within a hierarchical multiscale framework. *Journal of Applied Polymer Science*, 114, 3274–3291.

MESSERSMITH, P. B. and GIANNELIS, E. P. (1994). Synthesis and characterization of layered silicate-epoxy nanocomposites. *Chem. Mater.*, 6, 1719–1725.

MILTON, G. W. (2002). *The Theory of Composites*. Cambridge University Press, Cambridge.

MINELLI, M., BASCHETTI, M. G. and DOGHIERI, F. (2009). Analysis of modeling results for barrier properties in ordered nanocomposite systems. *Journal of Membrane Science*, 327.

MORGAN, A. B. (2007). Polymer-clay nanocomposites: Design and application of multifunctional materials. *Material Matters*, 2, 20–22.

MORI, T. and TANAKA, K. (1973). Average stress in matrix and average elastic energy of materials with misfitting inclusions. *Acta metallurgica*, 21, 571–574.

MORTAZAVI, B., BANIASSADI, M., BARDON, J. and AHZI, S. (2013). Modeling of two-phase random composite materials by finite element, mori–tanaka and strong contrast methods. *Composites Part B: Engineering*, 45, 1117–1125.

MOULINEC, H. and SUQUET, P. (1994). A fast numerical method for computing the linear and nonlinear mechanical properties of composites. *C.R. Acad. Sci. II, Mec. Phys. Chim. Astron. (France)*, 318, 1417 – 23.

MOULINEC, H. and SUQUET, P. (1998). A numerical method for computing the overall response of nonlinear composites with complex microstructure. *Comput. Methods Appl. Mech. Eng. (Switzerland)*, 157, 69 – 94.

MOUSSADDY, H. (2013). *A new definition of the reprentative volume element in numerical homogenization problems and its application to the performance evaluation of analytical homogenization models*, Université de Montréal, Ecole polytechnique de Montréal.

MURA, T. (1987). *Micromechanics of Defects in Solids* edition.

NEMAT-NASSER, S. and HORI, M. (1993). *Micromechanics: Overall Properties of Heterogeneous Materials.* north-holland, amsterdam edition.

NGUYEN, V.-D., BÉCHET, E., GEUZAINE, C. and NOELS, L. (2012). Imposing periodic boundary condition on arbitrary meshes by polynomial interpolation. *Computational Materials Science*, 55, 390 – 406.

OKADA, A. and USUKI, A. (1995). The chemistry of polymer-clay hybrids. *Materials Science and Engineering: C*, 3, 109–115.

OSMAN, M. A., MITTAL, V., MORBIDELLI, M. and SUTER, U. W. (2004). Epoxy-layered silicate nanocomposites and their gas permeation properties. *Macromolecules*, 37, 7250–7257.

OSTOJA-STARZEWSKI, M. (1999). Scale effects in materials with random distributions of needles and cracks. *Mechanics of Materials*, 31, 883–893.

OSTOJA-STARZEWSKI, M. (2002). Microstructural randomness versus representative volume element in thermomechanics. *Journal of Applied Mechanics*, 69, 25–35.

OSTOJA-STARZEWSKI, M. (2006). Material spatial randomness: From statistical to representative volume element. *Probabilistic Engineering Mechanics*, 21, 112–132.

PAHLAVANPOUR, M., MOUSSADDY, H., GHOSSEIN, E., HUBERT, P. and LÉVESQUE, M. (2013). Prediction of elastic properties in polymer-clay nanocomposites: Analytical homogenization methods and 3d finite element modeling. *Computational Materials Science*, 79, 206–215.

PIERARD, O. (2006). *Micromechanics of inclusion-reinforced composites in elasto-plasticity and elasto-viscoplasticity: modeling and computation*, Université Catholique de Louvain.

PIERARD, O., FRIEBEL, C. and DOGHRI, I. (2004). Mean-field homogenization of multi-phase thermo-elastic composites: a general framework and its validation. *Composites Science and Technology*, 64.

PINNAVAIA, T. J. and BEALL, G. W. (2000). *Polymer-Clay Nanocomposites.* John Wiley.

POWELL, C. E. and BEALL, G. W. (2006). Physical properties of polymer/clay nanocomposites. *Current Opinion in Solid State and Materials Science*, <u>10</u>, 73 – 80.

RAY, S. S. and OKAMOTO, M. (2003). Polymer/layered silicate nanocomposites: a review from preparation to processing. *Progress in Polymer Science*, <u>28</u>, 1539 – 1641.

SAB, K. (1992). On the homogenization and the simulation of random materials. *European Journal of Mechanics, A/Solids*, <u>11</u>, 585–607.

SARVESTANI, A. S. (2003). On the overall elastic moduli of composites with spherical coated fillers. *International Journal of Solids and Structures*, <u>40</u>, 7553–7566.

SCHJODT-THOMSEN, J. and PYRZ, R. (2001). The mori-tanaka stiffness tensor: diagolal symmetry, complex fibre orientations and non-dilute volume fractions. *Mechanics of Materials*, <u>33</u>, 531–544.

SCHMIDT, D., SHAH, D. and GIANNELIS, E. P. (2002). New advances in polymer/ layered silicate nanocomposites. *Current Opinion in Solid State and Materials Science*, <u>6</u>, 205–212.

SEGURADO, J. and LLORCA, J. (2002). A numerical approximation to the elastic properties of sphere-reinforced composites. *Journal of the Mechanics and Physics of Solids*, <u>50</u>, 2107–2121.

SHELLEY, J. S., MATHER, P. T. and DEVRIES, K. L. (2001). Reinforcement and environmental degradation of nylon-6/clay nanocomposites. *Polymer*, <u>42</u>, 5849 – 5858.

SHENG, N. (2006). *Multiscale micromechanical modeling of thermal/mechanical properties of polymer/clay nanocomposites*, MIT.

SHENG, N., BOYCE, M. C., PARKS, D. M., RUTLEDGEB, G. C., ABESB, J. I. and COHEN, R. E. (2004). Multiscale micromechanical modeling of polymer/clay nanocomposites and the effective clay particle. *Polymer*, <u>45</u>, 487–506.

SIKDAR, D., PRADHAN, S. M., KATTI, D. R., KATTI, K. S. and MOHANTY, B. (2008). Altered phase model for polymer clay nanocomposites. *Langmuir*, <u>24</u>, 5599–5607.

STROEVEN, M., ASKES, H. and SLUYS, L. (2004). Numerical determination of representative volumes for granular materials. *Computer Methods in Applied Mechanics and Engineering*, <u>193</u>, 3221–3238.

SUQUET, P. (1997). Effective properties of nonlinear composites. *Continuum micromechanics*, 197–264.

TALBOT, J., SCHAAF, P. and TARJUS, G. (1991). Random sequential addition of hard spheres. *Molecular Physics: An International Journal at the Interface Between Chemistry and Physics*, <u>72</u>.

TERADA, K., HORI, M., KYOYA, T. and KIKUCHI, N. (2000). Simulation of the multiscale convergence in computational homogenization approaches. *International Journal of Solids and Structures*, <u>37</u>, 2285–2311.

TORQUATO, S. (2002). *Random Heterogeneous Media*. Springer-Verlag, New York, NY, USA.

TRIAS, D., COSTA, J., TURON, A. and HURTADO, J. (2006). Determination of the critical size of a statistical representative volume element (srve) for carbon reinforced polymers. *Acta materialia*, <u>54</u>, 3471–3484.

TSAI, S. W. and HAHN, H. T. (1980). *Introduction to Composite Materials*. Technomic Pub.: Lancaster, Pennsylvania, USA.

TUCKER, C. L. and LIANG, E. (1999). Stiffness predictions for unidirectional short-fiber composites: Review and evaluation. *Composites Science and Technology*, <u>59</u>, 655 – 671.

TYAN, H.-L., WEI, K.-H. and HSIEH, T.-E. (2000). Mechanical properties of clay–polyimide (btda–oda) nanocomposites via oda-modified organoclay. *Journal of Polymer Science: Part B: Polymer Physics*, <u>38</u>, 2873–2878.

TZIKA, P. A., BOYCE, M. C. and PARKS, D. M. (2000). Micromechanics of deformation in particle-toughened polyamides. *Journal of Mechanics and Physics of Solids*, <u>48</u>, 1893–1929.

VANES, M. (2001). *Polymer composites, The importance of Particle dimension*, Delft University.

WANG, J. and PYRZ, R. (2004). Prediction of the overall moduli of layered silicate-reinforced nanocomposites–part i: basic theory and formulas. *Composites Science and Technology*, <u>64</u>, 925 – 934.

WITHERS, P., STOBBS, W. and PEDERSEN, O. (1989). The application of the eshelby method of internal stress determination to short fibre metal matrix composites. *Acta Metallurgica*, <u>37</u>, 3061–3084.

XIAO, J., HUANG, Y. and MANKE, C. W. (2010). Computational design of polymer nanocomposite coatings: A multiscale hierarchical approach for barrier property prediction. *Ind. Eng. Chem. Res.*, <u>49</u>.

XU, W., ZENG, Q. and YU, A. (2012). Young's modulus of effective clay clusters in polymer nanocomposites. *Polymer*, <u>53</u>, 3735–3740.

YANO, K., USUKI, A. and OKADA, A. (1997). Synthesis and properties of polyimide-clay hybrid films. *Journal of Polymer Science, Part A: Polymer Chemistry*, <u>35</u>, 2289 – 2294.

ZAOUI, A. (2002). Continuum micromechanics: Survey. *JOURNAL OF ENGINEERING MECHANICS*, <u>128</u>, 808–816.

APPENDIX I: FORMULATION OF THE TWO-STEP MT/EP MODEL

The stiffness tensor of a composites containing aligned EPs as reinforcements is calculated by the MT model (see Section 1 for details) as:

$$\mathbf{C}^{\mathrm{MT/EP}} = \mathbf{C}^{(0)} + \Phi_{(\mathrm{EP})}(\mathbf{C}^{(\mathrm{EP})} - \mathbf{C}^{(0)}) : \mathbf{A}^{\mathrm{MT}}. \tag{1}$$

The following relationship holds between the volume fraction of the phase j in the composite $\Phi_{(j)}$, its volume fraction in the coated particle $\phi_{(j)}$ and the EP volume fraction in the composite $\Phi_{(\mathrm{EP})}$ as:

$$\Phi_{(j)} = \phi_{(j)}\Phi_{(\mathrm{EP})}, \tag{2}$$

where $\Phi_{(\mathrm{EP})}$ can be calculated from

$$\Phi_{(\mathrm{EP})} = \sum_{j=1}^{n} \Phi_{(j)}. \tag{3}$$

In addition, the EP stiffness tensor $\mathbf{C}^{(\mathrm{EP})}$ under isotopic condition is calculated as:

$$\mathbf{C}^{(\mathrm{EP})} = \sum_{j=1}^{n} \phi_{(j)}\mathbf{C}^{(\mathrm{j})}. \tag{4}$$

Therefore, by simple substitution of Equations (2) to (4) into Equation (1) the composite stiffness tensor by the MT/EP model can be rewritten as:

$$\mathbf{C}^{\mathrm{MT/EP}} = \mathbf{C}^{(0)} + \left[\sum_{j=1}^{n} \Phi_{(j)}(\mathbf{C}^{(j)} - \mathbf{C}^{(0)})\right] : \mathbf{A}^{\mathrm{MT}}. \tag{5}$$

APPENDIX II: EXAMPLES OF CALCULATED STIFFNESS TENSORS

Calculated stiffness tensors for the exfoliated PCN with Case I (b) phase properties are presented for two RVEs in the ensemble. The RVEs contained 50 effective particles each and the effective particle volume fraction was 28%.

$$
\mathbf{C}_1 = \begin{bmatrix}
10.7977 & 3.3110 & 4.4060 & 0.0078 & 0.0090 & 0.0078 \\
3.3107 & 6.3123 & 3.3177 & -0.0048 & 0.0106 & -0.0048 \\
4.4060 & 3.3178 & 10.5964 & 0.0024 & 0.0043 & 0.0024 \\
0.0031 & 0.0034 & 0.0316 & 1.5348 & 0.0024 & 0.0037 \\
0.0089 & 0.0107 & 0.0042 & 0.0079 & 3.1658 & 0.0079 \\
0.0078 & -0.0048 & 0.0023 & 0.0037 & 0.0078 & 1.5348
\end{bmatrix},
\tag{6}
$$

$$
\mathbf{C}_2 = \begin{bmatrix}
10.7635 & 3.3109 & 4.4101 & -0.0086 & -0.0461 & -0.0196 \\
3.3109 & 6.3221 & 3.3032 & 0.0112 & -0.0067 & 0.0018 \\
4.4101 & 3.3034 & 10.6875 & 0.0038 & -0.0442 & -0.0052 \\
-0.0087 & 0.0112 & 0.0038 & 1.5349 & -0.0075 & -0.0026 \\
-0.0460 & -0.0067 & -0.0442 & -0.0075 & 3.1460 & 0.0031 \\
-0.0196 & 0.0017 & -0.0052 & -0.0026 & 0.0032 & 1.5380
\end{bmatrix}.
$$

It is worth reminding that the desired E_{11} was calculated for each of the RVEs and the ensemble average of E_{11} was then calculated form the averaging over all RVEs of the ensemble. Stiffness tensor of each realization is not perfectly transversely isotropic but the transverse isotropy criterion should be met for the average of ensemble (please refer to Section 3.5.2, criterion CR. II).